Republic of Iraq
Ministry of Higher Education and Scientific Research
University of Misan/College of Engineering
Department of Civil Engineering

Numerical Investigation into the Behavior of Concrete-Filled Aluminum Columns with Different Cross Sections

By

Rawa Layth Al-Jaroosh

B.Sc. civil engineering, 2020

A Thesis

Submitted in Partial Fulfilment of the

Requirements for the Degree of

Master of Science/Master of Structural Engineering

(in Civil Engineering)

Advisor Name: Prof. Dr. Mohammed S. Abd-Ali

بِسْمِ اللَّهِ الرَّحْمنِ الرَّحِيمِ

(وَأَن لَّيْسَ لِلْإِنسَانِ إِلَّا مَا سَعَىٰ (39) وَأَنَّ سَعْيَهُ سَوْفَ يُرَىٰ (40) ثُمَّ يُجْزَاهُ الْجَزَاءَ الْأَوْفَىٰ (41) وَأَنَّ إِلَىٰ رَبِّكَ الْمُنتَهَىٰ (42))

صَدَقَ اللهُ العَظِيمُ

Abstract

This study presents a numerical investigation into the behaviour of concrete-filled aluminium columns with different cross-sections. The parametric investigations used 34 specimens divided into four groups that present the influence of different parameters on the behaviour of a concrete filled with short aluminium columns, which have different cross-section shapes, different aluminium proof stress, different concrete cylinder strength, and different wall thicknesses of aluminium tube.

The first group analyses the cross-section behaviour, which is presented by six different cross-sections with equivalent section area, length and volume of the circular reference columns. This group indicates that circular cross-sections always outperformed the remaining geometric shapes. The columns having rectangular cross-sections exhibited the lowest efficiency of all cross-section-shaped columns, displaying reductions in ultimate load ranged from 12% to 14% compared with their circular reference equivalents. The shapes ranged in strength from the weakest to the strongest in the following sequence (rectangular, hexagonal, octagonal, elliptical, round ended, circular).

The second group investigated the effects of different aluminium proof stresses, which are 267 and 185 MPa. This group uses circular and rectangular sections. To understand the impact of proof stress of aluminium on the behaviour of these sections. The columns with circular cross section columns having aluminium proof stress equal to 267 MPa displayed an increase in ultimate load ranged from 14% to 20% when compared to columns that had aluminium proof stress equal to 185 MPa. The columns with rectangular cross-section columns having aluminium proof stress

equal to 267 MPa displayed an increase in ultimate load ranged from 12% to 18% when compared to columns that had aluminium proof stress equal to 185 MPa

The third group investigated the effects of different strengths of the cylindrical concrete, which are 44 and 70 MPa. This group uses circular and rectangular sections. To understand the impact of proof stress of aluminium on the behaviour of these sections. The columns with circular cross-section columns having a concrete compressive strength equal to 70MPa displayed an increase in ultimate load ranged from 25% to 33% when compared to columns that had concrete compressive strength equal to 40 MPa. The columns with rectangular cross-section columns having concrete compressive strength equal to 70MPa displayed an increase in ultimate load ranged from 26% to 36%, respectively, when compared to columns that had concrete compressive strength equal to 40MPa.

The fourth group analyses the effect of different aluminium wall thicknesses, which are (1.9, 3, and 5 mm). This group uses circular and rectangular sections. To understand the impact of proof stress of aluminium on the behaviour of these sections. For noncompact section columns that had an aluminium wall thickness of 3 mm, the ultimate load increased about 22% for circular sections and 19% for rectangular sections, compared with slender cross-section columns having a wall thickness of 1.9 mm. Also, compact cross-section columns having a 5 mm wall thickness exhibited improvements of 58% and 56% for circular and rectangular sections, respectively, compared to the same slender section.

Supervisor Certification

I certify that the preparation of this thesis entitled "**Numerical Investigation into the Behavior of Concrete-Filled Aluminum Columns with Different Cross Sections**" was presented by "**Rawa Layth Al-Jaroosh**", and prepared under my supervision at The University of Misan, Department of Civil Engineering, College of Engineering, as a partial fulfilment of the requirements for the degree of Master of Science in Civil Engineering (Structural Engineering).

Signature:

Prof. Dr. Mohammed S. Abd-Ali

Date:

In view of the available recommendations, I forward this thesis for discussion by the examining committee.

Signature:

Asst Prof. Dr. Mortada Abbas Abd Ali

(Head of Civil Eng. Department)

Date:

EXAMINING COMMITTTEE'S REPORT

We certify that we, the examining committee, have read the thesis titled **(Numerical Investigation into the Behavior of Concrete-Filled Aluminum Columns with Different Cross Sections)** which is being submitted by (**Rawa Layth Al-Jaroosh**), and examined the student in its content and in what is concerned with it, and that in our opinion, it meets the standard of a thesis for the degree of Master of Science in Civil Engineering (Structures).

Signature:
Name: **Prof. Dr. Mohammed S. Abd-Ali**
(Supervisor)
Date: / /2026

Signature:
Name: **Assist. Prof. Dr. Samir M. Chassib**
(Chairman)
Date: / /2026

Signature:
Name: **Prof. Dr. Haleem K. Hussain**
(Member)
Date: / /2026

Signature:
Name: **Assist. Prof. Dr. Hayder Al-Khazraji**
(Member)
Date: / /2026

Approval of the College of Engineering:
Signature:
Name: **Prof. Dr. Abbas Oda Dawood**
Dean, College of Engineering
Date: / /2026

Acknowledgements

In the name of Allah, the Most Gracious and the Most Merciful, all praise to Allah for His strength and his blessing in completing this thesis.

I would like to express my sincere thanks to everyone who supported me specially my supervisor (Prof. Dr. Mohammed S. Abd-Ali) during the completion of my thesis.

I am deeply grateful to my parents for their constant love, encouragement, and support. I also thank my brothers for their continued support.

My special thanks go to my husband for his patience and encouragement throughout this journey. I am also thankful to my beloved daughter Rayhana, who has been a source of motivation.

TABLE OF CONTENTS

List of Tables

List of Figures

List of Symboles

E	Aluminium Young's Modulus	MPa
f_y, $\sigma_{0.2}$	Aluminum 0.2% Proof Stress	MPa
f_u, σ_u	Aluminum Ultimate Stress	MPa
A	Area of The Section	mm^2
ε_c	Compressive Strain in The Concrete	mm/mm
σ_c	Compressive Stress in The Concrete	MPa
f'_c	Concrete Cylinder Strength	MPa
Ψ	Dilation Angle	
Δ0.85	Displacement at (0.85 From Ultimate Load) in Plastic Region.	mm
Δu	Displacement at Ultimate Load	mm
$\boldsymbol{\epsilon}$	Eccentricity	
K	Effective Length Factor	
ε_{0c}^{el}	Elastic Strain	mm/mm
ε_f (%)	Elongation (Tensile Strain) After Fracture Based on Gauge Length of 50 Mm	
P_{Exp}	Experimental Ultimate Load	kN
P_{FEA}	Finite Element Analysis Ultimate Load	kN
n	First Strain Hardening	
$\tilde{\varepsilon}_c^{in}$	Inelastic Strain	mm/mm
λ_p	Limiting Width-to-Thickness Parameter for Compact Member	
λ_r	Limiting Width-to-Thickness Parameter for Noncompact Member	
ε_{ln}^{pl}	Log Plastic Strains	mm/mm
I	Moment of Inertia of The Section	mm^4

ε_{nom}	Nominal Plastic Strains	mm/mm
σ_{nom}	Nominal Stresses of Aluminium Alloys	MPa
$f1, f2, f3$	Principal Stresses	MPa
r	Radius of Gyration	mm
M	Second Strain Hardening	
ε	Strain	mm/mm
$\varepsilon_{0.2}$	Strain At 0.2% Aluminium Proof Stress	mm/mm
ε_{ue}	Strain at Ultimate Load	mm/mm
f_{b0}/f_{c0}	Strength Ratio in The Biaxial State to Uniaxial Strength State	
f	Stress	MPa
$E_{0.2}$	Tangent Modulus At 0.2% Aluminium Proof Stress	MPa
Kc	The Ratio of The Second Stress Invariant in The Tensile Meridian to Compressive Meridian	
σ_{true}	True Stresses of Aluminium Alloys	MPa
Ɒ	Viscosity Parameter	
λ	Width-to-Thickness Ratio	

List of Abbreviations

6xxx	Aluminium alloy series made from Mg and Si
ACI	American Concrete Institute
AISC	American Institute of Steel Construction
CFRP	Carbon Fibre Reinforced Polymer
CHS	Circular Hollow Section
CDP	Concrete Damage Plasticity
CFAT	Concrete-Filled Aluminium Tube
CFST	Concrete-Filled Steel Tube
DI	Ductility Index
C3D8R	Eight-node linear brick element with reduced integration
FRP	Fibre-Reinforced Polymers
FE	Finite Element
FEA	Finite Element Analysis
FEM	Finite Element Method
S4R	Four-node doubly curved thin or thick shell with reduced integration
HAZ	Heat affected zone
kN	Kilonewton
LECA	Lightweight Expansion Clay Aggregate
MPa	Megapascal
mm	Millimetre
RHS	Rectangular Hollow Section
REHS	Round-Ended Hollow Section

Chapter One: Introduction

1.1 General

Columns are structural components which support loads during the compression condition. They typically support bending moments and compression forces on either or both axes of the cross-sections. Columns have a height-to-least lateral dimension ratio of 3 or greater [1].

In a composite column, the action occurs when two different materials are combined very tightly structurally so that they can work together like a single unit. Because of the combined action, the composite part is harder and stronger than the total individuals [2].

Recently, various composite material systems have been increasingly employed in the manufacturing of concrete columns to improve performance regarding strength, stiffness, and ductility, with many of these composite columns becoming totally encased in steel concrete. Much experimental and analytical investigation has been performed to understand the performance of composite columns since 1960. The negative aspect of this combination is its tendency to corrode over time in construction or buildings. It is currently essential to find a remedy for this conception, which means replacements for steel, such as stainless steel, that are costly and difficult to satisfy column demands. Therefore, alloys made of aluminium, which have developed greatly in applications in industry, can be mixed with particular components to produce an extremely strong alloy [3].

The preliminary usage of aluminium alloys in construction occurred in the 1950s, then expanded to multiple uses in structures. The growing popularity of aluminium alloys as building materials is related to their greater strength, low density, great resistance to corrosion, simple fabrication, little maintenance needs, high recycling ability, and attractive aesthetics. The steel weight is heavier than aluminium alloy by approximately three times that of aluminium alloy for the same volume. Aluminium alloys, because of their excellent corrosion resistance, often need no treatment, paint, or coating to avoid rust and corrosion, therefore decreasing repair costs. The recycling process of aluminium alloys requires only 5% energy of the production of the original metal, resulting in environmental and economic benefits. Moreover, recycled aluminium retains all the properties of virgin metal. Furthermore, the aesthetic appearance of aluminium alloys makes them suitable for architectural and structural applications. Despite these profound advantages, the low modulus of elasticity, welding complexity and low melting point of aluminium alloys affect the performance of aluminium alloy structures. The structural performance of aluminium alloy hollow members can be improved by filling concrete in the hollow space [4].

The stiffness of alumina alloy structural members is relatively lower than that of the carbon steel structural members due to low Young's modulus of aluminium alloy material. Also, due to higher ultimate strength and higher yield stress for carbon steel when compared with aluminium metal, the capacity for bearing load of aluminium columns is generally lower. Infilling aluminium tube

columns using a concrete core is a common technique for making them stiffer and increasing their capacity for bearing load. The columns composed of concrete and aluminium tubes can make excellent use of the high stiffness and strength supplied by both of these components. Zhou and Young [5] presented these results for concrete-filled aluminium rectangular and square hollow section short columns. Zhou and Young [6] examined the short columns for the circular hollow sections of concrete-filled aluminium.

1.2 Aluminium

The chemical symbol (Al) refers to the metallic element called aluminium. Following the oxygen and silica compounds in the crust of the Earth, aluminium is the third most common substance. It contributes eighty per cent of the total mass of the crust and is the most prevalent metal [7].

Pure aluminium is inappropriate for building purposes due to its weak mechanical properties. To make aluminium efficient as a structural metal, and because of the weakness of the pure aluminium metal, the production of proper alloys was required. Several alloys have been developed, exhibiting a various enhanced mechanical and physical characteristics. The optimal alloy is influenced by the exact purpose. The current 6xxx series alloys, which are most made from Mg and Si, exhibit the most common use of alloys that are suited to thermal strengthening. As a result of its strength, confluence, corrosion resistance, and weldability, the 6xxx series alloy of aluminium was suitable for building applications [7].

Aluminium, relatively, is a very recent material. It is also considered a very recent activity as aluminium alloys started to be used in structural engineering due to the nascent nature of this family of materials and its brief historical timeline. In fact, it wasn't until the end of the nineteenth century that aluminium and its alloys became available [8].

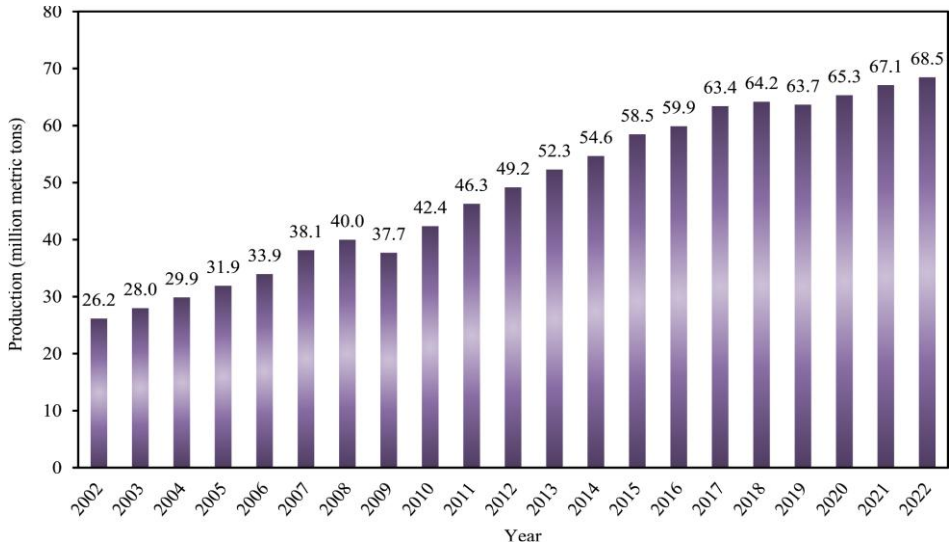

Figure 1.1 Aluminium Alloys Produced Globally From 2002 to 2022 [9].

During the last years (from 2002 to 2022), the production of aluminium alloy has been increasing in fixed steps, as illustrated in Figure 1.1. In 2022, around 68.5 million metric tonnes of aluminium alloys were produced globally, which is greater than the production in 2002 by 2.6 times. China is considered the largest aluminium alloy manufacturing country, where, in 2022, it produced approximately 60% of global production in that year [9].

1.2.1 Advantages and Disadvantages

The advantages of aluminium alloys [10] are:

1. Low density, about a third of that of steel.
2. Durability and high-strength characteristics, also at very low temperatures.
3. Elements formed by them are simply extrudable, enabling the construction of any cross-section.
4. Good workability.
5. High corrosion resistance due to a tough oxide layer
6. Aluminium alloys can be totally recycled without any change or effect on their physical or chemical characteristics.

The alloys of aluminium present several imperfections:

1. The main issue is the elevated cost of alloys made of aluminium in comparison to steel. The cost gap across alloys of aluminium and steel is gradually reducing. In addition, the absence of the requirement for regular painting of aluminium components results in decreased maintenance expenses[11].
2. The additional problem is that aluminium elements have weak resistance to fire. But it could be enhanced with the utilisation of passive fire resistance with thermally insulated materials as described in [11].
3. The following issue is that the alloys made of aluminium have a weaker elastic modulus compared to steel, nearly three times [11].
4. Connections with different metals may cause aluminium corrosion badly if appropriate procedures are not applied. This could be occurring even when dealing with very durable alloys [7].
5. Corrosion of aluminium in concrete stems from the material's amphoteric nature, where the highly alkaline pore solution (pH 12.5–13.5) from cement hydration dissolves the protective oxide layer [12]. A barrier coating, such as bitumen, epoxy, or enamel paint, isolates aluminium from the alkaline electrolyte, preventing ion transport and gas evolution.

1.2.2 The Main Characteristics of Aluminium Alloys Different from Those of Steel [13]

1. A large range of strength can be offered with aluminium alloys when compared with steel. Therefore, it appears that aluminium alloys are more appropriate in metal construction for the concept of a fourth dimension than steel. Aluminium is very ductile (ε_t 40 %), but on the other hand, for structural application, it has a very low strength (where $f_{0.2}$=20 MPa). A cold-working procedure could be applied to increase strength; however, the strength increase by this process is not great ($f_{0.2}$=100 MPa), while a great decrease in ductility will happen (up to one-tenth of the initial value). A further approach for improving the material's strength is to combine aluminium with other elements (AlMn, AlMg alloys). According to this method, strength might exceed 100 MPa, having a ductility of (ε_t 10 %). High strength may be attained with the utilisation of heat treatment. The strength of yield approaches $f_{0.2}$ = 250 MPa for AlSiMg alloys and may achieve a range of yield strength ($f_{0.2}$ = 350-400 MPa) for alloys made up of AlZn and AlCu. The behaver of AlMgSi alloy and Fe360 steel is shown in the stress-strain graph in Figure 1.2. The alloys of aluminium exhibit a strain-hardening area without a horizontal line indicating yield. The steel obviously has more elongation than aluminium alloy, and for aluminium alloy, the ($ft/f0.2$) ratio is smaller compared to steel (1.2 instead of 1.5). The two substances show linear elastic performance up until the elastic limit, which essentially limits the range of operation of the construction. They are different, alternatively, in their inelastic behaviour.

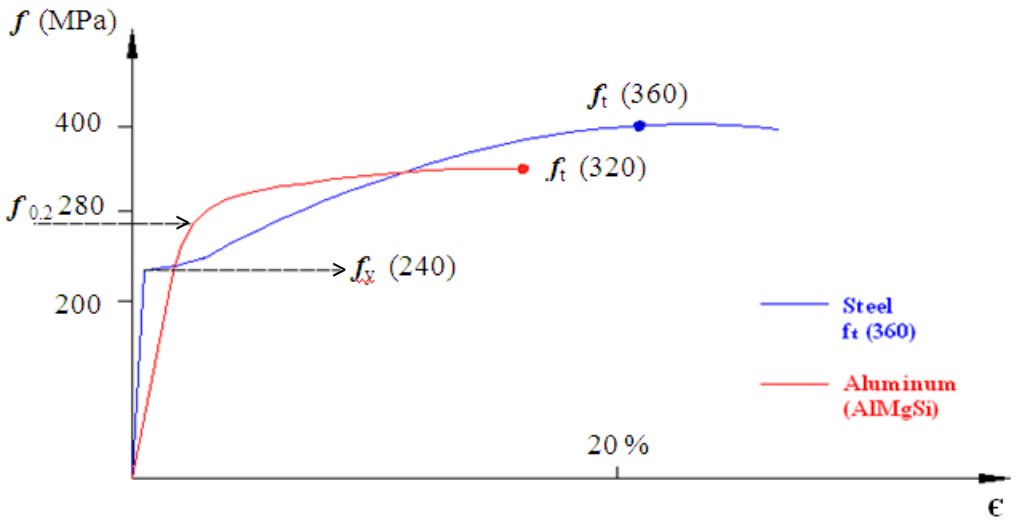

Figure 1.2 Comparation Between AlMgSi Aluminium Alloy and Fe360 Steel Behaviour in Stress-Strain Graph [13].

2. Aluminium is more lightweight than steel, having a specific weight of 2700 kg/m³, meaning it's a third of that of steel.
3. Aluminium alloys have three times less Young's modulus compared to steel; therefore, deformation and instability problems appear more frequently. In aluminium alloy structures, buckling is more probable to happen than in steel structures, due to aluminium alloys under compression, having low Young's modulus value.
4. Aluminium has a thermal expansion coefficient two times greater than that of steel. This means that the structure is more sensitive to thermal variations and thus has higher deformation when it is not constrained. When a structure is constrained against thermal deformation, residual stress will be about 30 per cent lower than that in steel structures since they are proportional to the product (αE). Unlike steel, aluminium doesn't tend to fragile fracture in low temperatures; thus, aluminium is very suitable for cryogenic applications. As the temperature goes down, the mechanical properties of the aluminium steadily improve.
5. By using gas-shielded processes, arc welding can be done on most of the aluminium alloys as readily as steel. The speed of the weld is faster. On the other side, alloys separate from the heat-affected zone (HAZ), softening at welds, where the welded joints in some alloys tend to experience a serious local drop in strength. Adhesive bonding is used as a valid technique to create a structural joint in aluminium.
6. Aluminium sections are produced by the extrusion process as a standard way; it is much more flexible compared to the rolling procedures in steel.
7. Components from aluminium tend to fail by fatigue compared to the components from steel.
8. Aluminium is naturally rust-resistant and frequently does not require painting; nonetheless, its strongest alloys may experience corrosion under extreme conditions. In such cases, taking preventative measures is essential.

1.2.3 Aluminium Application

The following part defines the different uses of alloys of aluminium in building elements for the construction industry [11]:

1. Aluminium alloy lightweight decks for bridges are employed for the substitution or rebuilding of damaged bridge decks.
2. storage facilities, interim structures, and elevations
3. anchoring cross-laminated timber shear walls
4. roofing panels, building roofing, and the exterior siding of platform bunker roofs
5. bridges
6. Strengthening of reinforced concrete beams.
7. Silos, domes, and tanks in wastewater treatment systems.
8. towers.

9. Offshore buildings and helidecks

The extrude property for alloys from aluminium makes them a multipurpose material in structural applications, and they have the capability to produce complex and different cross-sectional shapes; therefore, for constructions that could not be developed with steel and concrete, aluminium alloys were an appropriate material to utilise [14], as shown in Figure 1.3.

(a) Aluminium alloy support system (2004)

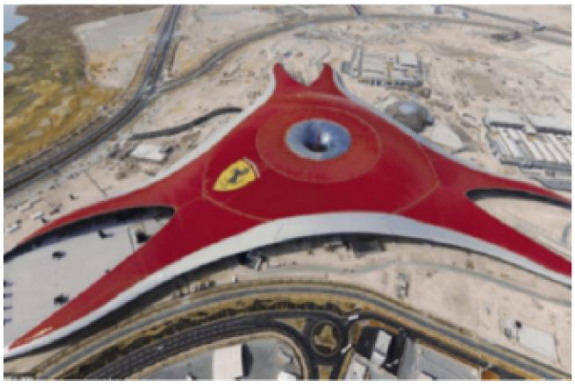

(b) Corrugated aluminium alloy roof (2010)

(c) Aluminium alloy curtain wall (2012)

(d) Aluminium tube truss pedestrian bridge (2021)

Figure 1.3 Typical Aluminium Alloy Structures [14].

1.3 Column

According to ACI Code 318 [15], a column is any member with a ratio of length-to-least lateral dimension equal to or exceeding three and used primarily to support compressive loads. Columns support total vertical loads from the beams, slabs and floor and convey loads to the footings. The axial compressive loads are supported by columns with or without bending. Despite the tensile stresses that may be produced, columns are commonly known as (compression members) because the compression forces or stress control their behaviour.

Figure 1.4 Classification of Columns [1].

Depending upon several conditions, there are different column types used in structures, based on shape, type of reinforcement and type of loading. Short and slender columns could be one or more of the above types [1].

1.3.1 Section Shape of Column

In most buildings, square or rectangular columns are used in the construction of buildings. Because of the flexibility of shuttering and reinforcement placement, these types of columns are both cost-effective and easy to construct.

For aesthetic reasons, circular cross-section tubes are commonly employed in piling and building elevations. According to their elevated deflection resistance, circular columns are also used as bridge pillars.

It is common for two walls to be crossed, forming T shapes, L shapes, or cross shapes at any point or at the building's corners. Specially shaped columns in a room eliminate noticeable corners, allowing for more usable floor space [16]. Ductility, deformation capacity, in addition to dissipating energy capacity of the specially shaped column with appropriate design, are good.

Structural safety and an affordable construction cost are the realistic goals of structural design. To accomplish this, a specially shaped column optimisation design should be carried out based on the overall structural design [17]. Figure 1.5 shows the specially shaped columns.

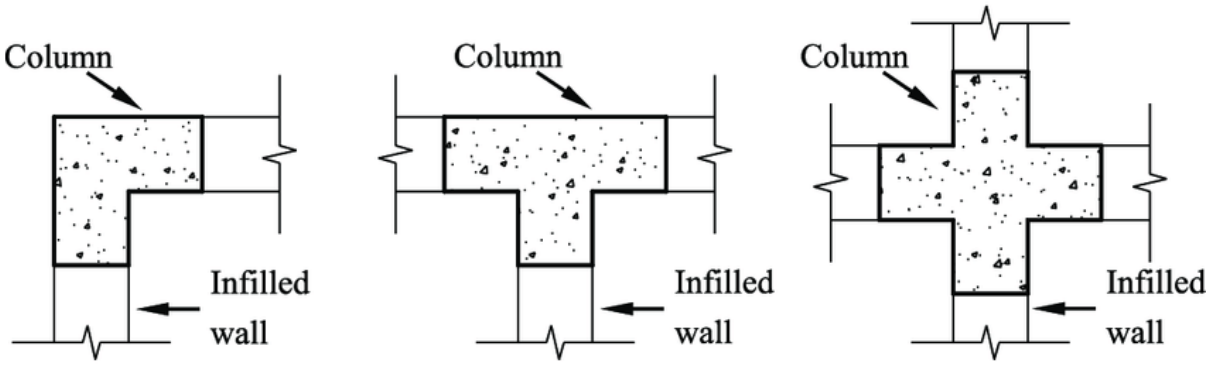

Figure 1.5 L- Shaped, T- Shaped, and Cross-Shaped Columns [18].

In addition to the previous shapes of columns, there are also elliptical, hexagonal, octagonal and Y-shaped columns.

1.3.2 Failure Mode of Columns

Columns may fail in one of the following mechanisms [19], as shown in Figure 1.6:

1. Crushing: This is the most common failure mode for columns. It occurs when the column is loaded with a compressive force that exceeds its load-carrying capacity, causing it to buckle or crush.
2. Buckling: Buckling happens when an axial compressive load is subjected to a column, causing it to bend or deform laterally. This can lead to sudden and catastrophic failure.
3. Combination of buckling and crushing: Columns can also fail due to a combination of different loading conditions, such as axial compression, bending, and shear acting simultaneously, leading to complex failure modes.
4. Shear Failure: Shear failure can occur in short columns when they are subjected to lateral forces that exceed their shear capacity, causing them to fail along a diagonal plane.

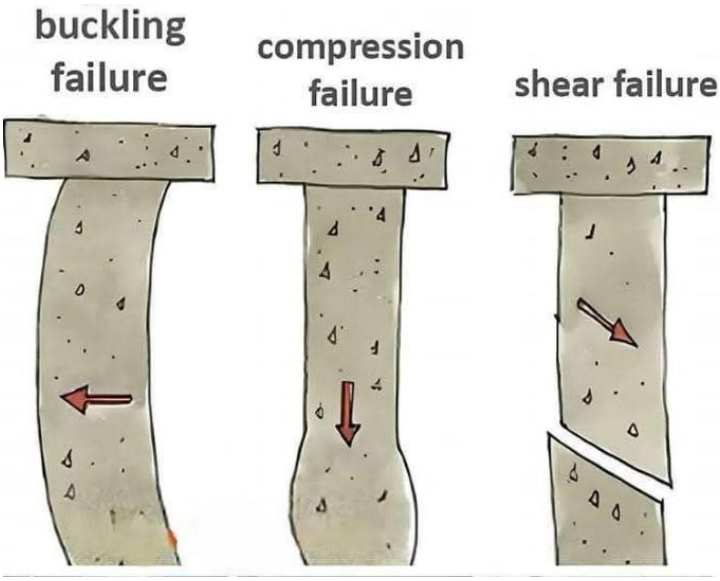

Figure 1.6 Mode Failure of Columns [19].

1.4 Aluminium-Concrete Composite Structures

In the past, steel or fibre-reinforced polymer tubes have been employed on the composite columns as a confinement material. But there are a number of challenges that make it hard to use these materials. This includes the fact that steel can rust in harsh settings, including subsea piling, as well as the high price for producing fibre-reinforced polymers (FRP). Although plastics have been used in construction and aesthetics for a wide range of applications [20].

The aluminium tubes could be filled with concrete to produce aluminium-concrete composite columns. The filling of concrete inside aluminium tubes has two main advantages: it increases the load capacity plus the columns' ability to resist fire. Using composite column technology can make structures and economies far more efficient. By making the columns smaller, developers can acquire more useful area, which is an important benefit in places where space is restricted, like parking facilities and office complexes [11].

These are two additional benefits of employing aluminium tubes externally of the concrete core, i.e., aluminium tubes become permanent moulds that improve the impact of confining. Furthermore, composite columns consisting of concrete and aluminium could display greater ductility when compared to an aluminium tube column, according to the higher quantity of material, in addition to the effect of confinement [11]. For composite columns, a major portion of the transfer of stress happens at the concrete-aluminium contact. There, the aluminium and concrete are essentially working together to give the column its great strength and ductility [21].

Aluminium tubes can possess circular, square, or rectangular hollow section shapes, as displayed in the Figure 1.7.

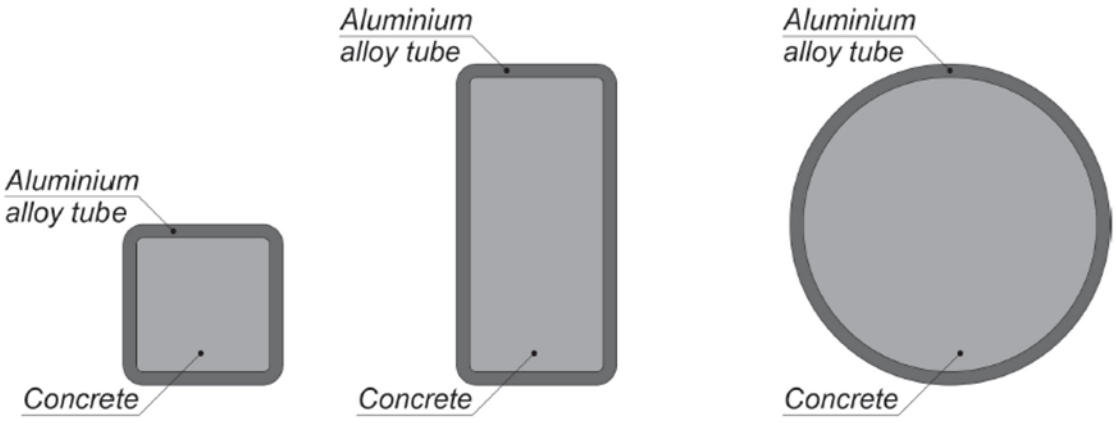

Figure 1.7 Square, Rectangular and Circular Column [11]

Circular cross-sections provide superior confinement compared to rectilinear designs, which demonstrate reduced effectiveness. Square or rectangular aluminium tubes are more likely to break because stress can build up in the corners. Circular tubes, on the other hand, are more stable [11].

The effect of confinement depends on [11]:

- generalised outer diameter-to-thickness ratio (as the ratio increases, the confining effect is less effective).
- Concrete strength (as concrete strength increases, the confining effect becomes less effective).
- the cross-section type (the confining effect is stronger in a circular cross-section than in a rectangular cross-section).

Generally, many design and construction advantages can be obtained from filling tubes with concrete, such as [22]:

1. Composite columns offer a higher load-bearing capacity than standard reinforced concrete columns of identical size. Consequently, this allows for a more efficient use of floor space within buildings.
2. The tube serves as a permanent mould for the concrete, which improves the construction process. This leads to significant reductions in project time and cost.
3. The external tube protects the concrete core from damage from machines and the environment, such as carbonation and chloride penetration.
4. A well-distributed reinforcement is provided by the tube. Where the reinforcement resists secondary bending moments due to its most efficient position.
5. The concrete prevents the tube from local buckling.
6. The confinement provided by the tube induces a significant increase in concrete strength and ductility.

1.5 Nonlinearity

In many nonlinear issues, multiple causes of nonlinearity are present in the mechanics of structure simulations: material, boundary, and geometric nonlinearity. As explained below [23]:

1. The material nonlinearity can be apparent in rubber materials and many metals. As an instance, at small strain values, the stress/strain relation for steel is relatively linear. Yet, because of yielding material, the relation turns extremely nonlinear at greater strains; in this stage, the response turns permanent.

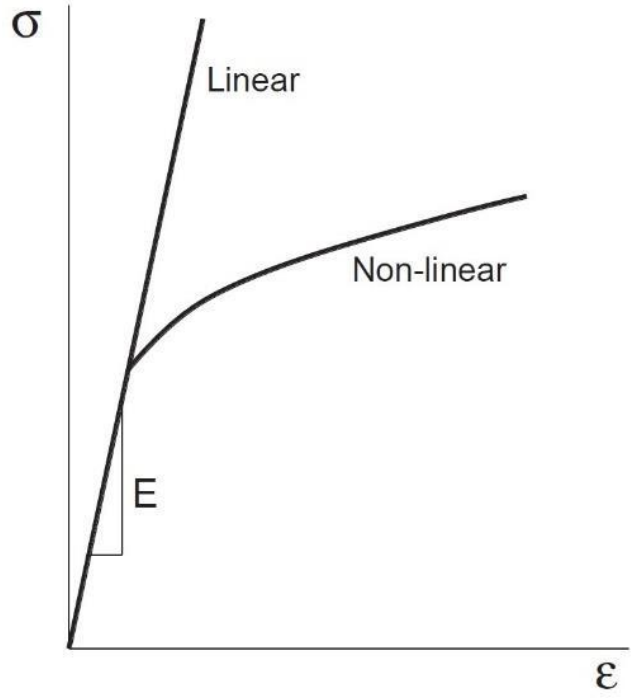

Figure 1.8 Material nonlinearity [1].

2. Boundary nonlinearity happens if the boundary conditions differ throughout the procedure. Analyse the cantilever beam illustrated in Figure 1.9 as a case. The beam-end vertical motion displays a linear relationship with the applied load prior to the beam end making contact with the stopping point.

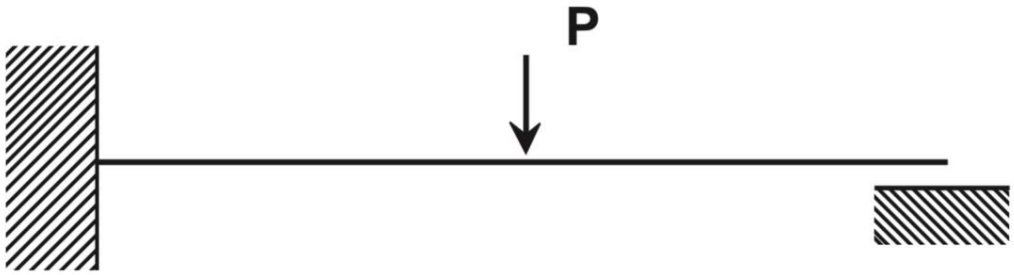

Figure 1.9 Cantilever Beam Hitting a Stop [23].

3. Geometric nonlinearity is the final reason for nonlinearity, which refers to variations in the geometry of the numerical model which produce significant variations in its stiffness throughout the investigation. That can happen from significant deflections or rotations, snap-through phenomena, and early stresses or load stiffening.

ABAQUS has two strategies of solution to treat the nonlinearity problems; the first one is (Standard Analysis), and the other is (Explicit Solution).

1.6 Aims of Research

The primary objective of this research will be to discuss the following parameters' effect on the ultimate load, stress-displacement curve, ductility index, and mode of failure:

1. Study numerically the structural behaviour of concrete core-filled aluminium tube columns having various cross-sections.
2. Study the effect of different aluminium proof stresses on circular and rectangular concrete-filled aluminium columns.
3. Study the effect of different concrete compressive stresses on circular and rectangular concrete-filled aluminium columns.
4. Study the effect of different aluminium tube thicknesses on circular and rectangular concrete-filled aluminium columns.

1.7 Thesis Layouts

The present thesis content is divided into five chapters, as follows:

1. **Chapter one (Introduction):** This chapter presents an overview of aluminium, columns, aluminium-concrete composite structures and nonlinearity.

2. **Chapter Two (Literature Review):** presented a literature review concerning the theoretical studies of confined columns.
3. **Chapter three (Finite Element Modelling):** Presents the main focus of this research, which was finite element modelling, and the setting up of the model's geometry, material properties, boundary conditions and meshing according to the finite element theory.
4. **Chapter four (Numerical Analysis and Results):** This chapter illustrates the finite element analyses and their discussions. In addition, a parametric study is carried out to investigate the impact of various parameters on the structural performance of short columns.
5. **Chapter five (Conclusions and Recommendations):** Includes the conclusions and recommendations.

Chapter Two: Literature Review

2.1 Introduction

Columns are actually the most essential part of structures. Due to the duty of transporting loads into the foundations. Therefore, any weakness in a column located at a critical location leads to failure at that point and all related structural components and may cause a complete collapse of the structure.

This chapter presents a historical background concerning the studies dealing with the composite columns, relatively related to the considered investigation, with a special importance on the concrete-filled aluminium tube columns. Composite columns have been commonly deployed in the construction industry for a long time. The rapid global development of composite columns is mostly due to the notable advantages they provide compared to conventional construction techniques.

In recent decades, there has been a growing trend in utilising various materials, such as concrete, steel tubes, aluminium and FRP, for confining columns, either external or internal. Extensive research has been conducted, spanning from as early as 1928, when Richart et al. [24] initiated experimental and theoretical studies, to recent years. These studies have explored a range of parameters and confining methods and have generally reported positive effects on the mechanical properties of columns.

2.2 Research on Aluminium Members.

Zhu and Young in 2006 [25], concerned experimental study on circular hollow section aluminium tubes with and without transverse welding at column ends, as shown in Figure 2.1. This paper studies 29 specimens divided into four test groups of various aluminium alloys and cross-section shapes tested against pure axial load; in addition, both ends are fixed. The 6061-T6 and 6063-T5 alloys of aluminium were extruded to fabricate the circular hollow section tube. The column height demand is between 300mm and 3000mm. Material yielding in the heat-affected region, yielding, and global buckling are the failure mechanisms for the column tests.

The study represents a comparison between the column strength provided by the experimental program and the designed value by the American, Australian/New Zealand, and European specifications for aluminium structures. The design specification strengths are conservative for non-welded columns, but for welded columns are even more conservative in contrast to non-welded tubes. The design strengths expected by the European Code are a little conservative compared to those expected by the American and Australian/New Zealand standards for aluminium

circular hollow section columns having transverse welds. The results indicated that the ultimate strength of welded tubes attained 54–76% of the ultimate strength of non-welded tubes.

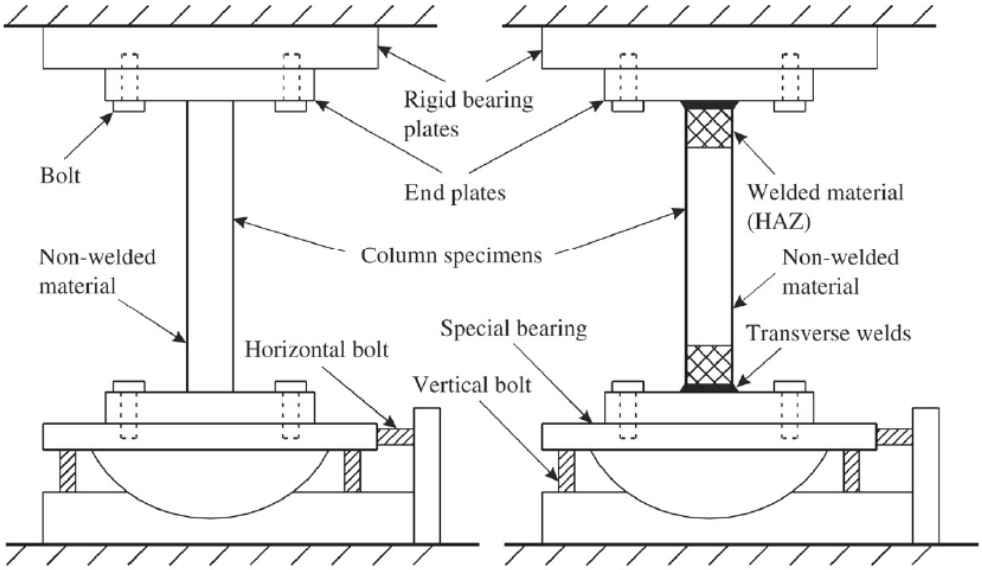

Figure 2.1 Illustration Drawings of The Column Test Setting [25].

Zhou and Young in 2008 [5], presented experimentally the performance of aluminium tube columns filled with concrete. This investigation studies 43 samples to understand the impact of various parameters, which are the cross-section shape of columns, concrete compressive strength, and aluminium thickness, on the structural performance of rectangular and square concrete columns confined with aluminium tubes, as displayed in Figure 2.2. The alloy of aluminium 6061-T6 heat-treated was extruded to fabricate the tubes filled with concrete cores having different compressive strengths (40, 70, and 100 MPa) and tested under axial compression. The column sections have a ratio of depth to wall thickness scope between 8.2 and 63.8. To avoid global buckling of columns, the column height was selected so that the column height to depth ratio stays at a constant value of 3. The test ultimate load of columns was compared to the design ultimate strength determined by Australian/New Zealand standards and American specifications of concrete and aluminium structures. The comparison shows that the results of the experimental study disagree with the results of the design standard. This disagreement is due to the column's failure due to the splitting of the aluminium tube close to the corner of the column. As a result, the tubes of aluminium are not completely utilised. The stiffness of the composite column was higher than that of hollow sections. On the other hand, the ductility of composite columns was slightly improved than hollow sections.

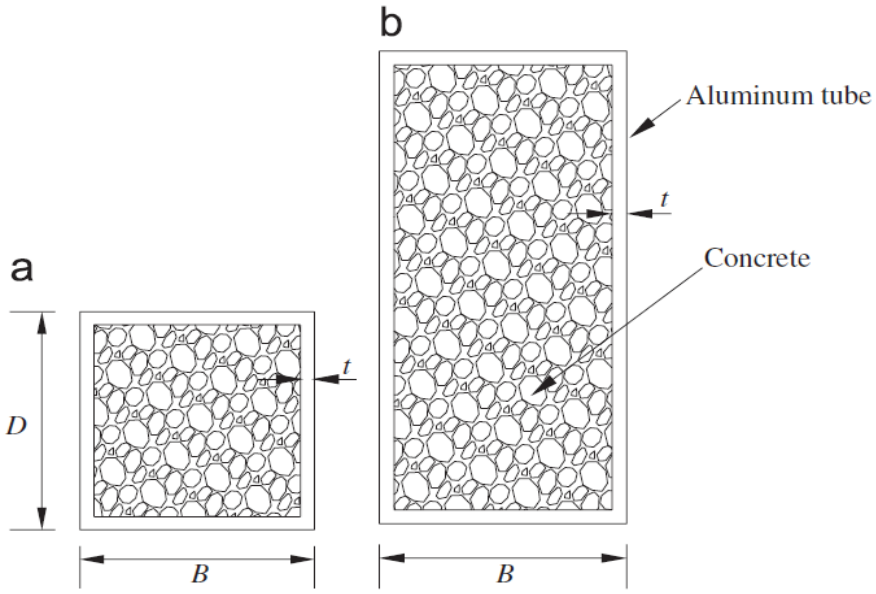

Figure 2.2 Details of Rectangular and Square Sections of Composite Columns [5].

Zhou and Young in 2009 [6], presented an experimental study of circular-section tube filling with a concrete core (CHS) and tested it under axial compression load. The study includes 42 specimens investigating the structural behaviour of concrete filling an aluminium tube short column with different geometric dimensions. The 6061-T6 alloy of aluminium was extruded to fabricate the circular hollow section tube and filling concrete having different compressive strengths (40, 70, 100 MPa). The ratio of diameter to aluminium thickness was demanded between 9.7 and 59. 7. To avoid the global buckling of columns, the column height was selected so that the column height to depth ratio stays at a constant value of 3. The study focused on ultimate load strength, load axial displacement relation, load axial strain, and mode of failure of columns. Crushing of concrete was obviously shown in the column having concrete compressive strength equal to 70 MPa, as shown in Figure 2.3. The test ultimate load of columns was compared to the design ultimate strength determined by Australian/New Zealand standards and American specifications of concrete and aluminium structures. The results shown that the American and Australian/New Zealand specifications are generally conservative and reliable for concrete-filled aluminium stub columns. From Figure 2.4, it was observed that samples filled with concrete have enhanced stiffness compared with hollow aluminium tubes, and increasing the concrete compressive strength led to a decrease in the ductility.

Figure 2.3 Failure Mode of Column Specimen [6].

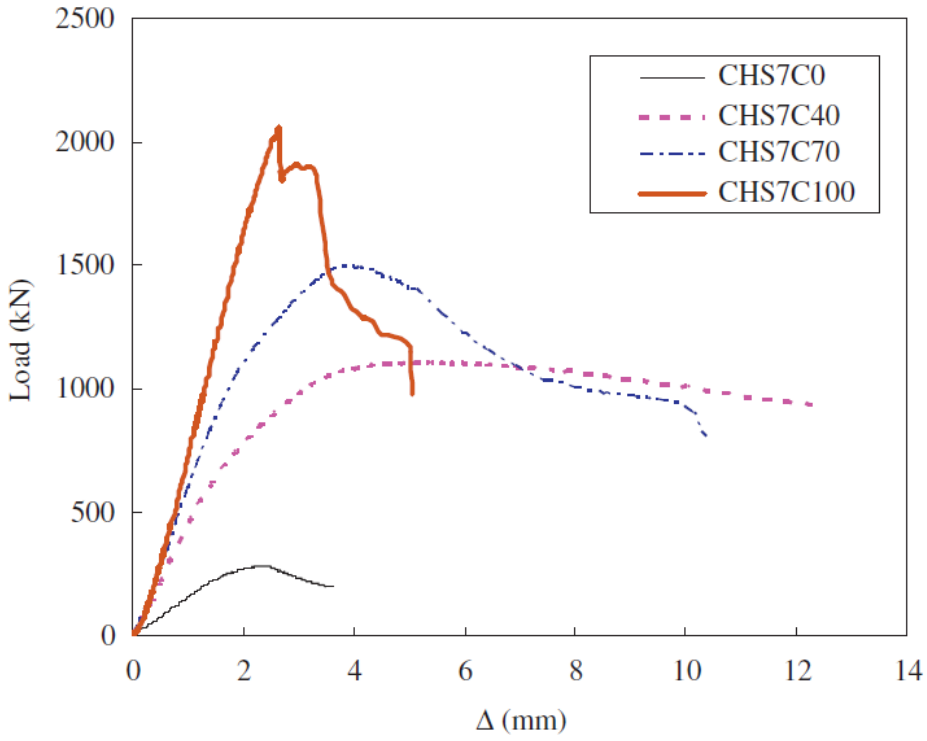

Figure 2.4 Load Axial Displacement Relation Curves [6].

Zhou and Young in 2012 [26], introduce numerical study on circular-section tubes filled with a concrete core (CHS). The model developed by the nonlinear finite element model was verified with experimental data. The parametric investigation discussed the impact of cross-section shape,

aluminium proof stress, and concrete compressive strength on the strength of composite columns. The study includes two aluminium alloys, which are T5 normal strength and T6 high strength, to model the tubes. The finite element model uses a concrete core with various compressive strengths (40, 70, 100 MPa). The ratio of diameter to aluminium thickness was scoped between 10 and 160. The comparison between the numerical strength and the experimental has its maximum value of 10%. The test ultimate load of columns was compared to the design ultimate strength determined by Australian/New Zealand standards and American specifications of concrete and aluminium structures. The results shown that the American and Australian/New Zealand specifications are generally conservative and reliable for concrete-filled aluminium stub columns.

Nasser in 2012 [27], presented both experimental and theoretical investigations about the response of aluminium concrete composite columns with circular sections against axial loading. The parameters that were studied in this paper are diameter, diameter-to-thickness ratio and slenderness ratio on the load strength of 24 specimen columns. This research is using 24 specimens having a different ratio of diameter to wall thickness ranging from 11.9 to 22.8; also, the ratio of column height to diameter ranges from 3 to 10. The 6061-T6 alloy of aluminium was extruded to fabricate the circular hollow section tube and filling concrete having compressive strength (24.1 MPa). The study aims to investigate the strength, load axial displacement relation curves and mode of failure. The expected strength of composite columns was the primary goal of the theoretical study.

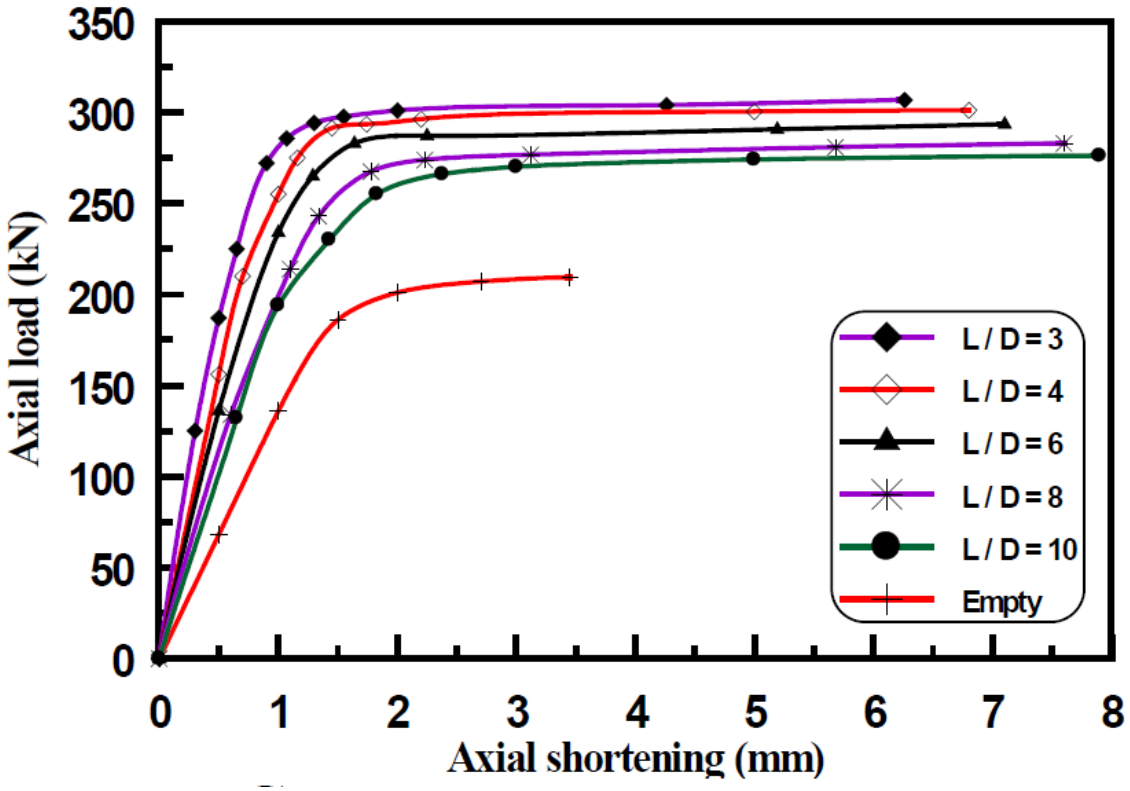

Figure 2.5 Load Versus Axial Displacement Relation of Specimens [27].

The average value of the experimental-to-expected value ratio of the ultimate load is 1.0104, which leads to considering empirical equations very efficient for the expected ultimate strength capacity of aluminium concrete composite columns. The stiffness of composite columns indicates a higher value for composite columns when compared with hollow aluminium tubes, as illustrated in load versus axial displacement relation curves in Figure 2.5. Columns with a slenderness ratio equal to 3 indicate that the composite column's strength to aluminium tube strength ratio is greater than one, defined from 1.405 to 1.751. On the other hand, the composite column's corresponding strain to the aluminium tube's corresponding strain ratio is greater than one demined from 1.814 to 1.997.

Nasser in 2014 [28], introduced experimental and computational research on the concrete core filling aluminium tubes having circular sections and tested under rising axial load compression. The study was introduced to understand the impact of various parameters, which are diameter, diameter-to-thickness ratio, and slenderness ratio, on the load strength of 24 specimen columns. This research is using specimens having a different ratio of diameter to wall thickness ranging from 23.3 to 47.8; also, the ratio of column height to diameter ranges from 3 to 10. The 6061-T6 alloy of aluminium was extruded to fabricate the circular hollow section tube and filled with concrete having different compressive strength (24-40 MPa). The possibility of employing a fuzzy inference system to predict the ultimate strength of composite columns was the primary goal of the computational investigation. With an average value of the ultimate load of the experimental to predicted ratio of 1.001, which leads to considering the fuzzy inference system model very efficient for predicting the ultimate strength of an aluminium tube confining a concrete core. As a result of L/d= 3, the ultimate strength capacity of the composite column to the ultimate strength of hollow sections ranged from 1.596 to 2.544. This enhancement because of the confinement effect. Encasing the concrete with aluminium tubes leads to an increase in the ductility, particularly in slender columns. Shear mode of failure was observed in columns having a length-to-diameter ratio range from 3 to 4. The global buckling failure mode was observed in the slenderest columns having a length-to-diameter ratio ranging from 6 to 10, as shown in Figure 2.6.

Figure 2.6 Failure Modes of Specimens [28].

Resan in 2014 [29], presented an experimental and theoretical analysis of lightweight concrete filling in aluminium tube columns. The study includes two different styles of loading as displayed in Figure 2.7; one style uses the aluminium wall just for confining the concrete, and the other style uses the aluminium wall to confine the concrete in addition to being axially loaded. The study is divided into four series depending on the loading style and the type of lightweight concrete. Columns with composite action indicate that the composite column's strength-to-aluminium tube strength ratio is greater than one defined from 1.5 to 2.14. while columns with confinement action decreased from 1.3 to 1.86. This indicates the aluminium wall offers effective lateral support and enhances the ultimate strength of composite columns.

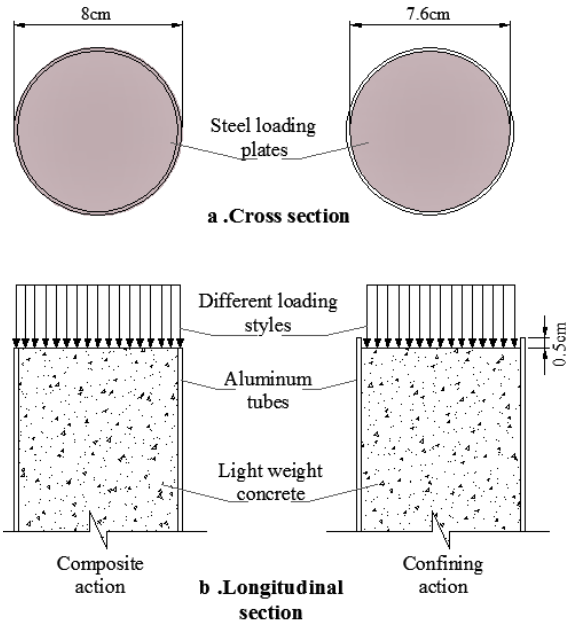

Figure 2.7 The Configuration of The Tested Columns [29].

Resan in 2014 [30], presented an experimental analysis of the lightweight concrete filling aluminium tubes enhanced with a fibre-reinforced polymer (FRP) sheet with circular sections as displayed in Figure 2.8. Lightweight expanded clay aggregate (LECA) is utilised to generate the lightweight concrete. The effect of external and internal confinement efficiency by CFRP and lightweight concrete on the composite columns. As a result, the constriction and composite interaction between both materials led to the energy dissipation capacity, and ductility of composite columns. Analysis indicates the composite column's strength-to-aluminium tube strength ratio is greater than one by 1.83. while the composite columns strength to concrete strength ratio is 2.54. The ductility of the columns increased significantly due to the confinement action, the ductility ratios ($\varepsilon/\varepsilon AC$) vary between (1.67 and 2.12) as the fibers orientation change from inclined to transverse mode. Although the strength increases with CFRP layers numbers, the ductility ratios dropped as CFRP jacket layers double in specimens, the same ratios became (1.54 and 2.02).

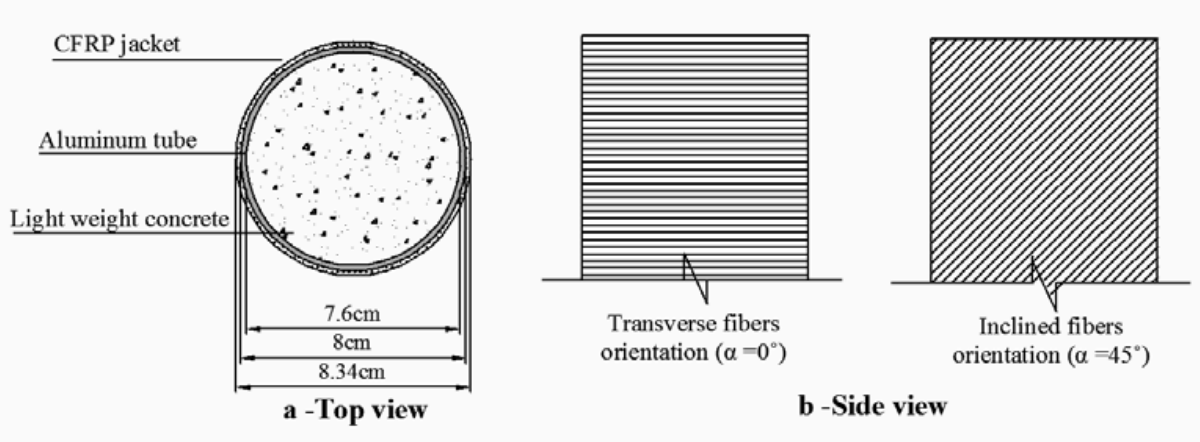

Figure 2.8 Column Specimens' Details and Fibre Orientation Configuration [30].

Nayak et al, in 2014 [31], proposed an experimental study on self-compacting concrete filling in aluminium tube columns. This paper includes a study of the column height-to-depth ratio and the depth-to-aluminium-thickness ratio on the composite columns. The 6063-T6 alloy of aluminium was extruded to fabricate the 24 circular hollow section tubes and fill them with concrete having different compressive strengths (214 MPa). The study includes 4 series, each one of which has different aluminium tube diameters. The slenderness ratio of columns ranges from 3 to 10, displays all failure modes, and the ratio of depth to thickness demanded is between 12 and 33.3. As a result, the aluminium wall provides great confinement to the concrete core, which causes enhancement of ultimate strength capacity. The analysis indicates that the composite column strength to aluminium tube strength ratio is greater than one, ranging from 1.47 to 2.9. Composite columns with slenderness of 3, 4, and 6 display a shear mode of failure, while composite columns with slenderness of 8 and 10 display buckling.

Alshimmeri in 2016 [32], investigated the structural behaviour of aluminium concrete composite columns, which were experimentally investigated in order to enhance the durability, strength capacity, and ductility. The study includes 7 composite columns. To study the influence of aluminium wall thickness using specimens with a uniform diameter of 100mm, constant column height of 450mm, and different aluminium wall thicknesses (0, 2, 3, 4, 5mm), the influence of column height using specimens with aluminium thickness was 5mm and height was 700mm; the durability of composite columns using specimens with aluminium thickness was 5mm and height was 450mm. As a result, the aluminium wall thickness increase influenced the improved compression load capacity in comparison with the reference column; using 2mm thickness led to an increase of 16%, and using 5mm thickness led to an increase of 224%. The (700 mm) column height and (5 mm) wall thickness reduced by 0.06% compared to the (450 mm) column height and the same wall thickness. The mode of failure in the short columns was local buckling, and in the long column it was global buckling. As shown in Figure 2.9, there is no clear difference between the column exposed to air and the column submerged in an aggressive solution.

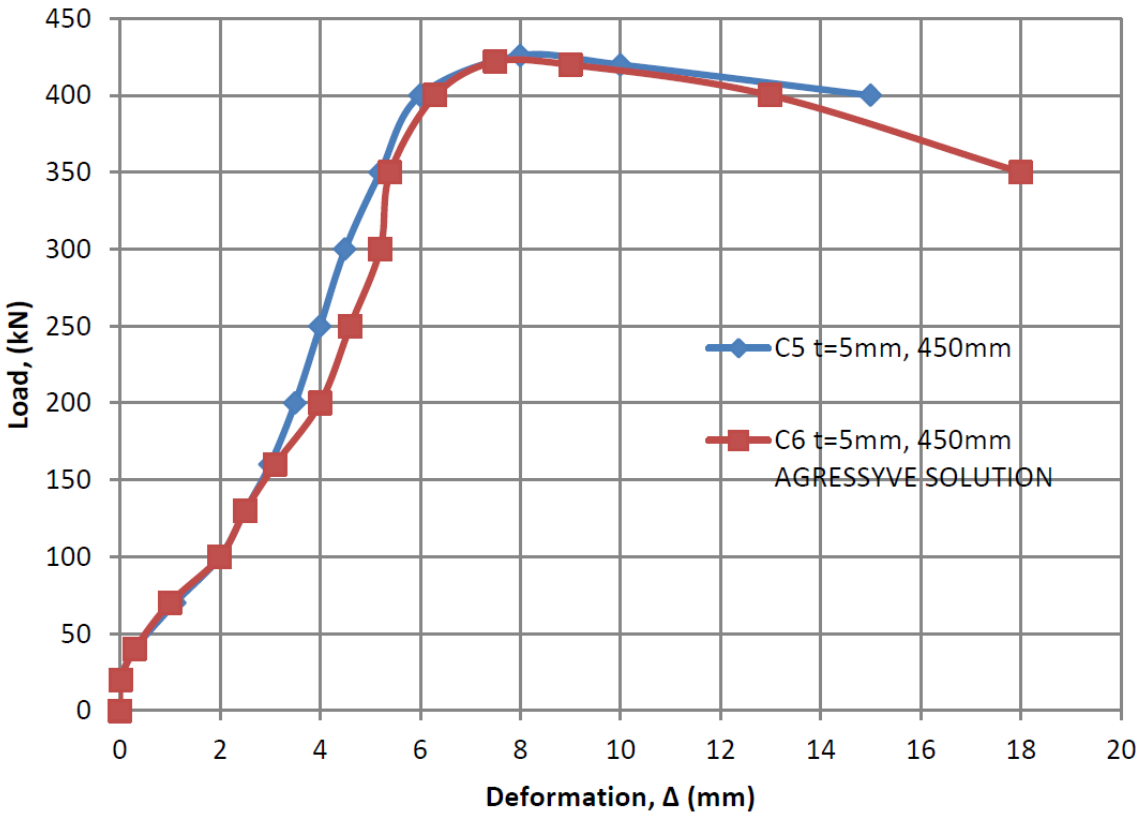

Figure 2.9 The Ultimate Load-Axial Deformation Curves for The Durability Study [32].

Al-Mazini and Chkhewier in 2017 [33], presented an experimental and numerical study on rectangular and square-section concrete aluminium composite columns. The investigation includes three parameters to examine 24 specimens: compressive strength of concrete (25, 40, and 60 MPa), slenderness ratio of columns ranging from 3 to 10, and the ratio of depth to thickness ranging from 25 to 62.5. Test results display that concrete compressive strength clearly effects on the strength of composite columns. The increasing of the ratio of height to depth led to a reduction in ultimate load capacity, and it is more clear in square-section columns compared with rectangular sections in the ratio of slenderness until L/d =7, and more than this ratio, there is no clear impact on ultimate capacity, as clearly displayed in Figure 2.10. This is because columns tend to lateral buckling failure with a slenderness ratio of more than 7. As a result of raising concrete compressive strength, raising the modulus of elasticity gives the composite columns improved initial stiffness. The ANSYS (12.0) program introduces a nonlinear three-dimensional finite element model employed to introduce numerical investigation. The (FE) model was verified through comparison with experimental data, which displayed high approval.

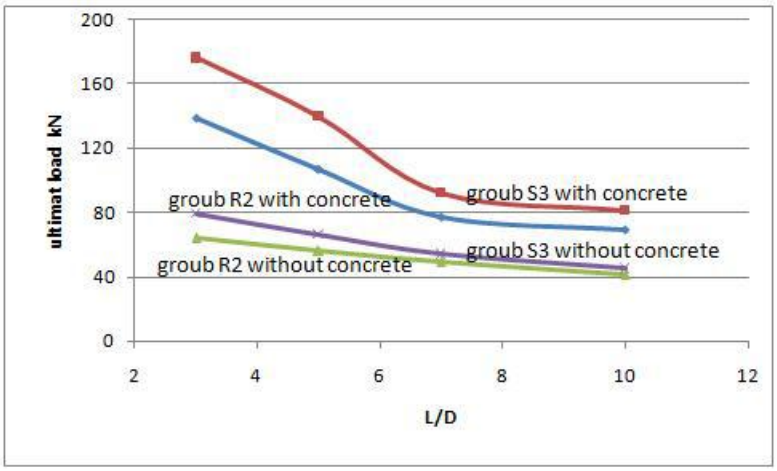

Figure 2.10 Effect of L/D Ratio on Ultimate Load [33].

Idan in 2017 [3], presented a nonlinear study that employed the ANSYS program to simulate the finite element model. The material properties of aluminium alloy and the concrete core, and the aluminium tube confining impact on the concrete, were used to generate the model. The strength capacity, mode of failure, and load axial displacement relation curves result from the finite element model compared with the experimental results to verify the model. The parametric study uses 9 specimen columns to study the effect of high compressive strength with various values (40, 80, 120 MPa) on the performance of composite columns. To concentrate the study on the effect of high-strength concrete on composite column performance, the length-to-diameter ratio was uniform in all specimens. The study indicates that the ultimate load was increased by increasing the concrete compressive strength to 120 MPa, while the ductility was reduced because the concrete core reached the ultimate capacity prior to yielding the aluminium tube. While the specimens with low compressive strength of the concrete core display greater ductility due to yielding of the aluminium tubes before the concrete core reaches its ultimate strength.

Wang et al, in 2019 [34], presented an FE model to discuss the behaviour of circular-section tubes filled with a concrete core (CHS) and examined it against axial compression load. The nonlinearity of the aluminium tube and concrete core, and the interaction between them, was used to generate the model. The strength capacity, mode of failure, and load axial strain relation curves result from the finite element model compared with the experimental results to verify the model. The parametric study employed the verified model to do an investigation on the geometric facilities and primary materials, which are the ratio of the aluminium tube and the strength of both concrete and aluminium, aluminium ratio a is defined as the cross-section area of the aluminium tube A_o normalized by the cross-section area of the concrete core A_c (a=Ao/Ac). The increase in strength of aluminium and concrete leading raises the ultimate strength capacity of composite columns. As shown in Figure 2.11, because of raising the ratio of aluminium, the ultimate load and ductility of the columns are also raised because of the improvement in the confining effect offered by the aluminium tube . The (ε_{scy}) strain at ultimate strength was investigated; therefore, a proposed

equation to determine the strain at ultimate strength of circular-section concrete-filled aluminium tube columns. The result show that for CFAT stub columns (ε_{scy}) can accurately reflect the minimum ductility required to achieve the ultimate strength.

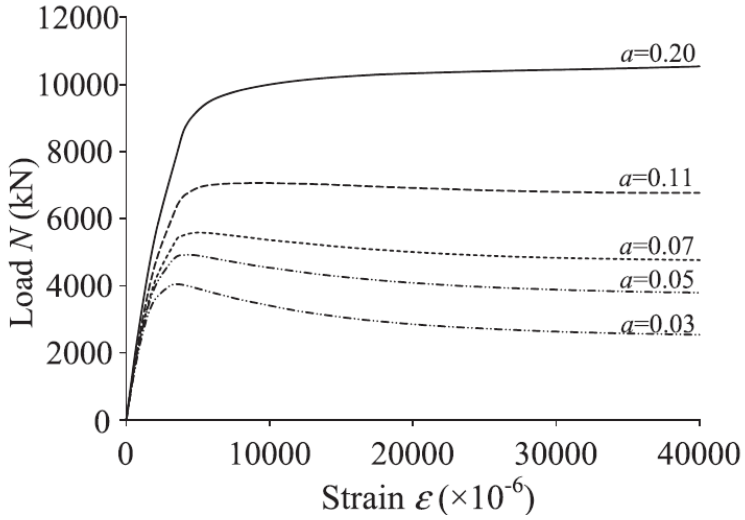

Figure 2.11 Impact of Different Ratios of Aluminium [34].

Jinlong et al, in 2012 [35], used FEM to examine aluminium concrete composite columns having cross-sections shaped square and circular. The mode of failure introduced by the FE model of square and circular composite columns was displayed in Figure 2.12. The mode of failure of circular composite columns displayed ductile "drum-like" deformation, indicated by bending at the middle height, where the outer diameter exceeds that at the ends, in the absence of local buckling indication. Local buckling was displayed at both ends close to the loading and supporting plates and in the middle height of the square composite columns. The results indicate that the circular sections provide higher confinement to the concrete than the square composite columns. Raising aluminium proof stress led to improving the ductility and ultimate strength for both sections of composite columns. Unlike raising the strength of concrete, which led to improving the ultimate strength while reducing the ductility for both sections. Raising the aluminium proof stress or decreasing the concrete strength is not efficient compared to raising the aluminium ratio for enhancing the ductility. The increase in the aluminium ratio not only affects the ultimate bearing capacity of both sections but also affects the third phase of load-displacement curves, potentially changing the slope of this stage from negative to positive, indicating a significant enhancement in ductility.

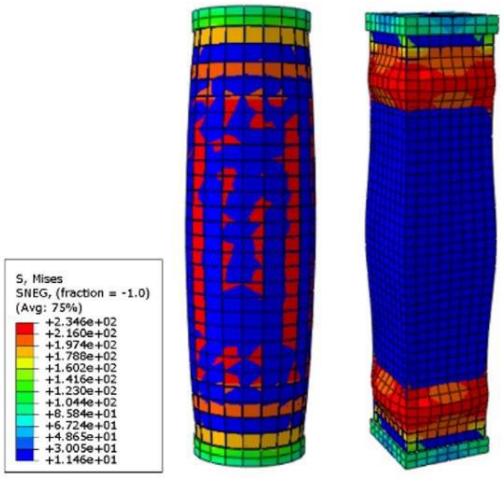

Figure 2.12 Model of Failure for Square and Circular Composite Columns [35].

Patel et al, in 2020 [36], concerned a numerical study of high-strength concrete filling circular stub aluminium tubes. The verified model can correctly identify the ultimate load capacity, and load strain relationship curves of concrete-aluminium composite columns with circular sections. Figure 2.13 displays an increase in the aluminium proof stress that led to an enhancement in the ultimate load of composite columns. Figure 2.14 displays a comparison between concrete aluminium composite columns and concrete steel composite columns. It indicates that the stiffness and ultimate strength capacity of concrete-steel composite columns are little higher than those of concrete-aluminium composite columns, due to the elastic modulus of steel being higher than the elastic modulus of aluminium.

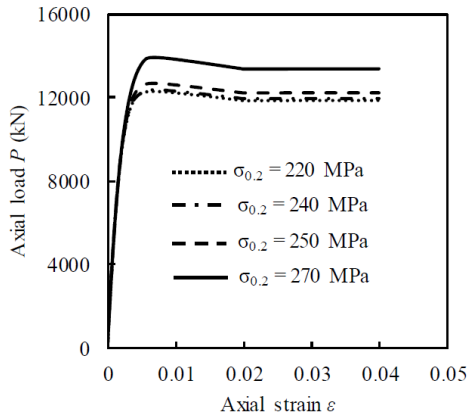

Figure 2.13 Axial Load-Strain Relationship Affected by Proof Stress of Aluminium [36].

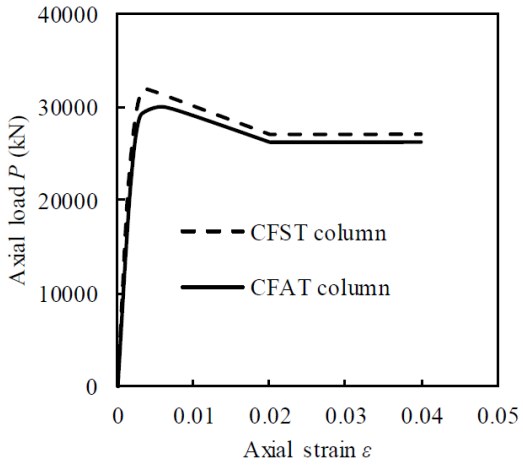

Figure 2.14 Load-Strain Relationship Curves of CFST And CFAT Columns [36].

Georgantzia et al, in 2021 [37], presented an experimental study on 10 specimens of aluminium concrete composite columns having cross-sections shaped square and rectangular. The boundary conditions of the tested columns were pinned ends. The 6082-T6 alloy of aluminium was extruded to fabricate the circular hollow section tube and filling concrete having compressive strength (30 MPa). It is investigating composite columns with a demand from 1 to 3.99 as an aspect ratio of the sections. The tensile coupon procedure was used to determine the properties of the aluminium material. The global buckling was shown in the majority of columns; also, a combination of local and global buckling was shown in a small number of columns. A comparison of strengths between the experimental and EC4 standard design strength was done, which introduced comparability demand between 0.99 and 1.18. Design strength of hollow sections was determined for reference objectives. As a result, an effective method to improve the resistance of local and global buckling of hollow columns is filling them with concrete, which gives them greater structural performance.

Zhang et al, in 2022 [38], conducted experimental and numerical research on the high-strength concrete filling in long aluminium tube columns against axial and eccentric compression. The study is divided into 9 series to understand the impact of eccentricity and different aspect ratios. The 7A04 alloy is a third of the steel metal density; on the other hand, it has great strength with a yield proof stress of 400 MPa and high resistance to corrosion. The FE model uses the ABAQUS program to simulate the experimental column as illustrated in Figure 2.15. The error of the experimental to predicted ultimate load ratio is 10%. The column compressed in the whole cross-section in the longitudinal direction once subjected to axial compression load. If the column attains the elastic-plastic phase, the compression turns from both directions to compress one direction and make the other direction tensile. The eccentric compression on a long column presents low bending stiffness, leading to slight deflection deformation in the initial loading phase, exhibiting strong compression on one side and tension on the other side. The column's stiffness and bearing capacity

reduced as eccentricity got higher, while ductility improved. The carrying capacity of composite columns reduces with a rise in aspect ratio and eccentricity; eccentricity has the greatest impact from aspect ratio. The result shows that the eccentric compression composite column attains the elastic critical point more quickly than the axial compression composite column. At last, an equation to estimate the bearing capacity of high-strength concrete long columns composed of 7A04 aluminium alloy tubes. This formula provides an important reference for the structural design.

Figure 2.15 Numerical and Experimental Failure Mode [38].

Bu et al, in 2023 [39], investigated both experimental and theoretical investigations on the response of aluminium concrete composite columns with round-ended sections against axial loading. This paper studied the effect of the aluminium content of the cross-section and the aspect ratio of the cross-section on the behaviour of composite columns using four columns. The ABAQUS program was used to test parameters throughout the mode of failure, the load versus strain relationship, the load versus displacement relationship, and the capacity of ultimate bearing. As a result of local bulging in the aluminium wall, which led to exposure to oblique shear failure, on the other hand, a complete failure due to instability. The results display reduced stiffness, ductility, and improvement coefficient of bearing capacity with raising the aspect ratio. It also displays reduced initial stiffness of the column with the increase in the content of aluminium, so they recommend the ideal aluminium content to be in the range between 8.5% and 13.5%. The lateral strain of columns was enhanced more quickly, and a better confinement effect was observed

in columns with an aspect ratio of (2). As illustrated in Figure 2.16, the (v)-shaped internal failure of concrete and oblique shear bulging of the tube can be correctly displayed in the FE model. The axial compression bearing capacity of the columns was enhanced more by increasing the strength of the aluminium alloy than by increasing the strength of the concrete.

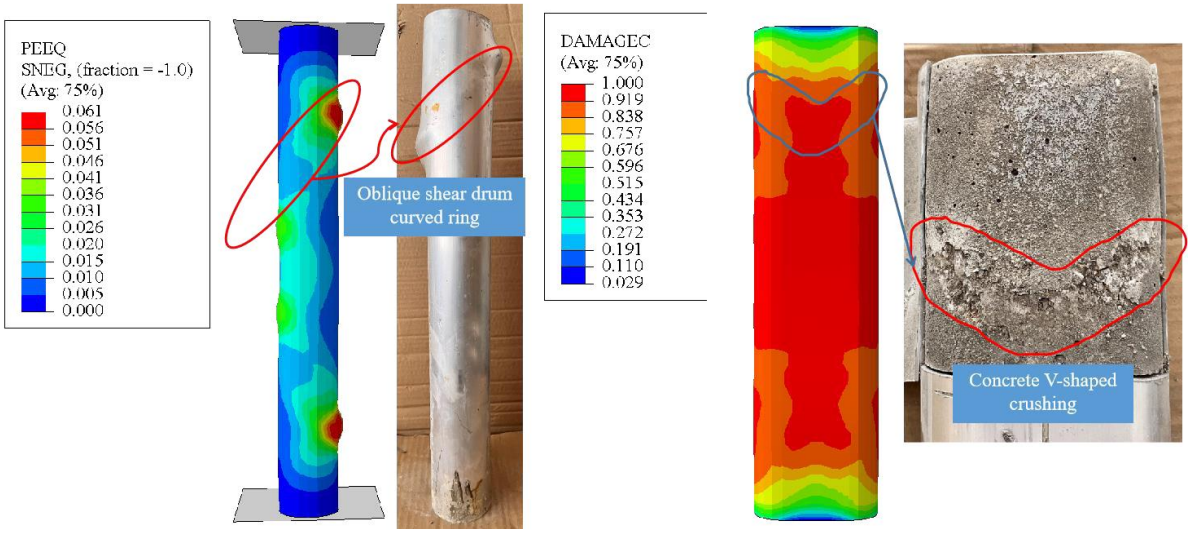

Figure 2.16 Comparison of Failure Modes [39].

2.3 Summary

A brief presentation of the main studies related to the present study are summarised in Table 2.1. Based on the previous review and Table 2.1, the main topics studied by researchers are presented in the following summary:

1. The circular CFAT column has slightly lower initial stiffness than the equivalent circular CFST column because of the low elastic modulus of aluminium.
2. The aluminium concrete composite column strength to aluminium tube strength ratio is greater than one.
3. Raising the proof strength of aluminium leads to an enhancement of ultimate strength.
4. Raising concrete compressive strength led to an improvement in the initial stiffness of composite columns.
5. Concrete with high strength, extremely enhanced ultimate strength of concrete and aluminium composite and decreasing the ductility.
6. A higher aluminium ratio enhanced the ductility of concrete aluminium composite columns better than decreasing concrete compressive strength or increasing aluminium proof stress.
7. Raising the ratio of diameter to aluminium thickness by using uniform diameter and different aluminium wall thickness, it was clearly reduced the ultimate strength and ductility of concrete aluminium composite columns and aluminium tubes.

8. Raising the ratio of column height to depth led to a reduction in ultimate load; when the column height-to-depth ratio exceeds 7, it indicates no clear influence on ultimate load capacity for composite columns and hollow aluminium tubes.
9. A concrete core filled the aluminium tubes to prevent the internal local buckling of hollow aluminium tubes.
10. Shear and local buckling mode of failure were observed in columns having a length-to-diameter ratio range from 3 to 6. The global buckling failure mode was observed in the slenderest columns having a length-to-diameter ratio ranging from 6 to 10.
11. the welded columns reached 54–76% of the test strength of the non-welded columns..

Table 2.1 Previous studies on CFAT columns.

Reference number	Explain	Alloy type	Cross section	Height of column	D/T Range	Test No.	parameter
[25]	Experimental study	6061-T6, 6063-T5	CHS	$300 \le L \le 3000$	$16.66 \le D/t \le 31.25$	29	Welding, cross-section geometry, aluminium strength
[5]	Experimental study	6061-T6	RHS, SHS	Stub column	8.2-63.8	11	Column length, D/T ratio, and concrete strength
[6]	Experimental study	6061-T6	CHS	Stub column	9.7 - 59.7	10	Column length, D/T ratio, and concrete strength
[26]	Numerical study	6061-T6, T5	CHS	Stub column	10 – 160	8	Column length, D/T ratio, concrete strength, aluminium strength
[27]	experimental and theoretical study	6061-T6	CHS	$3 \le L/D \le 10$	11.9 -22.8	4	Column length, D/T ratio
[28]	experimental and computational study	6061-T6	CHS	$3 \le L/D \le 10$	23.3 -47.8	4	Column length, D/T ratio
[29]	An experimental and theoretical study	-	CHS	4.25	40	4	concrete strength, loading styles
[30]	experimental study	-	CHS	3.75	40	9	concrete strength, external confinement effectiveness
[31]	Experimental study	6063-T6	CHS	$3 \le L/D \le 10$	12 - 33.3	4	D/T ratio and L/D ratio
[32]	Experimental study	6061-T6	CHS	4.5 – 7	20-5	7	Column length, D/T ratio
[33]	Experimental and Analytical Study	6063-T6	SHS, RHS	$3 \le L/D \le 10$	25-62.5	5	D/T ratio, slenderness ratio and concrete strength
[3]	Numerical study	-	CHS	Stub column	9.7 23.6	3	Column length, D/T ratio, and concrete strength

[34]	Analytical study	6061-T6	CHS	Stub column	9.7 - 59.7	10	Column length, D/T ratio, and concrete strength
[35]	Numerical study	7020-T6, 6082-T6, 5083-T6, and 6063-T6	CHS, SHS	-	-	-	aluminium proof stress, strength of concrete, and aluminium ratio
[36]	numerical analysis		CHS	Short column	40-100	4	D/T ratio, proof stress of aluminium, concrete strength and comparison between CFST and CFAT
[37]	Experimental study	6082-T6	SHS, RHS	Long column	1-3.99	10	D/T ratio
[38]	Experimental and Analytical Study	7A04	CHS	Long column	33.33	9	L/D ratio and eccentricity
[39]	experimental and Numerical study	-	R-EHS	$3.8 \leq L/D \leq 5$	2-4	4	section aspect ratio and aluminium content of cross section

2.4 Current Study Coverage

Previous studies fewer investigate different cross-section shapes and their impacts on the structural behaviour of short composite columns; they were limited to circular, rectangular, and square cross-sections. To improve this gap in previous studies, this research aimed to numerically analyse the structural performance of concrete-filled aluminium tube columns with various cross-section geometries, specifically those that have equivalent section areas, lengths, and volumes compared to the circular reference column. The first group consists of two branches (curved or rounded cross-sections, polygon cross-sections). Curved cross-sections include three section shapes that were selected (circular, elliptical, and round-ended). Polygon cross-sections with sharp corners include three section shapes that were selected (rectangular, hexagonal, and octagonal). To understand the structural behaviour of these sections. The second group investigated the effects of different aluminium proof stresses on short CFAT, which are 267.9 and 185.9Mpa. The third group investigated the effects of different strengths of the cylindrical concrete on short CFAT, which are 44.8 and 70.2Mpa. The fourth group analyses the effect of different aluminium wall thicknesses on short CFAT, which are (1.9, 3, and 5 mm). The second group investigated the effects of different aluminium proof stresses, which are 267.9 and 185.9Mpa reported by [6], and [25]. The third group investigated the effects of different strengths of the cylindrical concrete, which are 44.8 and 70.2Mpa reported by Zhou and Young [6]. The fourth group analyses the effect of different aluminium wall thicknesses, which are (1.9, 3, and 5 mm). The second, third, and fourth groups uses the most common cross-sections used in buildings, which are circular and rectangular sections.

Chapter Three: Finite Element Modelling

3.1 Introduction

The finite element method (FEM) quickly evolved as the primary numerical analysis instrument for technicians and applied mathematicians because of its beneficial properties against traditional methods [40]. Its key benefit is that it may be used in any shape in any number of dimensions. The FEM is a typical method for turning governing energy principles or governing differential equations into a matrix equation system that may be solved for an approximate solution. Finite element analysis (FEA) is the term used when the finite element method is used in a particular subject of research, for example, stress measurement, thermal investigation, or vibrational study. [41].

Engineering education has changed substantially since the invention of the digital computer. In today's world, everything but the simplest problems are solved using computer software that speeds up computations and allows for the presentation of results in fancy graphics [42].

This technique involves splitting the entire system into individual parts joined by nodes. The elements are organised in a specific pattern, defined as a mesh. Numerically, meshes can be expressed by a collection of mathematical formulas that have to be calculated to estimate variables that are unknown.

Many academics recognise the significance of combining experimental and numerical studies in advanced structural engineering design. Numerical simulation techniques, specifically the finite element method, are essential for discovering how effective concrete and aluminium composite structures are.

There are several types of FE simulation software, such as Abaqus, ANSYS, ATINA, ADINA, DIANA, OpenSees, VECTOR2, etc. Abaqus is one of the most powerful software used in finite element analysis [43]. This chapter presents a nonlinear FE model to study the performance of an aluminium concrete composite column with different cross-sections using ABAQUS/CAE/2019.

3.2 ABAQUS Description

Abaqus software is one of the successful finite element packages that was developed in 1978 and has been used since then for numerical simulation of complex problems in various fields, such as civil and especially structural engineering [44].

ABAQUS (FEA) utilises the finite element method (FEM) to solve partial differential equations that control the behaviour of intricate systems. The FEM breaks down the system into smaller elements, making it easier to approximate the system's behaviour using mathematical models for

each. With Abaqus, users can develop detailed finite element models of structures, components, or materials by considering factors like geometry, material properties, boundary conditions, and loading conditions [45].

After creating a model, ABAQUS enables users to investigate how the system behaves by solving the equations obtained from the finite element discretisation. This examination can offer an understanding of different mechanical phenomena such as stress distribution, deformation, heat transfer, fluid flow, and structural reaction to dynamic loads [46].

ABAQUS has a diverse set of analytical features, such as linear and nonlinear static analysis, dynamic analysis, thermal analysis, coupled field analysis, and optimisation. Moreover, it has a vast array of post-processing tools for visualising and interpreting simulation results, which helps users gain a better understanding of the system's behaviour [47].

In general, ABAQUS Finite Element Analysis allows engineers and researchers to model and analyse intricate systems accurately and efficiently. This tool helps them make informed design choices, improve performance, and reduce risks [48].

3.3 ABAQUS Modelling Procedure

ABAQUS has become one of the most commonly employed FEA applications. ABAQUS/CAE includes an extensive selection of input choices for simulation, which involve geometry, element types, material characteristics, solver controls, loads, graphical user interfaces, automated meshing, boundaries, interaction, and post-processing controls.

1) The modelling processes of the ABAQUS system can be separated into four key phases, as illustrated in Figure 3.1, which are:
    - Stage 1- Modelling of geometry and materials.
    - Stage 2- boundary conditions and contact interaction.
    - Stage 3- Analysis output.
    - Stage 4- Results of post-processing.

Stage 1: Includes modelling the section in the part field, defining the section properties, assembling the pieces and meshing each part in the field.

(a) The concrete column, aluminium column, CFRP, supporting plate and loading plate are modelled.
(b) The material property contains both linear and nonlinear stress-strain graphs of the material, acting as input for the elements in the part domain.
(c) The different parts are meshed employing different kinds of elements, and a member mesh number is selected.

Stage 2: Adding surface interactions, constraints, and contact condition methods to the ABAQUS. This stage also defines the border and conditions for loading.

Stage 3: Discusses the ABAQUS analysis procedure and outputs the results of the composite aluminium-concrete column, such as the ultimate strength, deflections, and strain. Time increment, time period and load case are the inputs of the step field, which is created in this stage during an analysis.

Stage 4: In this stage, the results are presented in tables and figures for the test comparison and validation.

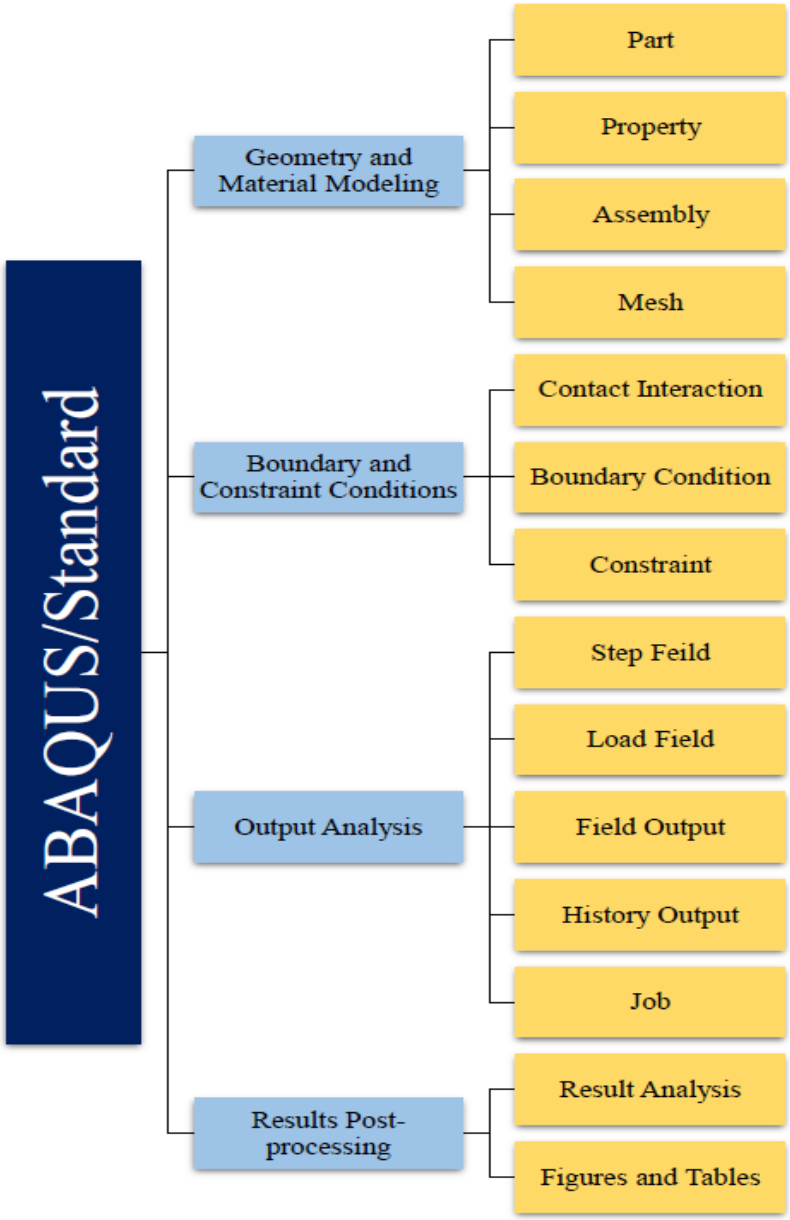

Figure 3.1 ABAQUSE Finite Element Procedure.

3.3.1 Geometry and Material Modelling

Material and geometry modelling in ABAQUS is a critical step in creating accurate simulations of engineering structures. Here's an overview of both aspects:

3.3.1.1 Part Modelling

Part modelling in ABAQUS involves creating or importing the geometric representation of the individual components or parts that make up the entire structure to be analysed. Here's an overview of the part modelling process in ABAQUS:

1) **Geometry Creation:**
- ABAQUS provides tools within its graphical user interface (ABAQUS/CAE) for creating geometric models directly. Users can define basic geometric entities such as points, lines, curves, surfaces, and volumes to construct the desired part geometry.
- Geometric operations like extrusion, sweeping, lofting, and revolving can be used to create complex shapes and features within the part model.

2) **Importing Geometry:**
- Alternatively, users can import part geometry from CAD software using standard file formats such as IGES, STEP, or Parasolid. This allows for seamless integration of existing CAD models into the ABAQUS environment for analysis.
- Imported geometry can undergo further editing or manipulation within ABAQUS to prepare it for finite element analysis.

3) **Geometry Editing:**
- ABAQUS offers a range of editing tools to modify imported or created geometry as needed. Users can perform operations such as filleting, chamfering, splitting, and merging to refine the part geometry for analysis.
- Geometry editing capabilities in ABAQUS enable users to adjust and make modifications to the part model to accurately represent the physical component being analysed.

3.3.1.2 Material Property

Material modelling is important in ABAQUS because it helps engineers simulate how different materials behave when they are under different types of stress. The material library in the Abaqus program attempts to offer a wide range of isotropic and anisotropic, linear and nonlinear material responses. Here are some important properties and features of material modelling in ABAQUS:

1- Concrete

When working with ABAQUS, creating a concrete model requires specifying the material characteristics and choosing appropriate models to accurately replicate its response to different

loads. Key concrete properties usually consist of variables like modulus of elasticity, Poisson's ratio, mass density, compression resistance, and tensile strength. These attributes may differ depending on factors like the specific mix used and the curing process.

ABAQUS provides a variety of material models that can accurately simulate concrete's behaviour. These models range from simple linear elastic models to more complex nonlinear models that consider concrete response to stress and strain, as well as factors like cracking and damage. Among these models, the damaged concrete plasticity model is frequently used to study behaviour under different loading scenarios.

Concrete behaves in a nonlinear manner because of cracking and crushing characteristics that ABAQUS material models can represent with stress-strain relationships. Nonlinear models enable the modelling of the intricate performance of concrete when subjected to both monotonic and cyclic loading. This material is susceptible to cracking, spalling, and ultimately failing when exposed to excessive loads or unfavourable conditions.

With the ABAQUS material models, engineers can accurately simulate concrete damage and failure by including criteria for crack initiation, propagation, and concrete crushing. By specifying concrete properties and choosing the right material models in ABAQUS, engineers can effectively analyse, design, and optimise concrete structures for different engineering scenarios.

In aluminium-concrete composite columns, aluminium walls offer passive containment to the concrete during the first elastic period; the confining impact is low because of the variance in the Poisson's ratio of the two substances. The containing pressure gets apparent as the lateral strain of concrete rises, reaching a stage where the concrete compressive stress becomes 80% of its unconfined strength, as illustrated in Figure 3.2. Past investigations have shown that the confinement afforded by the aluminium tube notably enhances the ductility and strength of concrete in CFAT columns. Investigations indicate that in an aluminium-concrete composite column, the aluminium wall improves the compressive strength capacity of concrete through the confinement effect, and concrete reduces the interior local buckling of the aluminium tube [49].

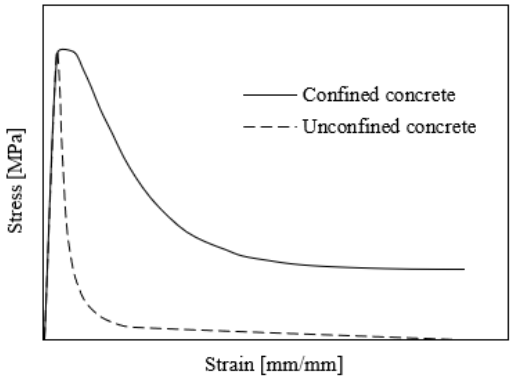

Figure 3.2 Confinement Effect on The Concrete Stress-Strain Curve [49].

I. Elastic Property of Concrete

The elastic properties of concrete refer to its ability to deform reversibly under applied stress within the linear elastic range. In ABAQUS, these properties are typically characterised by density and two main parameters, as shown in Table 3.1 for parametric study.

Table 3.1 Elastic Properties of Concrete.

Type	Density (ton/mm^3)	Young Modulus (MPa)	Poisson's Ratio
Isotropic	2.4*10-9	31458	0.2

II. Concrete Damage Plasticity (CDP)

The CDP simulation tool ABAQUS offers an entire framework for simulating concrete and other brittle materials throughout many structural forms, such as trusses, beams, solids, and shells. The model uses the principles of isotropic tensile and compressive plasticity, together with isotropic damage elasticity, to express the inelastic behaviour of concrete. The developed CDP applies to concrete tested dynamically with or without monotonic loads at little confinement pressure. The CDP model of isotropic damage elasticity and non-associated multi-hardening plasticity displays the irreversible harm produced throughout the fracturing operation.

Additionally, CDP enables operator modification on stiffness restoration impacts throughout cyclical load reversals and is characterised by sensitivity of strain rate[50]. In ABAQUS, Concrete Damage Plasticity (CDP) depends on a lot of things that determine how it reacts to different loads. Some of the main parameters that are often used in CDP are mentioned below:

A. The strength hypothesis and its parameters

Drucker–Prager theory is one of the many commonly used strength theories for concrete, as illustrated in Figure 3.3.

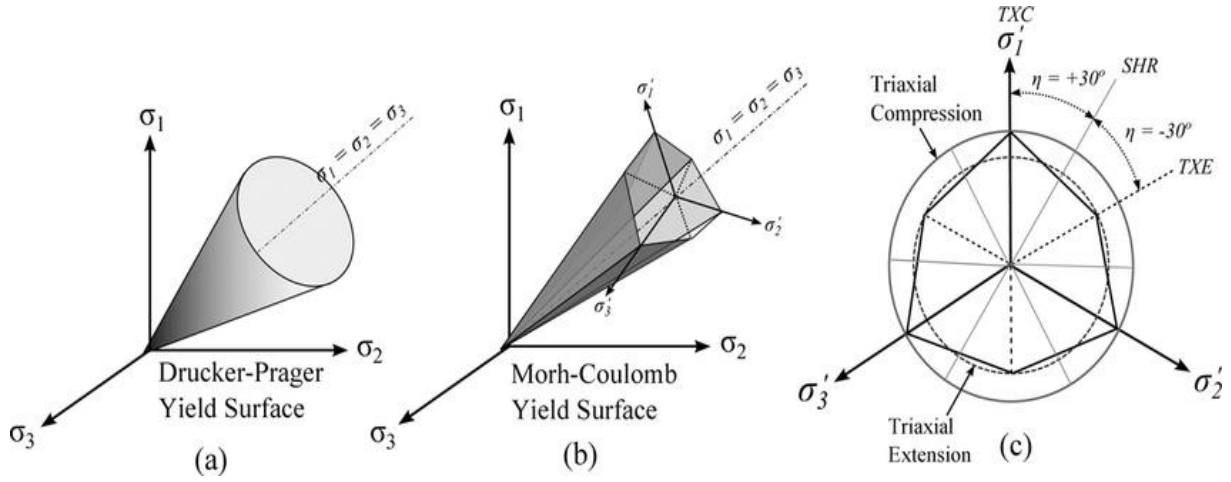

Figure 3.3 Drucker-Prager Boundary Surface [51].

Failure is determined by non-dilatational strain power, and the limit surface in the stress field takes the form of a cone. The benefit of adopting these criteria is achieving surface smoothness, which in turn reduces problems in numerical computations [52]. The concrete damage plasticity concept utilised by the ABAQUS program is a modification of the Drucker–Prager strength criterion.

a) Dilation angle (Ψ)

The slope angle of the failure surface respects its hydrostatic axis, calculated in the meridian level. While the dilation angle is minimal, the concrete indicates brittle performance; conversely, as it increases, its performance approaches ductility. Laboratory findings from academics on a 4-point loaded beam indicated the dilation angles value ranged from 20 to 45 degrees. At the same time, additional studies reported dilation angle ranging from 30 to 55 degrees [42]. In the ABAQUS program, the standard setting is 36. The dilation angle Ψ is known as the angle of internal friction of concrete. Usually, in modelling, Ψ = 25° to 40° or more, depending on concrete compressive strength. In the context of the thesis, the inclination angle was 31 degrees.

b) Eccentricity (ϵ)

A plastic potential eccentricity is a tiny positive parameter that indicates how quickly the plastic potential hyperbola approaches its asymptote. The hydrostatic axis represents the distance between the vertex of the hyperbola and the intersection of the hyperbola's asymptotes (the centre). Eccentricity can also be interpreted as a ratio of compressive strength to tensile strength. In the Concrete Damage Plasticity (CDP) model, a value of ϵ = 0.1 is commonly recommended [53]. Additionally, in the meridional plane, the surface is represented as a straight line when ϵ = 0, following the strength hypothesis of Drucker-Prager. In this thesis, a value of ϵ = 0.1 was used.

c)f_{b0}/f_{c0} Parameter

The parameter f_{b0}/f_{c0} represents the strength ratio of concrete under biaxial compression to its strength under uniaxial compression. Equation 3.1 provides an understanding of how the material performs under different types of loading.[54] suggested a corresponding formula for estimating the f_{b0}/f_{c0} ratio according to the experimental results.

$$\frac{f_{b0}}{f_{c0}} = \frac{1.5}{[f_{c0}]^{0.075}} \qquad 3.1$$

In ABAQUS, this ratio is commonly used to describe how the material reacts to biaxial compression. The default value provided in the ABAQUS user manual for this ratio is f_{b0}/f_{c0} = 1.16, indicating that the concrete's strength under biaxial compression is around 1.16 times greater than its strength under uniaxial compression, as shown in Figure 3.4.

In ABAQUS, the value of f_{b0}/f_{c0} is set to 1.16, which is likely based on empirical correlations. This value is a trusted default for simulating concrete behaviour under biaxial compression. Users

have the option to tweak this parameter to better match their material properties or experimental data for more precise simulations [54].

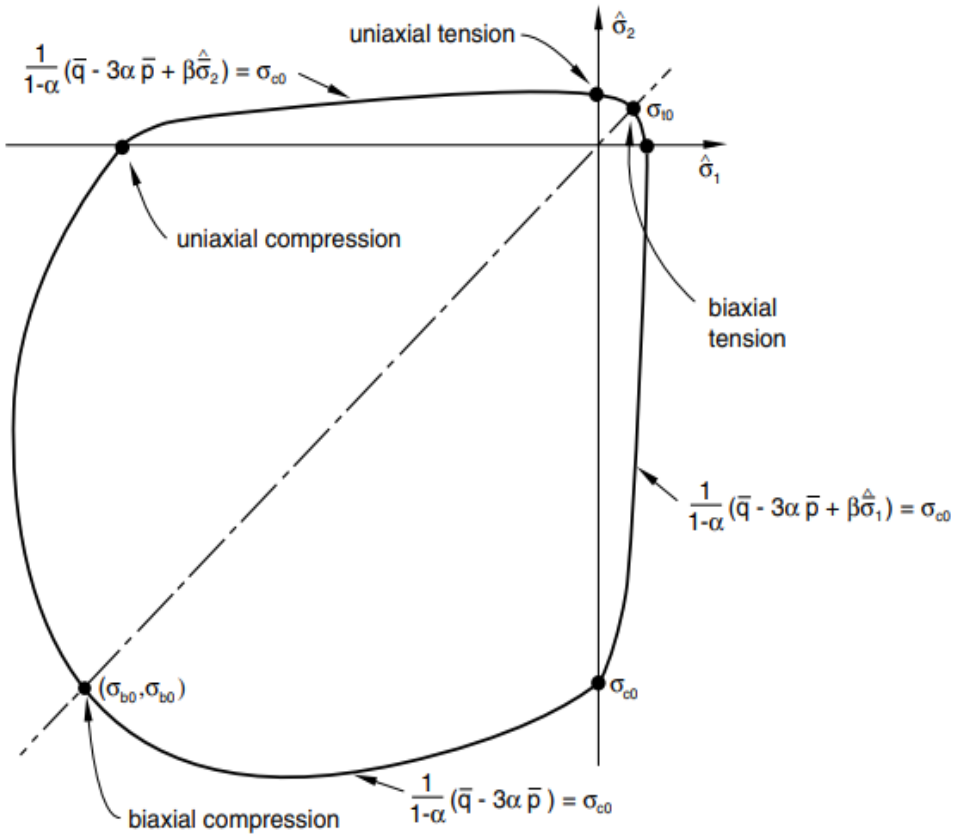

Figure 3.4 Concrete Subjected to Biaxial Stress According to Concrete Damage Plasticity Simulation [53].

d) *Kc* Parameter

Kc is a parameter that can be defined as the quotient of distances between the hydrostatic axis and the compression meridian. A tension axis exists within the deviatoric sectional region. Figure 3.5 illustrates how it determines what shape the deviatoric cross-sections of the failure surface will take [55]. suggests that the Kc range varies from 0.5 to 1, and Equation 3.2 can be utilised for determining Kc:

$$K_c = \frac{5.5 \times f_{b0}}{3 \times f'_c + 5 \times f_{b0}} = 5.5 \times \frac{1}{5 + 2 \times (f'_c)^{0.075}} \qquad 3.2$$

When Kc is greater than 0.5, it indicates that the compression meridian is closer to the hydrostatic axis than the tension meridian. As Kc approaches 1, the deviatoric cross-section becomes more circular, resembling the classic Drucker–Prager strength hypothesis where the failure surface is a circle.

Experimental results indicate that for a mean normal stress of zero, Kc is approximately 0.6 and tends to increase slightly with decreasing mean stress. However, the Concrete Damage Plasticity (CDP) model recommends assuming Kc = 2/3 as a default value.

The shape described by Kc = 2/3 is like the strength criterion formulated by William and Warnke, which consists of a combination of three mutually tangent ellipses. This criterion is a theoretical-experimental approach based on triaxial stress test results and provides a representation of the failure surface under various stress conditions [54].

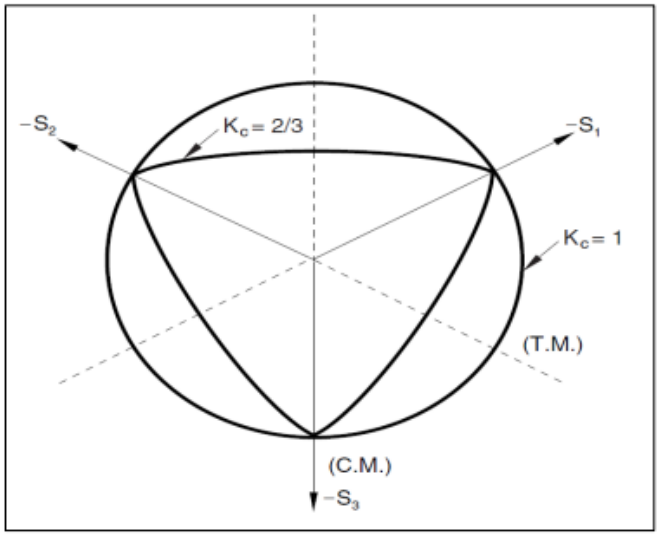

Figure 3.5 Deviatoric Failure Surface in The Concrete Damage Plasticity Model [54].

e) Viscosity Parameter (ŋ)

It can be referred to in the form of relaxing time. Improved substance models that display stiffness deterioration and strain decreasing, which causes convergent problems. A common method for solving this challenge is the regularising of constitutive formulas, where the tangent stiffness of a substance turns positive for short-period steps.

In general, the value of the viscoplastic regularisation parameter is one hundredth of the maximum load values. Using small values generally helps the convergence development rate in the softening regime of the model, without compromising results. The standard setting for the (ŋ) in the ABAQUS program is (0); thus, no viscoelastic regularisation is employed [50]. To improve convergence and stability, it is necessary to assign a non-zero value for the viscosity parameter, usually a small one; a value of ŋ=0.00002 was selected to aid in convergence and guarantee the reliability of the results. The obvious advantages of the concrete damage plasticity concept derive from its basis on variables with a clear physical meaning.

The particular function of the mentioned parameters and the techniques of math adopted for defining the progression of the border surface in 3-D stress space are clarified in the ABAQUS

user reference. The further features that define concrete's behaviour are established under single-axial stresses. In the ABAQUS program, the default parameters of the model characterising its performance under compound stress are shown in Table 3.2.

Table 3.2 Default Parameter of CDP Model Under Compound Stress.

Parameter	Standard Value	Utilised in the Current Study
ϵ	0.1	0.1
Ψ	36	31
f_{b0}/f_{c0}	1.16	1.16
Kc	0.667	0.667
ŋ	0	0.00002

B) Concrete Compressive Behaviour

When concrete is under pressure after being squeezed in one direction, it goes through different stages of reaction. First, it bends without permanently changing shape, then it starts to bend more easily until it reaches a limit. After that, it starts to act in a way that isn't perfectly predictable, with the resistance increasing quickly as it gets squeezed more. Once it reaches its maximum ability to resist being squished, it starts to show signs of damage, like small cracks. If the pressure keeps increasing, the concrete will eventually break apart completely, which can look like it's being crushed, breaking into pieces, or splitting apart.

After a failure occurs, the material might start to soften after reaching its peak, leading to a quick drop in strength because of cracks spreading and the release of elastic energy. It is essential to comprehend these stages to guarantee the longevity and safety of concrete buildings when subjected to different types of loads. The conversion of uniaxial stress-strain curves to stress against plastic strain is assumed. This procedure is done immediately by ABAQUS using the provided stress against "inelastic" strain information, as detailed below.

The concrete stress-strain relation can be precisely described according to the Saenz relation in terms of equivalent uniaxial strain (Elwi and Murray, 1979) yields. Once the graph is obtained, the variables must transform Figure 3.6. In CDP, the inelastic strains are utilised. To define them, the elastic part must be deducted (according to the undamaged material) from the uniaxial compression for the total registered strains from Equations 3.3 and 3.4:

$$\tilde{\varepsilon}_c^{in} = \varepsilon_c - \varepsilon_{0c}^{el} \quad 3.3$$

$$\varepsilon_{0c}^{el} = \frac{\sigma_c}{E_0} \quad 3.4$$

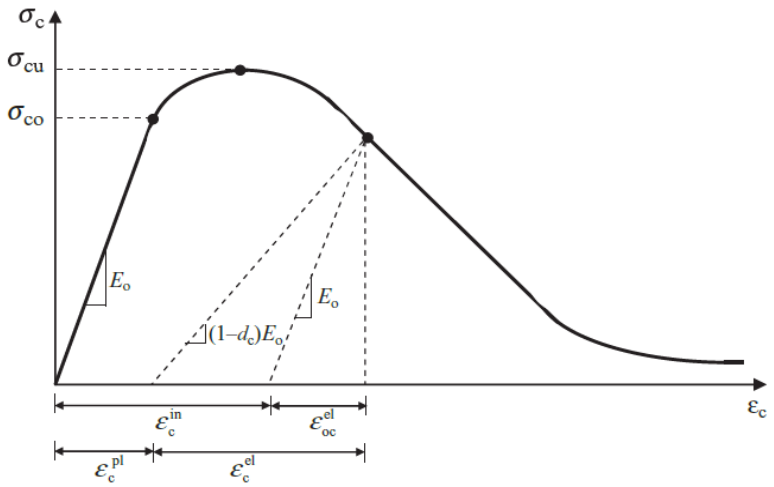

Figure 3.6 Inelastic Compressive Definition of Strain $\tilde{\varepsilon}_c^{in}$ [50].

C) Concrete Tensile Behaviour

When concrete is stretched in one direction, it goes through a series of changes. At first, it stretches elastically in a straight line, following Hooke's Law, until it reaches the point where it can no longer hold the stress, σt0, which is when tiny cracks start to form within the material. After this, as shown in Figure 3.7, the relationship between stress and strain weakens, showing a decrease in both stiffness and strength as the cracks spread.

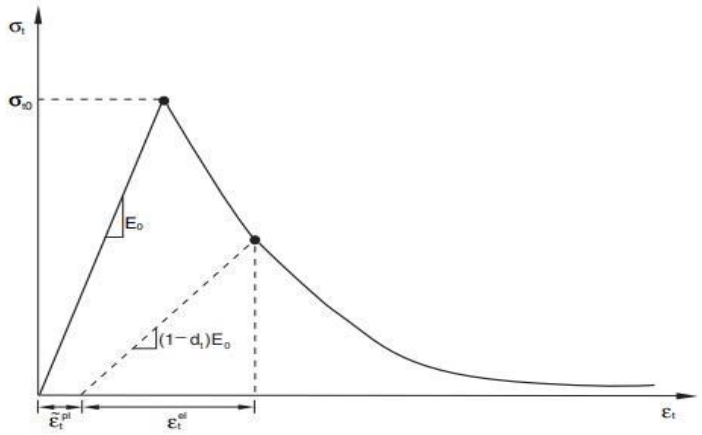

Figure 3.7 Response of Concrete to Uniaxial Loading in Tension [53].

This weakening response causes localised strain within the concrete and eventually leads to a complete breakdown. Understanding this process (from stretching without damage to the start of cracks and then to weakening) is essential for assessing how well concrete structures can handle being stretched. Uniaxial stress-strain curves can be transformed into plastic strain curves against stress. (This automatic conversion is performed by ABAQUS, using user-defined stress versus "inelastic" strain).

Concrete properties of elastic and concrete damage plasticity (CDP) parameters and for compressive and tension behaviour can be entered into the ABAQUS to simulate concrete behaviour, as shown in Figure 3.8 and Figure 3.9.

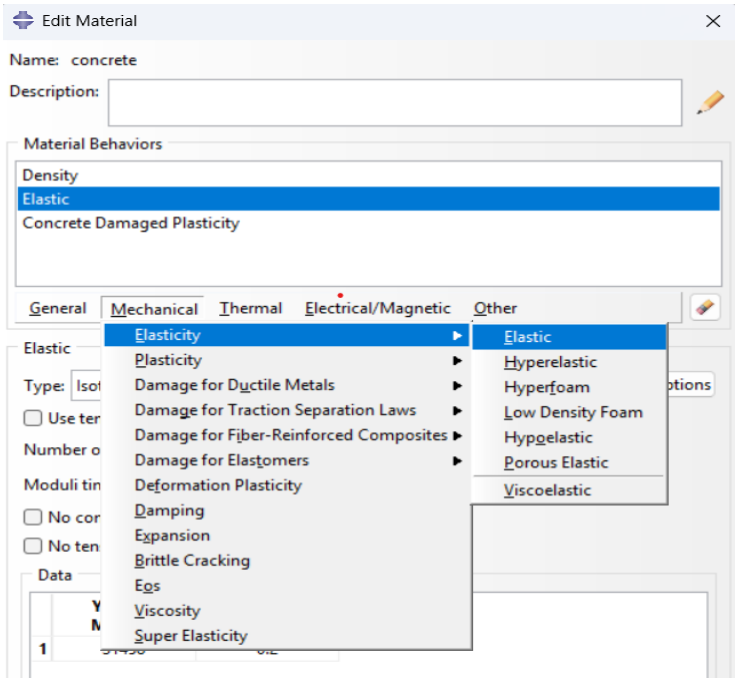

Figure 3.8 Elastic Property Details.

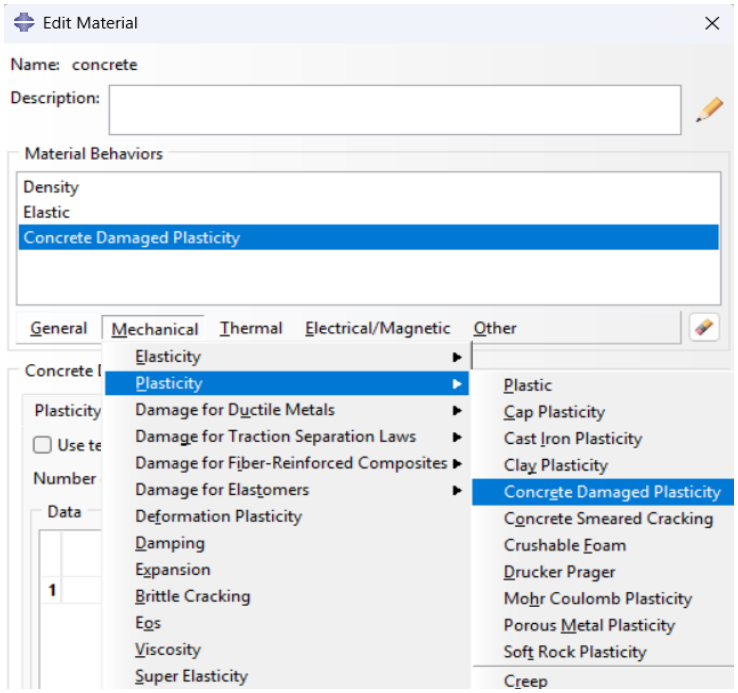

Figure 3.9 Utilisation of The Concrete Damage Plasticity Model to Identify The Plasticity Features of Concrete.

2- Aluminium Properties

In Abaqus, the aluminium tube was modelled as a shell element with the concrete core being the inner part. For clarifying the fundamental structure of aluminium, the elastic-plastic model was adopted. It is accepted that aluminium displays isotropic material characteristics. The density was given as (tonne/mm³), which is the same as the standard density of structural aluminium alloys. The elastic properties were set up with a modulus of elasticity and Poisson's ratio that are in line with the values for structural aluminium in validation and parametric studies. Next, to simulate the nonlinear material behaviour, plasticity was assigned to aluminium via its stress-strain curve. At first, the engineering stress-strain curve was calculated as per the two-phase Ramberg-Osgood model, along with the prescribed values and forecasting expressions for the key input parameters, for characterising the stress-strain relationship of aluminium alloys, which is condensed in this section [56]. The basic structure of the model is described by Equations (3.5),(3.6),(3.7), and (3.8):

$$\varepsilon = \frac{f}{E} + 0.002\left(\frac{f}{f_y}\right)^n, \text{ for } 0 < f < f_y \quad 3.5$$

$$\varepsilon = \frac{f-f_y}{E_{0.2}} + \left(\varepsilon_u - \varepsilon_{0.2} - \frac{f_u - f_y}{E_{0.2}}\right)\left(\frac{f-f_y}{f_u - f_y}\right)^m + \varepsilon_{0.2}, \text{ for } f_y < f < f_u \quad 3.6$$

Where:

$$E_{0.2} = \frac{E}{1+0.002n\frac{E}{f_y}} \quad 3.7$$

$$\varepsilon_{0.2} = \frac{f_y}{E} + 0.002 \quad 3.8$$

where f indicates the stress and ε indicates the strain of aluminium, f_y is 0.2% aluminium proof stress, f_u is the aluminium ultimate stress, $\varepsilon_{0.2}$ is the strain at 0.2% aluminium proof stress, E is aluminium Young's modulus, $E_{0.2}$ is the tangent modulus at 0.2% aluminium proof stress, n is the first strain hardening, m is the second strain hardening, E is Young's modulus, and Poisson's ratio is 0.3.

Most ductile materials yield at stress points far lower compared to their modulus of elasticity; this indicates the right measurements of stress and strain are "true" stress and logarithmic strain. The engineering values were transformed into true stress and logarithmic plastic strain using Equations (3.9 and 3.10) that are in accordance with the input requirements of Abaqus for plastic material modelling.

$$\sigma_{true} = \sigma_{nom}\,(1+\varepsilon_{nom}) \quad 3.9$$

$$\varepsilon_{ln}^{pl} = ln\,(1+\varepsilon_{nom}) - \frac{\sigma_{true}}{E} \quad 3.10$$

Where σ_{true} and σ_{nom} are the true and nominal stresses of aluminium alloys, respectively, ε_{nom} and ε_{ln}^{pl} are the nominal and log plastic strains, respectively.

The true stress-plastic strain curve thus produced was input into the plasticity module to describe the aluminium shell's inelastic response. Such a technique has been commonly used in finite element studies that analyse the performance of concrete-filled aluminium or steel tubes since it allows for the direct. The elastic behaviour of the aluminium tube was evaluated employing an elastic modulus determined by the coupon test and a Poisson's ratio equal to 0.33. The von Mises yield criterion and isotropic hardening were applied to handle the plastic response. The Von Mises yield criterion indicates the yielding limit for metallic materials. Yielding happens when the second constant of deviatoric stress attains a crucial point, but the stress-strain curve is until elastic till a certain point is reached. The requirement in the multiaxial stress condition may be defined by Equation (3.11) (von Mises, 1913).

$$f_y = \sqrt{0.5\left[(f_1 - f_2)^2 + (f_2 - f_3)^2 + (f_3 - f_1)^2\right]} \qquad 3.11$$

*f*1, *f*2 and *f*3 indicate the principal stresses. As illustrated in Figure 3.10, this formula produces a cylinder yield surface having a radius of √2/3 *fy* around the hydrostatic axis (*f*1 = *f*2 = *f*3). In metallic parts, isotropic hardening is indicated by the yield surface keeping its form in addition to evenly expanding about the hydrostatic axis as stress [4].

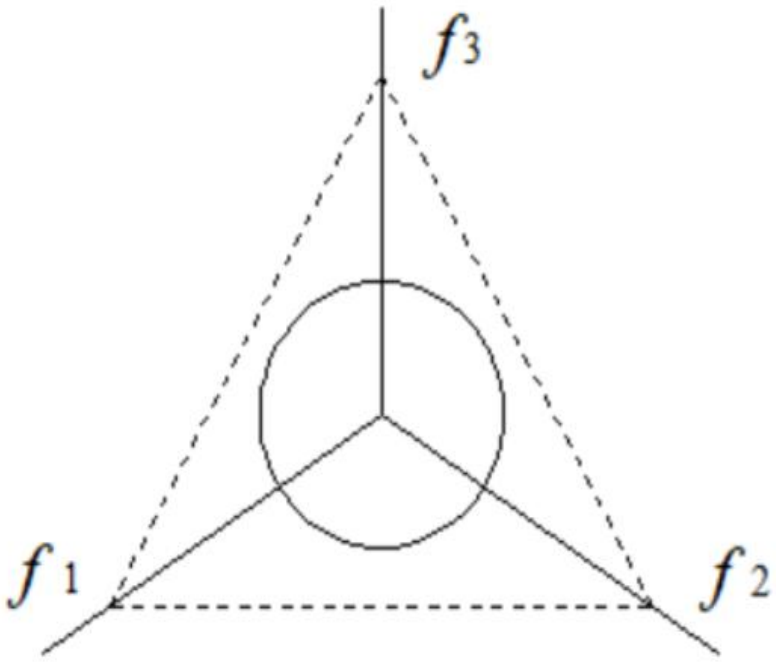

Figure 3.10 The Yielding Criteria of Von Mises [4].

3- CFRP Properties

FRP composites are strong and lightweight materials utilised in the construction domain to improve the strength and stiffness of existing constructions. They are composed of fibres of carbon embedded within a polymer resin [9]. Besides specifying the characteristics of aluminium and concrete, which are the principal components of the composite columns, the properties of Carbon Fibre Reinforced Polymer (CFRP) were also imported into the numerical model with the aim of enhancing the end performance of the composite columns. The major goal of applying CFRP wrapping at the ends of the columns is to postpone or prevent the occurrence of local buckling, which is often referred to as "elephant foot failure" and is normally a result of high compressive stresses and the resulting instability at the base area of the column [57]. In the Abaqus material property module, the CFRP definition was deliberately simplified to capture its elastic contribution, as the confinement role of CFRP in this study is mainly ruled by its stiffness and not its post-yield behaviour. The density of CFRP was set to 1.8e-9 (ton/mm3), a value that is in line with the commonly used carbon fibre composites. The elastic properties were established by providing an isotropic linear elastic behaviour with a Young's modulus of 230,000 MPa and a Poisson's ratio of 0.33. Although the material is generally anisotropic, this modelling assumption was affirmed as the direction of the maximum resistance to load is along the fibre, which is accurately indicated by the chosen modulus of elasticity. Therefore, treating the material as isotropic allowed the Abaqus model to be computationally efficient while still accurately capturing the confinement effect of CFRP at the column ends. This method has been used in several earlier numerical studies where the emphasis was on simulating the global confinement effect of FRP composites rather than their complete anisotropic response.

4- Steel Properties

The steel plates employed at the ends of each specimen were characterised. The lower plate served as a support plate to give a stable base and guarantee uniform stress distribution to the boundary conditions, while the upper plate worked as a loading plate to convey the applied axial load uniformly to the column cross-section. The plates were not included in the loading or the structural system under investigation, and thus, the assumption was made that the steel material had a constant elastic response over the entire analysis, which was a common practice in finite element modelling. The aforementioned assumption is shared among all modelling techniques where boundary or loading plates solely act as load transfer facilitators and do not influence the overall nonlinear response of the tested element. Steel was thus modelled in Abaqus via a simplified linear elastic definition. Material density was determined to be 7.8e-9 (ton/mm3), as per standard values for structural carbon steel. The elastic behaviour was defined through Young's modulus and Poisson's ratio, specified as 200,000 MPa and 0.3, respectively. No plasticity or damage parameters were assigned since they were not pertinent to the function of the plates. This method resulted in providing a realistic yet computationally efficient portrayal of the support and loading conditions, thus ensuring an accurate simulation of the column's behaviour while maintaining numerical stability and simplicity in the finite element model.

3.3.1.3 Assembly of Modelling

When working in ABAQUS, assembling models requires putting together different parts to create complex structures. To start, parts need to be formed, which can be achieved using ABAQUS's tools or by importing designs from CAD software. Each part embodies a specific element of the assembly and may vary in materials, characteristics, and shapes, as shown in Figure 3.11. After creating the part geometries, they are then arranged and adjusted in relation to one another to create the final assembly. ABAQUS offers a range of tools and capabilities to simplify this assembly process, enabling users to accurately specify connections, interfaces, and interactions between the parts. These can involve tie constraints, equation constraints or interactions to simulate the interactions between the parts.

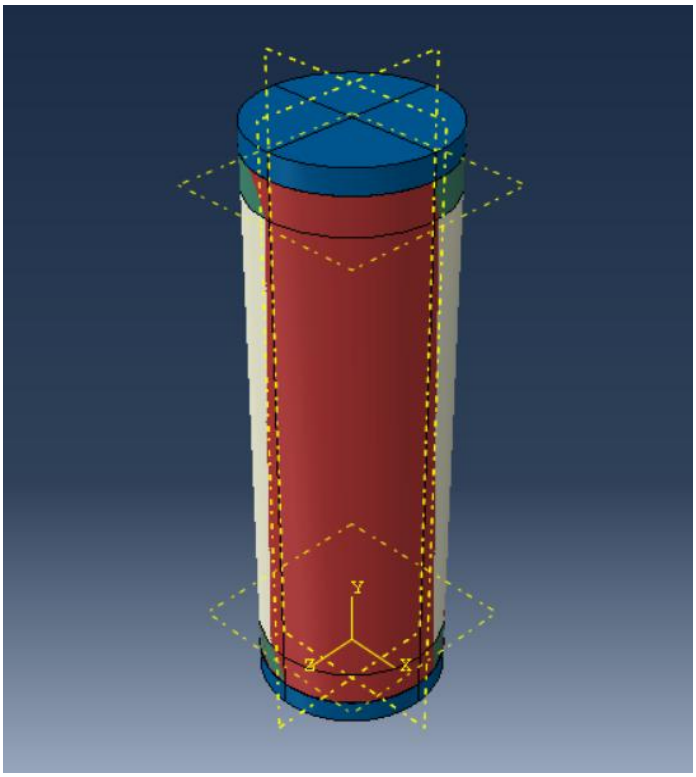

Figure 3.11 Assembly of Modelling Parts.

3.3.1.4 Element Mesh and Type

Meshing in ABAQUS is a key step in finite element analysis (FEA) that is essential for accurately representing complex geometries and predicting structural behaviour under different loads. The mesh generation process then takes place, offering automatic, manual, and controlled meshing options to divide the geometry into finite elements. Quality checks are important after mesh generation to ensure that elements meet specific criteria for accuracy and reliability. Mesh refinement may be needed for complex models to improve solution accuracy. ABAQUS also offers

visualisation tools for users to examine and assess mesh quality and distribution. For engineers to achieve accurate and reliable analysis results for their designs, it is crucial that they have a deep understanding and effectively use meshing techniques.

For exact findings from the finite element model, all concrete and aluminium elements were specifically chosen to have an equal mesh size to guarantee that both materials occupy the same nodes [58].

The main difference among various elements in families is the geometrical shape each family adopts. The starting character or characters of an element's title denote its familial category. S4R is a shell element, while C3D8I is a continuum element. The quantity of nodes within an element is typically provided in its title. The eight-node brick element is known as C3D8, whereas the four-node shell element is known as S4R. The degrees of freedom are the fundamental variables calculated during the analysis. For a stress/displacement simulation, the degrees of freedom are the translations and the rotations at each node. Abaqus defines reduced integration elements by adding the character 'R' to the element title. The meshing of the whole model is displayed in Figure 3.12.

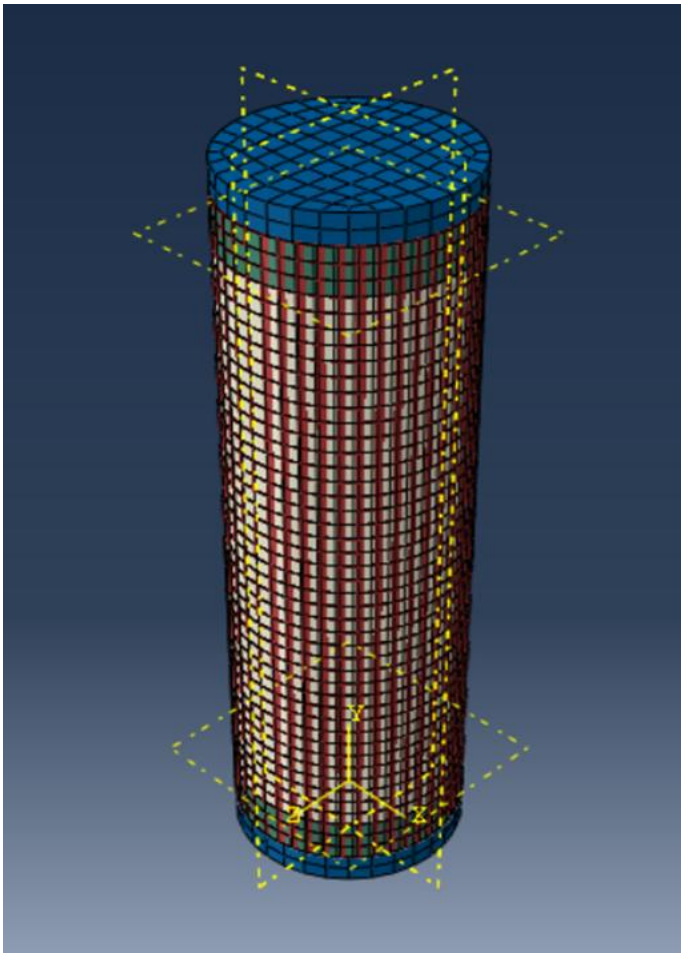

Figure 3.12 The Meshing of The Whole Model

A. Solid Element Description

Three-dimensional solid elements are volumetric components made of a singular homogenous substance or could be made up of multiple layers of different material for large deformations, plasticity and contact behaviour during linear and nonlinear analyses. A three-dimensional (3D) solid element can be considered to be the most general of all solid finite elements because all the field variables are dependent on x, y and z. Since the 3D element is said to be the most general solid element, the truss, beam, plate, 2D solid and shell elements can all be considered to be special cases of the 3D element. Each node of the element will have three translational degrees of freedom. The element can thus deform in all three directions in space. Elements that have nodes only at their corners, such as the 8-node brick, use linear interpolation in each direction and are often called linear elements or first-order elements. Figure 3.14 and Figure 3.15 illustrate the utilising of concrete columns and steel loading and support plates; an eight-node three-dimensional element (C3D8R) can be identified in Figure 3.13. Employing linear displacement approximation, decreased integration with hourglass control, 8node, and three moving degrees of freedom were chosen. Stress at different layers within the element thickness can be defined at every integration point. First-order interpolation elements, for example, hexahedra, indicate possible stiffness with a delayed converging velocity, although they eliminate the risk of mesh lock if employing a decreased integral analytical technique. While second-order elements offer improved accuracy [52]. First-order elements have been utilised to modify the simulation for interfaces and avoid compacted contact situations. The steel loading and supporting plate model are utilising solid elements to make sure the concrete-filled aluminium columns do not penetrate the steel plates.

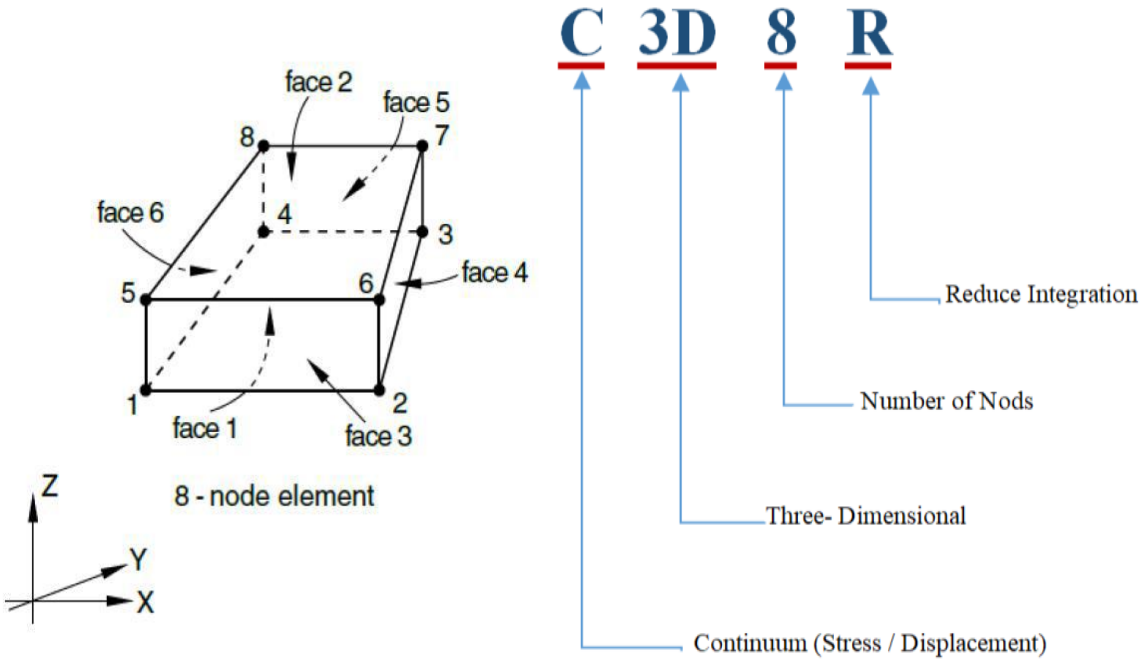

Figure 3.13 C3D8R Element Description [52].

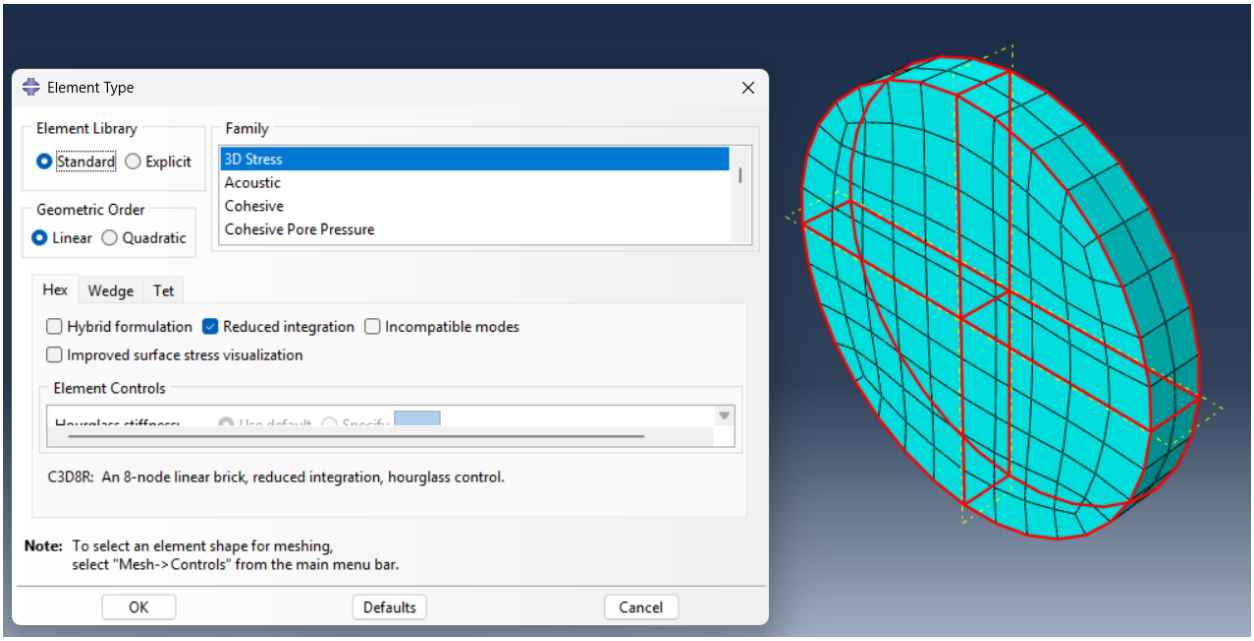

Figure 3.14 Illustration of Chosen Elements for The Plate Model

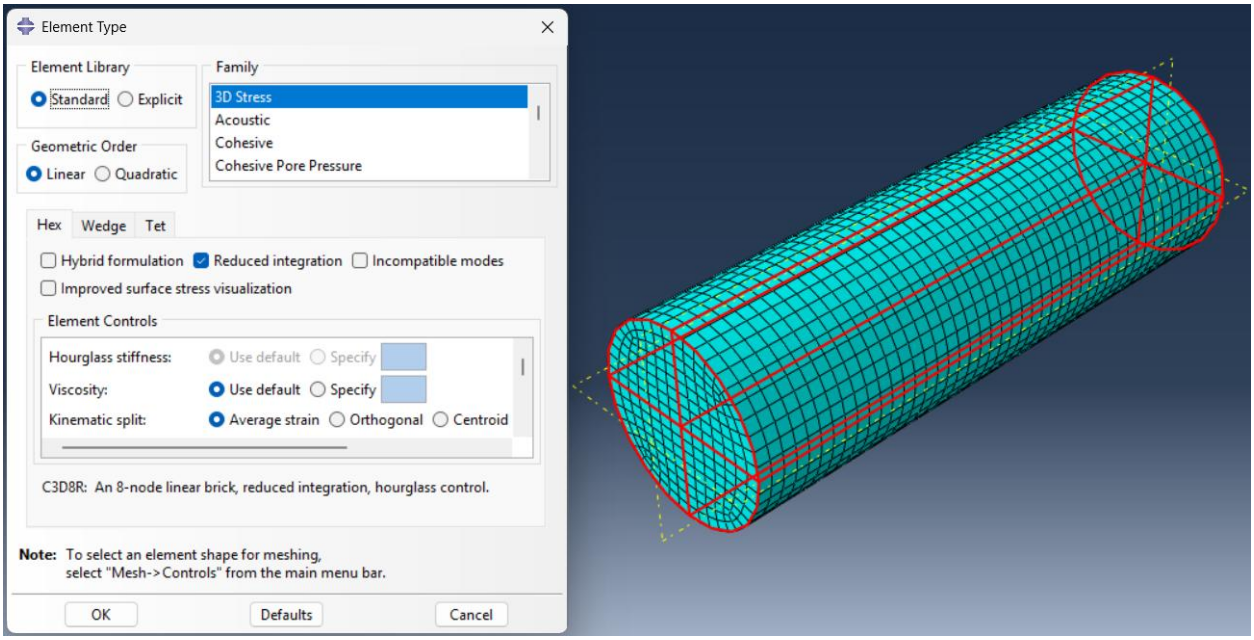

Figure 3.15 Illustration of Chosen Elements for The Concrete Model.

B. Shell Elements

Shell components have a thickness that is far less than both their length and width. Thin or thick-shell FE analysis can be performed on shell structures. Classical Kirchhoff theory describes thin shells, while Reissner-Mindlin theory regulates the kinematics of thick shells. To precisely imitate the thin-walled characteristics of the aluminium enclosure and CFRP

layers, the outer aluminium tube and CFRP wrapping were designed using shell elements. In particular, S4R was the element type for the aluminium shell and CFRP shell, as shown in Figure 3.16. The S4R model is a four-node quadrilateral shell element with a stress/displacement formulation, hourglass control and reduced integration. This element type is specifically suitable for the simulation of thin-walled members. The reduced integration formulation helps shear and membrane locking effects to a lesser extent, while the hourglass control technique ensures stable and realistic results by eliminating the occurrence of spurious deformation modes. Using S4R instead of S8R (eight-node shell elements) was a decision made considering both physical and computational factors. It is true that higher-order elements, such as S8R, might give the local curvature effects slightly more accurately, but they will also increase the computational cost and complexity to a large extent, particularly in large-scale nonlinear analyses.

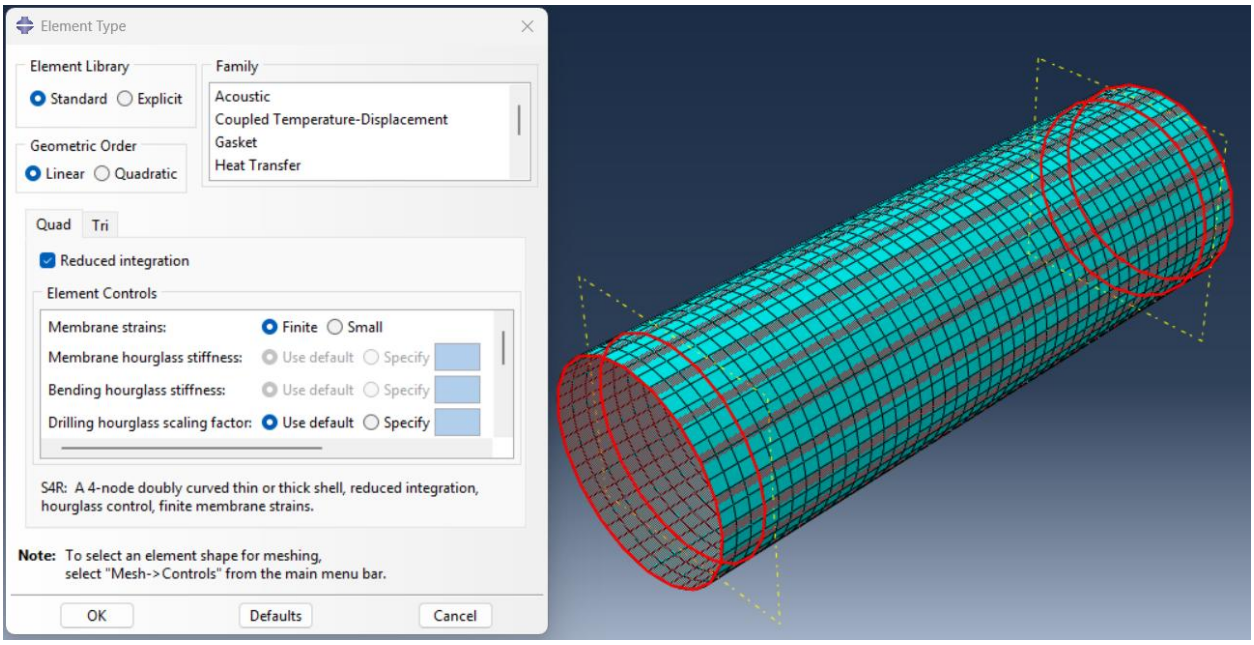

Figure 3.16 Illustration of Chosen Elements for The Shell Model for The Aluminium Tube and CFRP Wrapping.

3.3.2 Contact Interaction and Boundary Conditions

Following the assembly of every component into its specified position, a suitable constraint is applied to indicate the relationship across the different parts. as presented in Figure 3.17 and Figure 3.18. Boundary conditions specify how loads or displacements are applied to model surfaces, reflecting actual loading situations. In the finite element method, contact relationships are an essential feature. Physical procedures are essential details that have to be included in the conditions of boundaries and surface relationships throughout computer modelling. An incorrect formulation could negatively influence the modelling expense, especially in the current thesis, due to the

presence of several components in the simulation, such as the concrete column, aluminium shell, CFRP shell and steel plate. The ABAQUS program includes various approaches for identifying connections, such as tie contact, equation contact, and surface-to-surface contact [59]. 2D and 3D structures may be under either finite or small movement, such as the interface contact surfaces between the aluminium shell and concrete column.

3.3.2.1 Boundary and Loading Conditions

Boundary conditions are essential characteristics which define the interaction of an FE model and its outside setting. They contain instructions such as force, movement, speeds, and temperature, in addition to other physical parameters applied on the simulation's borders or surface. Researchers apply these circumstances to model actual loading situations, including loads on structures or influences from the environment, to accurately represent the structures during examination. Boundary conditions are important for estimating the simulation's performance and getting important knowledge into the structure, heating, or fluid mechanics in ABAQUS models. The loading and boundary conditions employed in this study are explained in this section. The lower surface of support plate is displayed in Figure 3.17, the upper surface of loading plate is displayed in Figure 3.19, and the load is applied on the top surface of the upper plate according to Figure 3.18. Axial compression load must be evenly distributed throughout the two composite components, which are the aluminium tube and concrete core. Two steel plates are placed on the top and bottom of the composite columns. The bottom steel plate is completely fixed against the (X, Y, Z) directions, while the upper steel plate is fixed against the (X, Z) directions. Axial displacement is applied on the top surface of the loading plate in the (Y axis) normal direction with gradual raising until it attains the load that caused the column deformation.

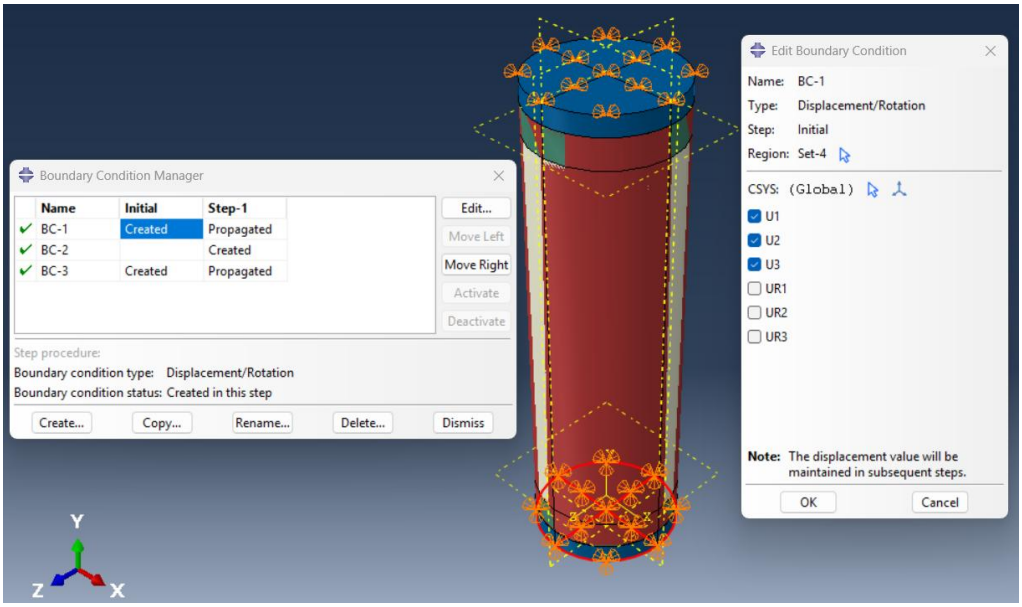

Figure 3.17 Illustration of Boundary Conditions at The Lower Surface of The Supporting Plate.

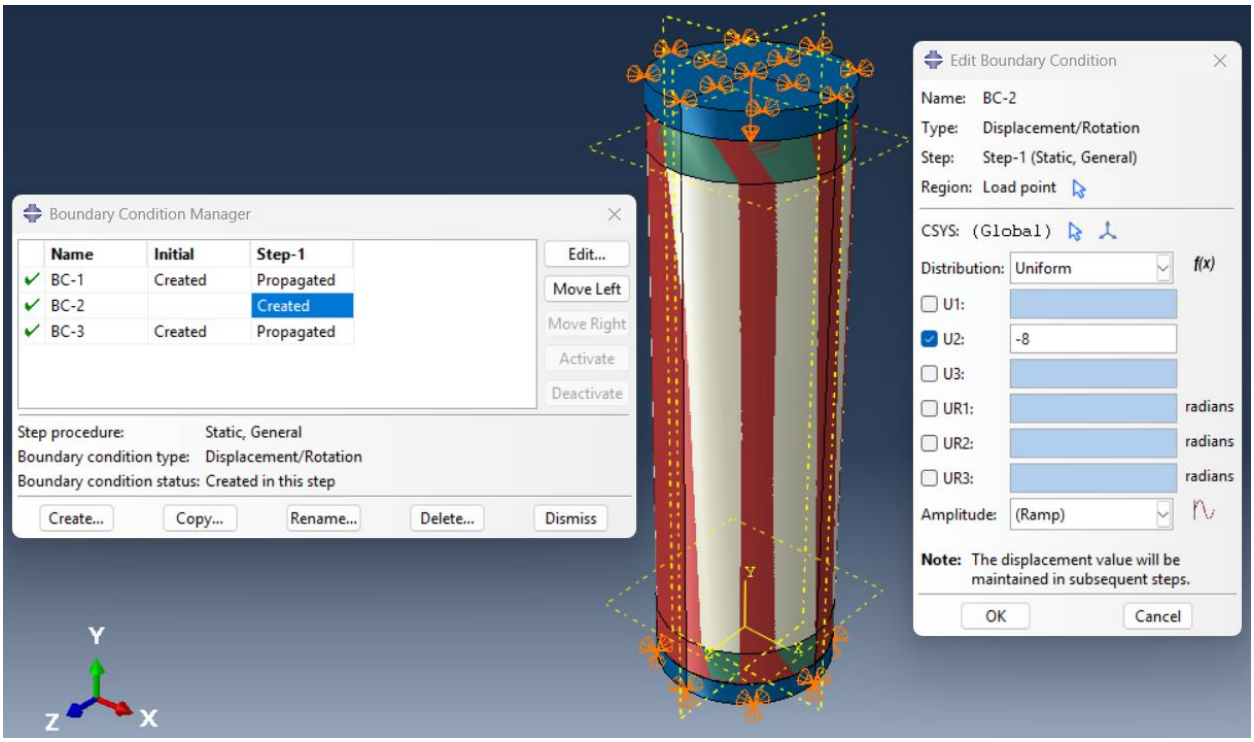

Figure 3.18 Applied Load on the Top Surface of the Loading Plate.

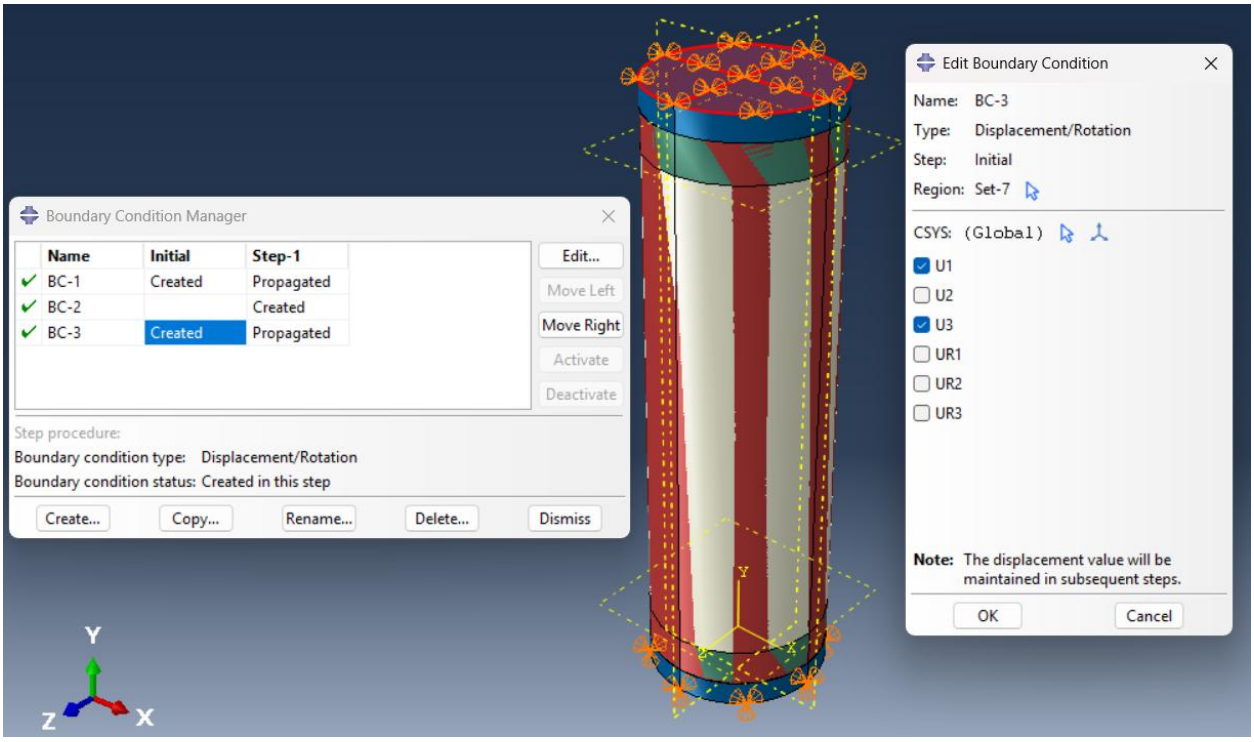

Figure 3.19 Illustration of Boundary Conditions at the Upper Surface of the Loading Plate.

3.3.2.2 Constraint and Interaction Conditions

In ABAQUS, constraints and interactions are critical for managing performance and interactions inside FE models. Constraints control the motion of a node or element through either limiting certain locations or connecting elements together. These constraints are necessary for properly expressing actual-life constraints, such as rigid support or interdependent surfaces, which improve the reliability and accuracy of the investigation. Contact interactions in ABAQUS enable designers to model friction, separation, or adhesion among surfaces, while also applying tie constraints to guarantee consistency of displacements among linked areas. According to Figure 3.20 and Figure 3.21, a tie constraint was adopted between the core concrete and the loading, supporting plates and used between aluminium tube edges and plate edges. According to Figure 3.26, the connection between the aluminium wall and the concrete core was simulated as a surface-to-surface contacting relationship. The concrete core having the smaller modulus of elasticity was chosen as the slave surface, and the aluminium tube having the larger modulus of elasticity was chosen as the master surface. Between interaction surfaces, contact characteristics can be generated, especially when a penalty function with a 0.4 friction coefficient in the tangential direction as shown in Figure 3.24 and hard contact in the normal direction is used in Figure 3.25. The contact couple surfaces permit the separation of surfaces under the impact of tensile force. The magnitude of the interface's coefficient of friction was uncertain because there was not enough investigation on this composite column. Thus, test analyses were done on the models, and it was discovered that, for (0.4), the model obtained an excellent level of agreement. According to Figure 3.23, an equation constraint was adopted to link the applied load element as shown in Figure 3.22a with the other upper surface elements in Figure 3.22b, which ensures equal pressure is distributed on the upper loading plate surface.

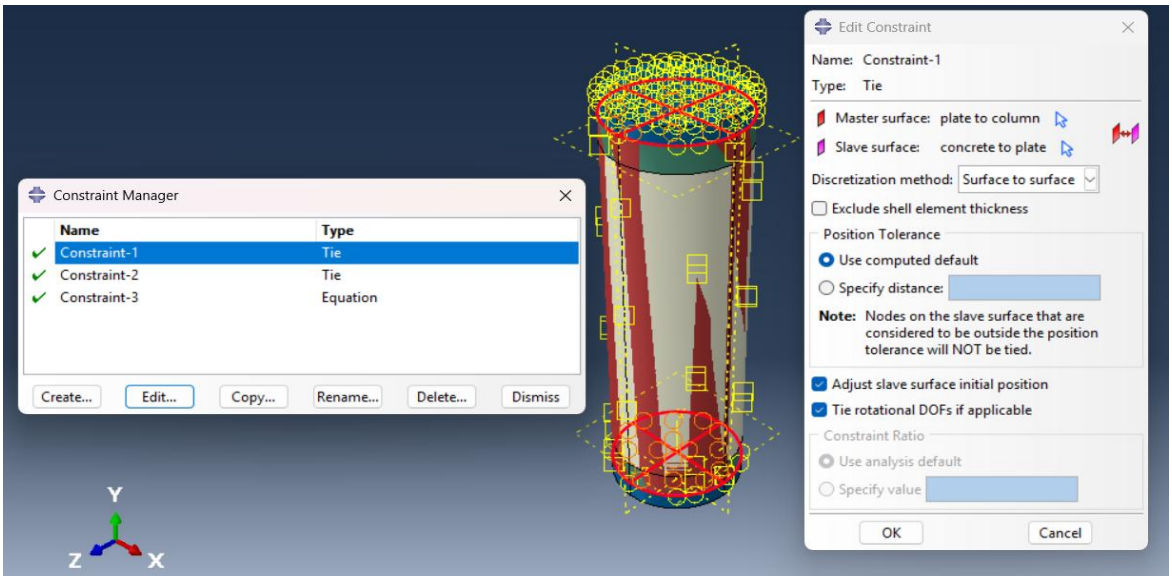

Figure 3.20 Tie Constraint Connecting the Concrete Column Surfaces and The Steel Plate Surfaces.

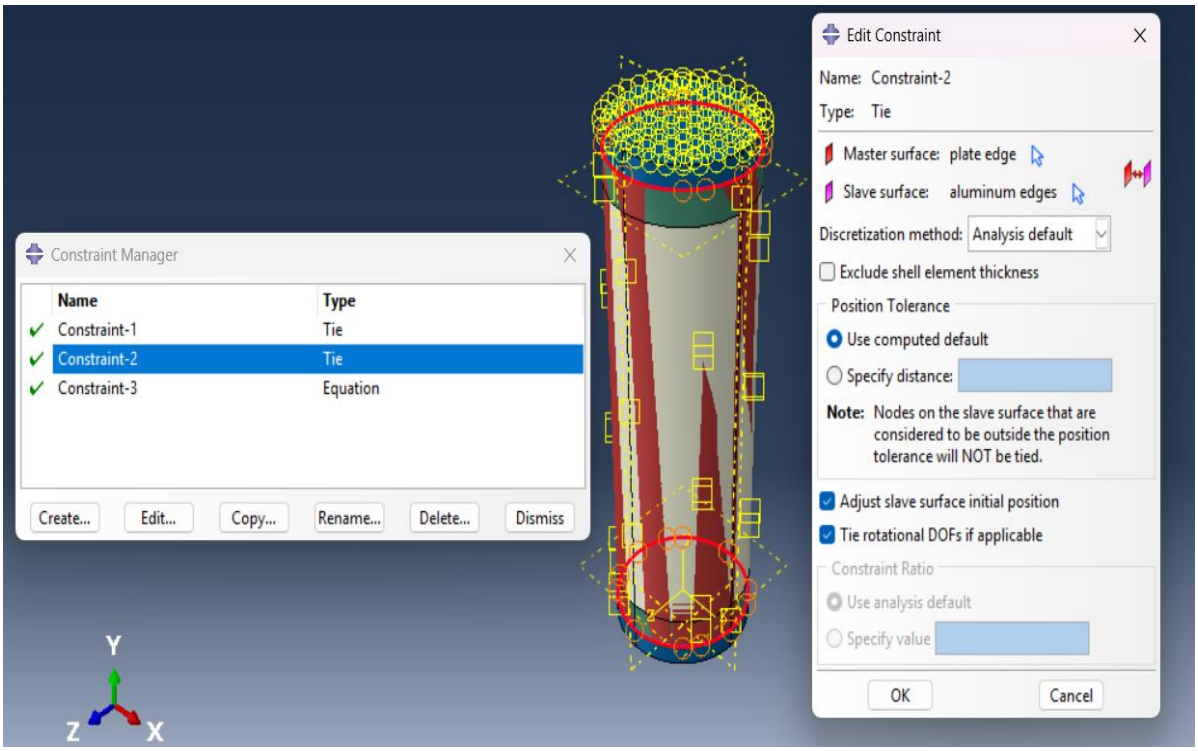

Figure 3.21 Tie Constraint Between Plates Edges and Aluminium Edges.

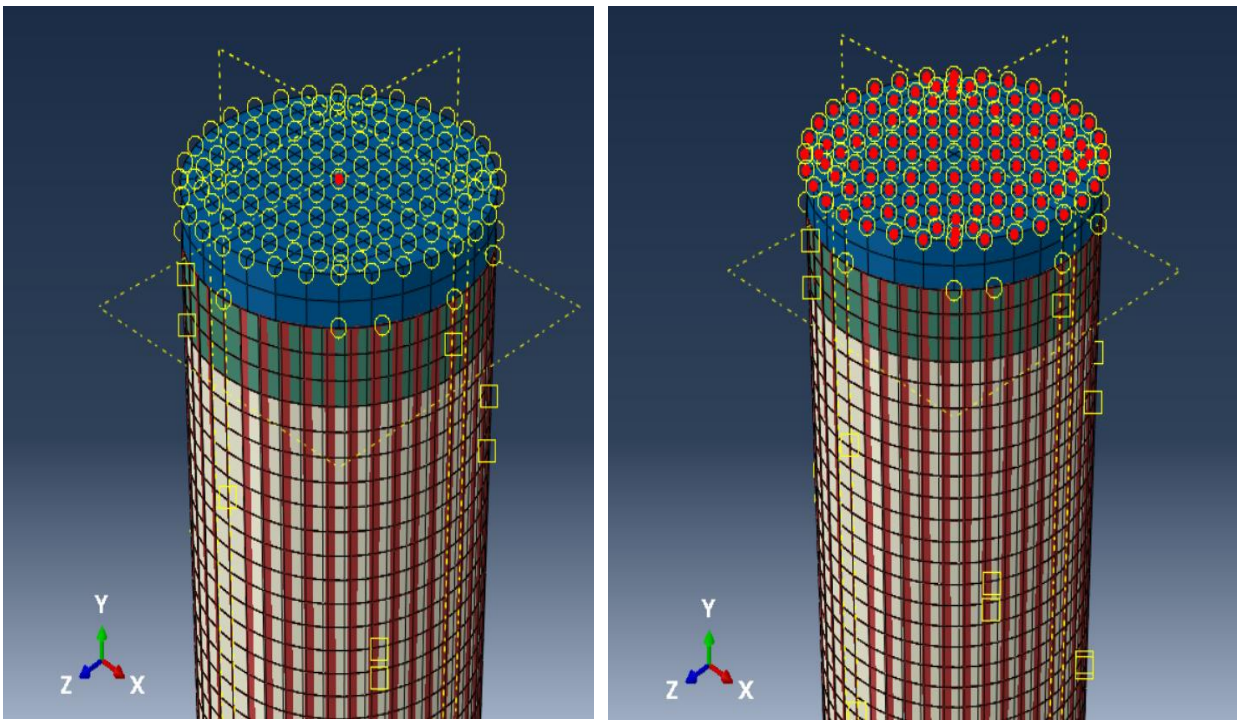

(a) Load point (b) Load area

Figure 3.22 Illustrate the Load Point and Load Area Elements' Positions.

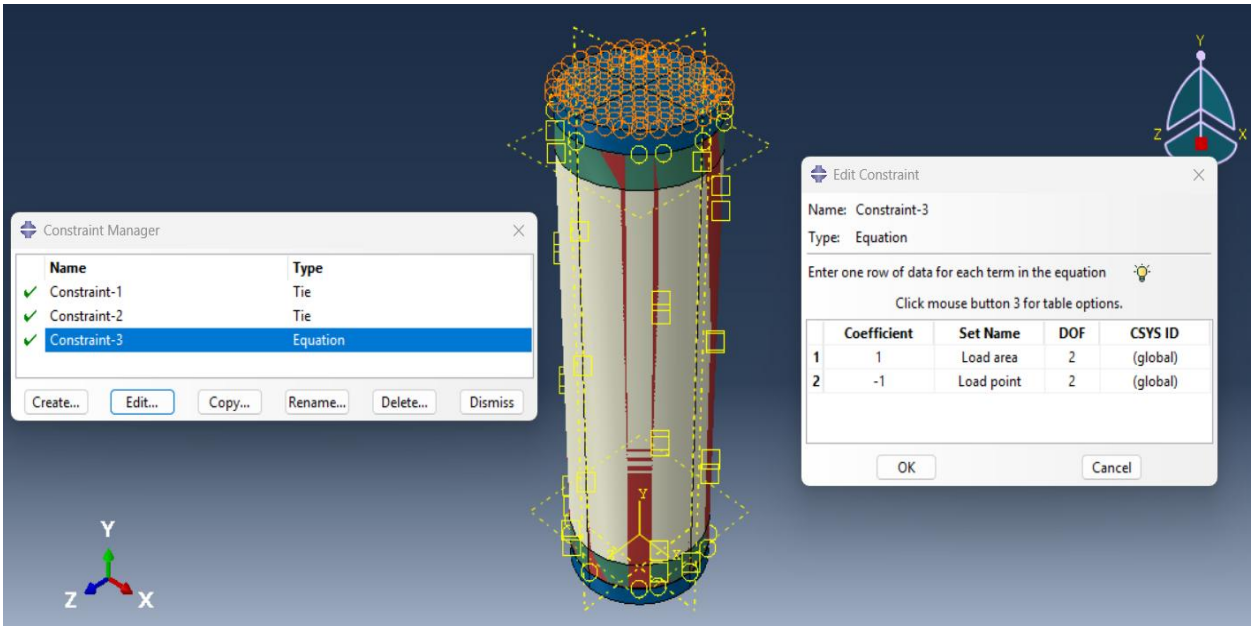

Figure 3.23 Using the Equation Constraint Between The Load Point and The Load Area.

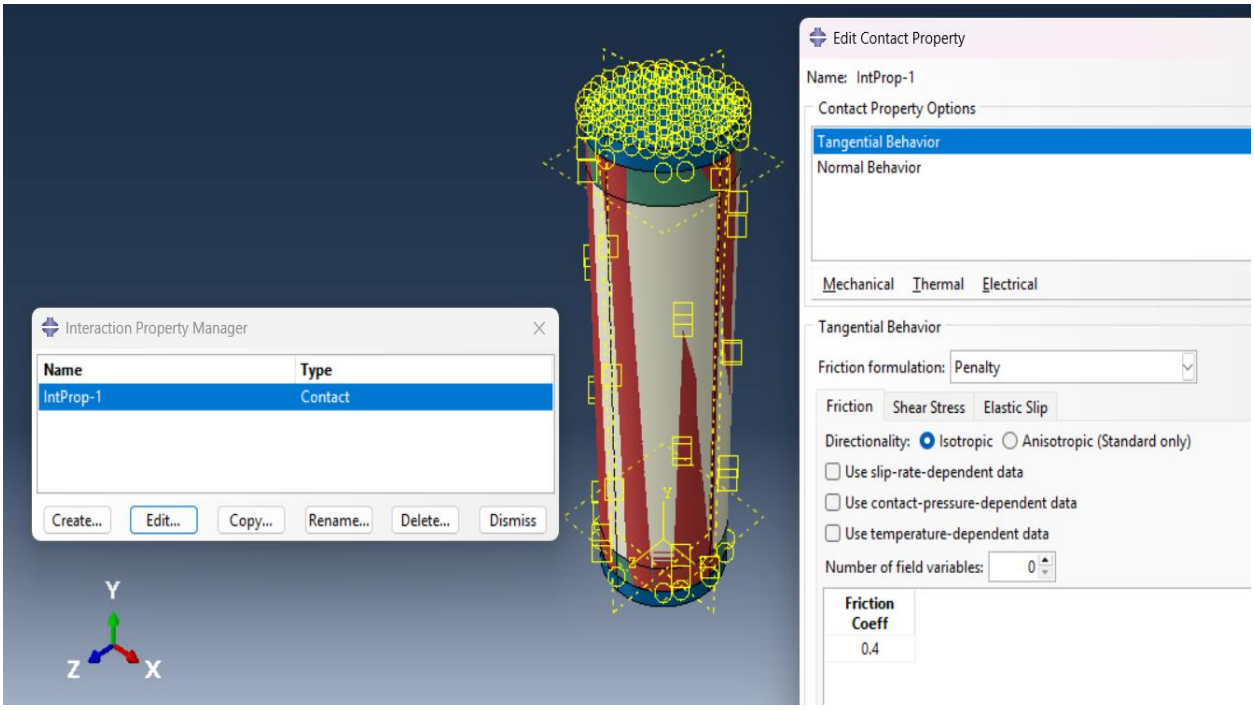

Figure 3.24 Input of Contact Properties Interaction of Tangential Behaviour Between the Outside Surface of Concrete and The Inside Surface of Aluminium.

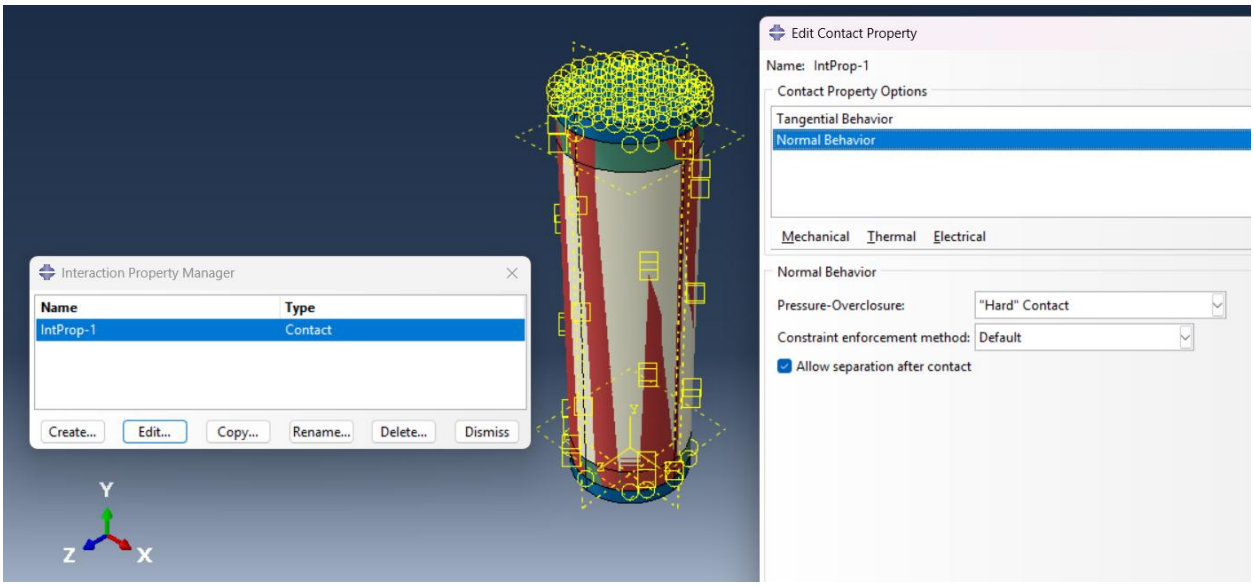

Figure 3.25 Input of Contact Properties Interaction of Normal Behaviour Between the Outside Surface of Concrete and The Inside Surface of Aluminium.

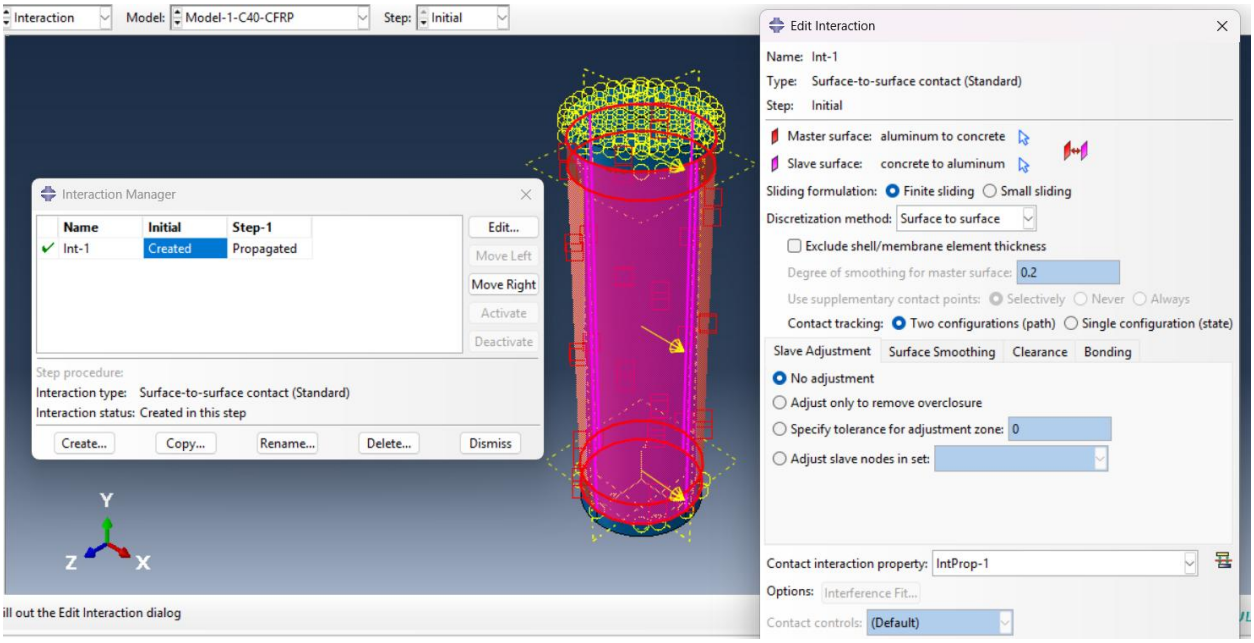

Figure 3.26 Surface-To-Surface Contact Among External Surface of Concrete and The Inside Surface of Aluminium.

3.3.3 Output Analysis

When using ABAQUS, analysing output involves looking at and making sense of the results from finite element simulations. This includes visualising the data, finding details like displacements

and stresses, and processing the information to draw useful conclusions. Comparing the results to real-world data or theoretical solutions helps ensure they are accurate, and sensitivity analysis shows how the system reacts to changes in parameters. The goal of output analysis in ABAQUS is to gain insights into the behaviour of complex systems, which in turn guides decisions and improvements in engineering.

3.3.3.1 Step Field

In ABAQUS, a step represents a unique phase or stage in a finite element analysis. Each step corresponds to a particular loading condition, boundary condition, or material behaviour that is applied to the model during the simulation. Steps are defined in order and can involve different actions like applying loads, displacements, temperature changes, or modifying material properties. Usually, a simulation consists of several stages, each depicting a specific aspect of structural response or material performance. For instance, in a structural examination, the stages could involve an initial phase for setting boundary conditions, followed by subsequent phases where forces or displacements are gradually applied. Similarly, in a material simulation, the stages could indicate various levels of material deformation, like elastic loading, plastic deformation, and eventual failure. The Step module in ABAQUS offers tools for defining, managing, and analysing each step of the simulation process. Users can choose the type of analysis, set boundary conditions, specify loadings, and adjust other parameters for each step. This organisation allows for accurate simulation of complex behaviours and loading conditions, leading to a thorough understanding of the system's response. Both static and large deformations are taken into account when figuring out what kind of solution to use, as shown in Figure 3.27.

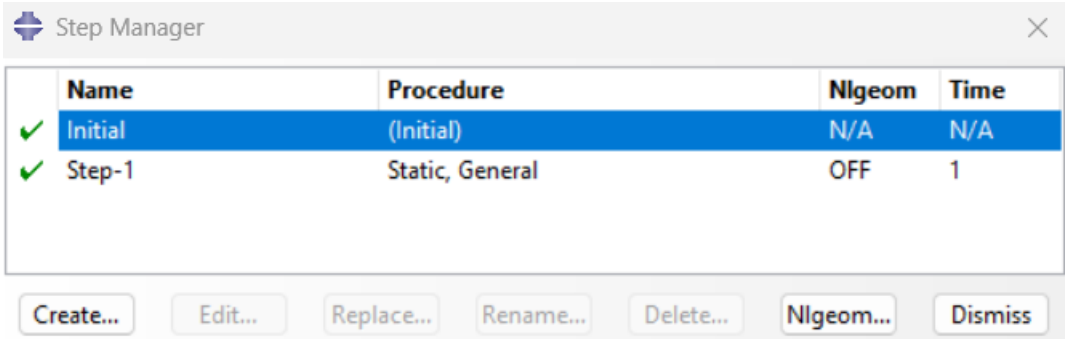

Figure 3.27 Determine the Solution Type Static.

3.3.3.2 Output Field and History

The output field and history are connected parts of the finite element analysis process, important for extracting and analysing simulation results over time or specific intervals. The Output field includes tools for visualising, extracting, and processing data produced during simulations. Users can view different quantities like deformations, stresses, strains, and displacements, understanding

the simulated system's behaviour. With post-processing methods, users can find more quantities or examine specific parts of the simulation results. History in the simulation context refers to the changing values of certain parameters over time. For instance, users may want to monitor how stress or displacement changes at nodes or elements throughout the simulation. ABAQUS offers features to specify and keep track of such historical data, enabling users to gather information at set intervals or specific time points. By merging the output field with historical data, users can efficiently study the evolution of different parameters throughout the simulation duration. This allows for a deeper understanding of temporary behaviours, dynamic reactions, and the development of deformation and stress patterns. Moreover, historical results help in comparing with real data or analytical forecasts, which assist in confirming and checking simulation outcomes. In general, the output section and historical results within ABAQUS are essential for examining and understanding finite element simulations, allowing users to obtain important insights and understand the behaviour of complicated systems being studied.

3.3.3.3 Job Field

For solving any FE problem, a suitable job analysis must be performed. Once completing the job analysis, the information has to be validated and submitted for findings to be analytically displayed.

- Model Setup: Users define the geometry, material properties, boundary conditions, loads, and other parameters necessary for the simulation within the job environment. This involves creating or importing the finite element model and specifying the analysis type (e.g., static, dynamic, thermal, etc.).
- Job Submission: Once the model setup is complete, users submit the job for analysis. ABAQUS then performs the calculations based on the specified parameters and settings. Users can submit multiple jobs simultaneously for efficient use of computational resources.
- Job Monitoring: During the analysis, users can monitor the progress of the job, including its status, computational progress, and any potential errors or warnings. This allows users to intervene if necessary and ensures the successful completion of the simulation.
- Results Post-Processing: After the job has finished running, users can access and analyse the simulation results within the job environment. This involves visualising the results, extracting relevant data, and performing further analysis or interpretation as needed.
- Job Management: The job field also includes features for managing simulation jobs, such as organising them into projects or folders, renaming, copying, deleting, or archiving completed jobs for future reference.

3.3.4 Results Post-Processing

Results post-processing involves two main aspects: results analysis and visualisation through figures and tables.

- Results Analysis: This aspect entails examining and interpreting the simulation outcomes to gain insights into the behaviour of the analysed system. It involves extracting relevant data from the simulation results, such as displacements, stresses, strains, reaction forces, etc. Users can analyse this data to understand the performance and response of the structure or material under various loading conditions. Analysis may include calculating derived quantities, comparing results against design criteria or standards, identifying critical areas or failure modes, and drawing conclusions about the system's behaviour.
- Figures and Tables: ABAQUS provides tools for visualising simulation results through figures and tables. Figures can display graphical representations of data, such as contour plots, stress-strain curves, displacement plots, and mode shapes. These visualisations help users to intuitively understand the distribution and variation of different quantities across the model. Tables present numerical data in a structured format, allowing for detailed analysis and comparison.

Figures (from Figure 3.28 to Figure 3.33) illustrate the cross-section shapes of parametric specimens.

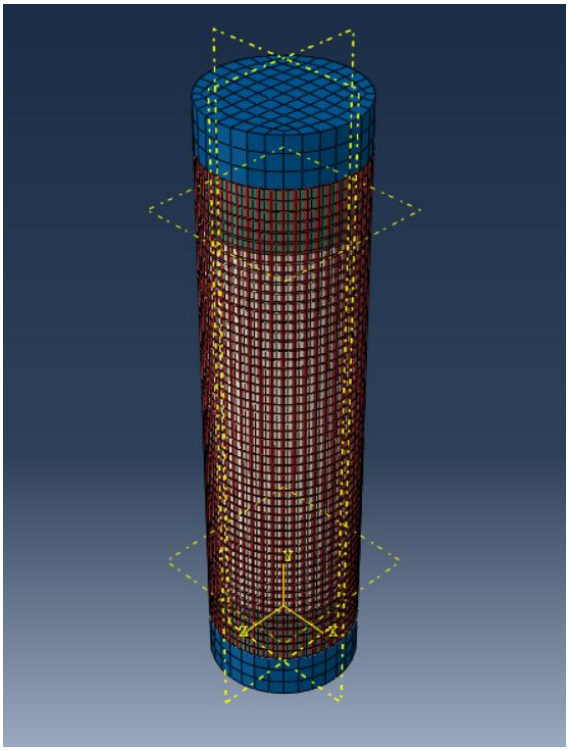

Figure 3.28 Circular Cross-Section Composite Column.

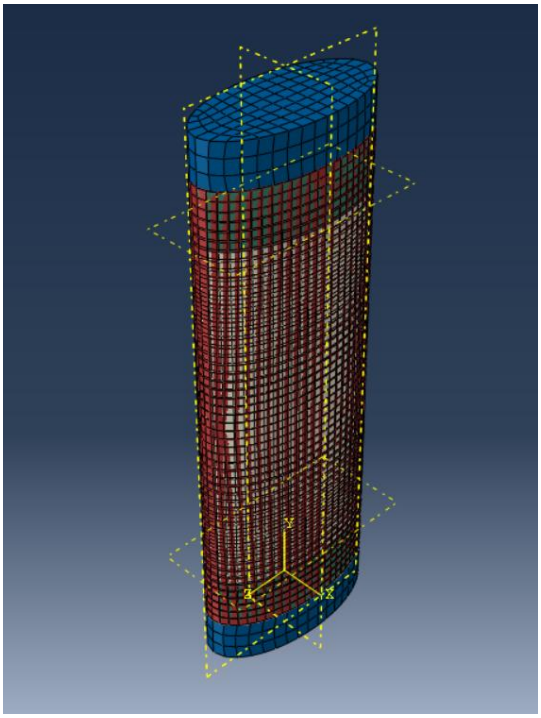

Figure 3.29 Elliptical Cross-Section Composite Column.

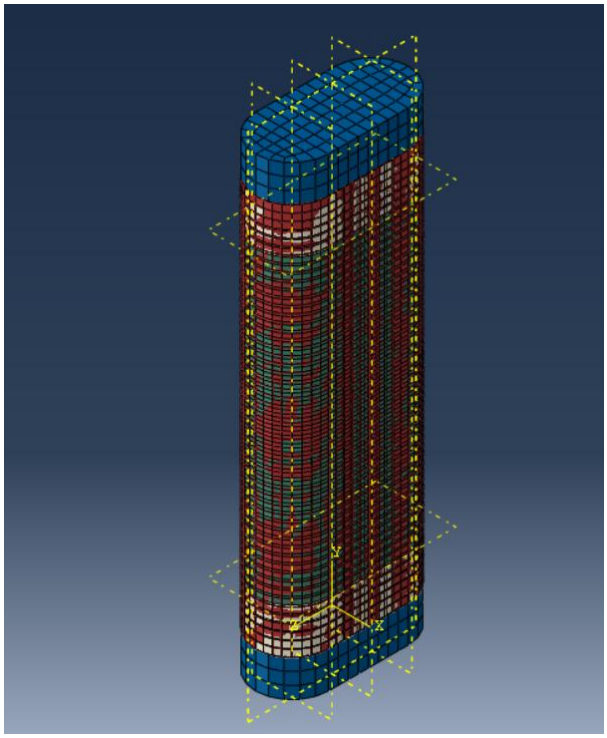

Figure 3.30 Round Ended Cross-Section Composite Column.

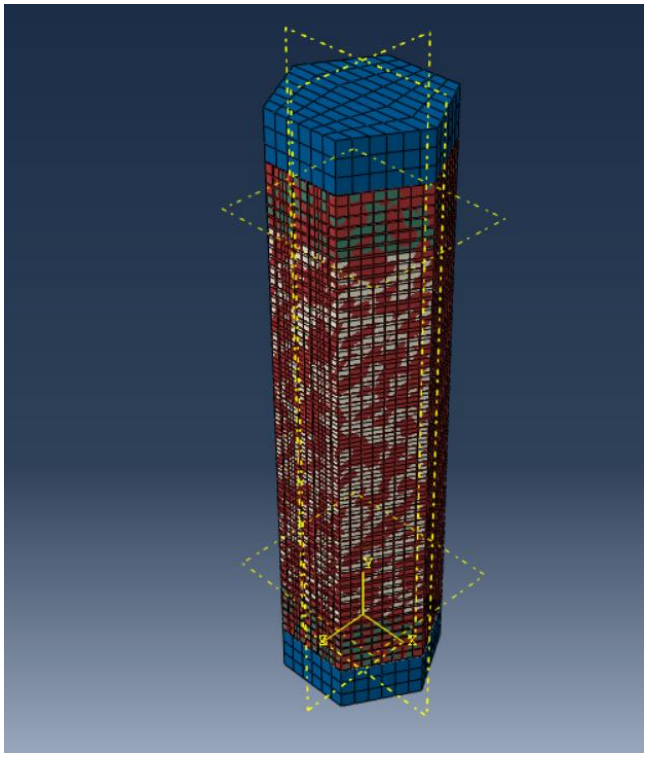

Figure 3.31 Hexagonal Cross-Section Composite Column.

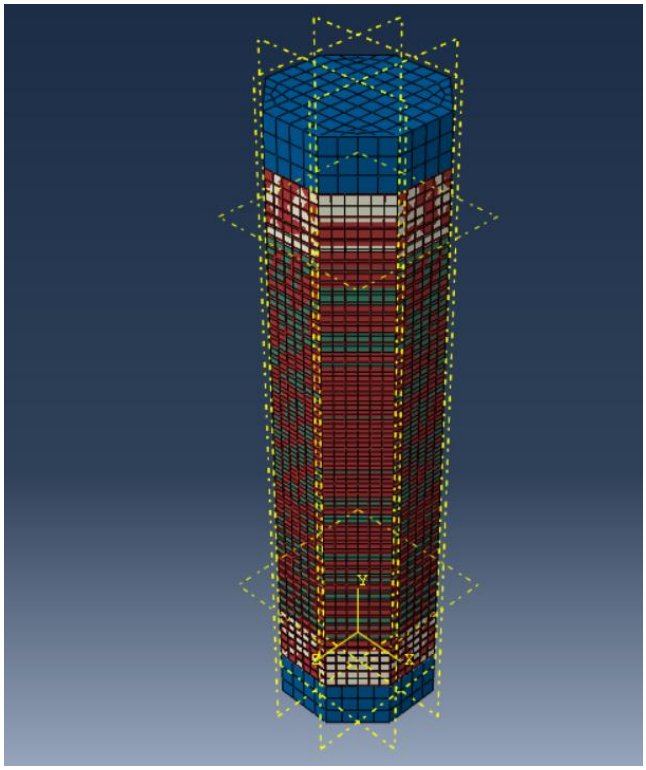

Figure 3.32 Octagonal Cross-Section Composite Column.

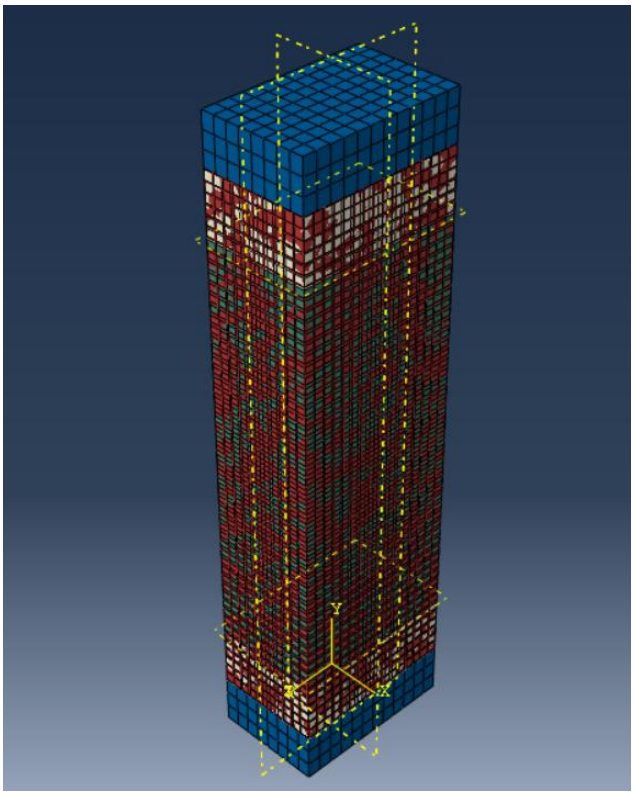

Figure 3.33 Rectangular Cross-Section Composite Column.

Chapter Four: Results and Discussions

4.1 Introduction

In this chapter, the experimental results obtained from previous studies of concrete-filled aluminium short columns of the rectangular and circular cross-sections will be compared with the theoretical results obtained from the finite element method simulation using ABAQUS/Standard 2019 software in terms of the load-axial strain relationship and ultimate load. Also, some important parameters that may affect the behaviour of such columns will be discussed through a parametric study conducted to determine the ultimate load, load deflection curves, and mode of failure patterns.

It is necessary to provide detailed descriptions about the methodologies utilised in numerical simulations (those carried out with the usage of ABAQUS / Standard 2019) and in experiments to ensure that there are clarity and rigour. Moreover, for the study to be credible, it would be worthwhile to highlight any shortcomings or uncertainties inherent within any of them.

4.2 Procedure of the Study

Using existing experimental data by [6] and [25] this study simulates the structural behaviour of different cross-sections for the aluminium-concrete composite short columns. Four groups of composite columns with different parameters are analysed.

The first group analyses the cross-section behaviour, which is presented by six different cross-sections with equivalent section area, length and volume of the circular reference column. The first group consists of two branches (curved or rounded cross-sections, polygon cross-sections). Curved cross-sections include three section shapes that were selected (circular, elliptical, round-ended). Polygon cross-sections with sharped cornered include three section shapes that were selected (rectangular, hexagonal, and octagonal). To understand the structural behaviour of these sections.

The second group investigated the effects of different aluminium proof stresses, which are 267.9 and 185.9Mpa reported by [6], and [25]. This group also uses the most common cross-sections used in buildings, which are circular and rectangular sections. To understand the impact of proof stress of aluminium on the behaviour of these sections.

The third group investigated the effects of different strengths of the cylindrical concrete, which are 44.8 and 70.2Mpa reported by Zhou and Young [6]. This group uses the most common cross-sections used in buildings, which are circular and rectangular sections. To understand the impact of compressive concrete strength on the behaviour of these sections.

The fourth group analyses the effect of different aluminium wall thicknesses, which are (1.9, 3, and 5 mm). This group also uses the most common cross-sections used in buildings, which are circular and rectangular sections. To understand the impact of different aluminium wall thicknesses on the behaviour of these sections.

4.3 Modelling Verification

Modelling verification is a crucial step in the development of reliable computational models, ensuring that the numerical model accurately represents the underlying theoretical formulation. In structural engineering, where simulations are often used to predict the behaviour of materials and components under various loading conditions, verification ensures that the model is solving the equations correctly, free from numerical errors.

Verification differs from validation in that it does not focus on comparing numerical results with experimental data but rather on confirming the mathematical and algorithmic accuracy of the simulation. This involves testing the model under controlled conditions, such as simplified loading scenarios or analytical benchmarks, where the expected outcomes are known. Any discrepancies between the numerical results and theoretical expectations can then be attributed to issues like mesh sensitivity, time-stepping errors, or incorrect implementation of material models.

In this study, the process of modelling verification has been conducted by examining key factors such as mesh independence, time step convergence, and algorithmic stability. Various model parameters will be systematically adjusted to ensure that the results are robust and independent of numerical artefacts. This verification process is essential to establish confidence in the model before it can be used for more complex simulations or further validation against experimental results. Through rigorous testing and refinement, the verified model can be relied upon for accurate predictions in structural analysis.

4.3.1 Summery of Experimental Data

The experimental data presented by [6], and [5] were adopted to verify the present FE model. The models used in this analysis are identical in terms of size, material characteristics, and boundary conditions.

This study employed the experimental study of aluminium-concrete composite with circular and rectangular cross-section columns by [6] and [5] to validate the finite element model (FEM) that was created. To understand the specimen labelling of the verification models it will be explained below

- The first four letters indicate the shape of aluminium tube and the test series, for example CHS is the circular hollow section. The fourth letter defines the specimen belonged to test series

- The designations (C70) and (C40) refer to concrete cylinder strength, where (C70) represents (f'_c=70.2MPa), and (C40) represents (f'_c=44.8MPa).

4.3.1.1 Circular Sections

To achieve this objective, two circular sections from [6] were adopted. The properties of material and dimensions for the above specimens are presented in Table 4.1 and Table 4.2. Experiments were conducted on concrete-filled tubes produced via extrusion using a high-strength 6061-T6 heat-treated aluminium alloy.

To reduce overall column buckling, for all stub column specimens, a constant L/D ratio of 3 was employed by selecting the lengths (L) of each one in relation to their diameters. The compressive strengths of concrete cores equal to 40MPa and 70MPa were employed to test the column samples. The concrete strength is marked by the letter "C" in the group label, which is followed by the compressive strength of the concrete core in MPa.

Table 4.1 Summarize of The CHS Column Test [6].

Samples	**Length, L (mm)**	**Thickness, T (mm)**	**Diameter, D (mm)**	**L/D**	**D/t**	**Aluminium tube, f_y (MPa)**	**Concrete, f'_c (MPa)**
CHS7C40	450	2.53	150.1	3	59.3	267.9	44.8
CHS7C70	451	2.54	150.1	3	59.1	267.9	70.2

Table 4.2 Aluminium Property of CHS Column Test [6].

Test group	Section D×t (mm)	$f_{0.2}$ (MPa)	f_u (MPa)	E_o (GPa)	ε_f (%)
CHS7	150×2.5	267.9	282.9	64.9	10.1

4.3.1.2 Rectangular Sections

To achieve this objective, two rectangular sections from [5] were adopted. The properties of the material and dimensions of these samples are presented in Table 4.3 and Table 4.4. Experiments were conducted on concrete-filled tubes produced via extrusion using a high-strength 6061-T6 heat-treated aluminium alloy.

In order to avoid global buckling of composite columns, the ratio of column height to the depth of the cross-sectional in uniform value is equal to 3. The structural performance of the (CFAT) columns was analysed using two concrete strengths of 40Mpa and 70MPa. The concrete strength is marked by the letter "C" within the group label, which is followed by the concrete strength in MPa.

Table 4.3 Summarize of The RHS Column Test [5].

Samples	Width, B (mm)	Thickness T (mm)	Length, L (mm)	Depth, D (mm)	L/D	D/t	Concrete, f'_c (MPa)	Aluminium tube, f_y (MPa)
RHS1C40	44.1	1.57	300	100	3	63.8	36.1	263
RHS1C70	44.1	1.57	300	100	3	63.7	74.4	263

Table 4.4 Aluminium Property of RHS Column Test [5].

Test group	Section D×B×t (mm)	$\sigma_{0.2}$ (MPa)	σ_u (MPa)	E_o (GPa)	ε_f (%)
RSH1	100×45×1.5	263	284	68.1	9.0

4.3.2 The Comparison Between Numerical Simulations and Laboratory Testing

To verify the proposed finite element model's (FEM) accuracy, the ultimate load capacity and the load-axial strain are two measurements which are utilised to analyse and compare the present model with experimental studies. Analysing and verifying the finite element design's validity is the main aim of this comparison.

Table 4.5 shows a comparison between the predicted FE column strength (P_{FEA}) and the test results. Initially, Table 4.5 clearly illustrates the good agreement between experimental research for ultimate load capacity and the results obtained from the ABAQUS (2019) model. The results of the numerical and experimental analyses for the specimens indicated an upper limit difference of 10%.

Table 4.5 Verification of Finite Element Model [5], [6].

Specimen	D/t	P_{Exp} (kN)	ε_{Exp}	P_{FEA} (kN)	ε_{FEA}	P_{Exp}/P_{FEA}	$\varepsilon_{Exp}/\varepsilon_{FEA}$
CHS7C40	59.3	1111.1	0.602154	1228.63	0.509663	0.9	1.1
CHS7C70	59.1	1496.4	0.510905	1643.18	0.497557	0.91	1
RHS1C40	63.8	182	0.518338	193.847	0.40461	0.94	1.2
RHS1C70	63.7	296	0.52594	296.595	0.44498	0.99	1.1

Four concrete-filled aluminium tube specimens were selected depending on the available experimental data, and their load-strain behaviour was also evaluated. The load-strain relationship comparing the experimental and proposed FE model is displayed in Figure 4.1.

The provided current model format presents a good high standard for its experiment match, and the present model effectively shows the relationship between load and strain. It can also be illustrated how the FE current model correlates with experiments through elastic and plastic phases.

It can be seen that the test curve is slightly lower compared to the corresponding FE curve of the specimen. Such a phenomenon is likely to occur for many reasons; one is that there might be a difference between coupon test data and actual material properties of specimens. Errors in geometrical measurements of the coupons, especially during the recording of the decimal values, can cause errors to arise in the cross-sectional area. Therefore, the tensile stress values calculated could be an artefact from the real mechanical response. The other reason is translating a mathematical model into a finite-element one, where the number of degrees of freedom is finite. The finite element analysis solution is impacted by various factors such as the number of elements, nodes per element, element shape functions, integration rules, and formulation details of specific elements. Except for these, experimental load versus strain curves can be predicted via the developed FE models.

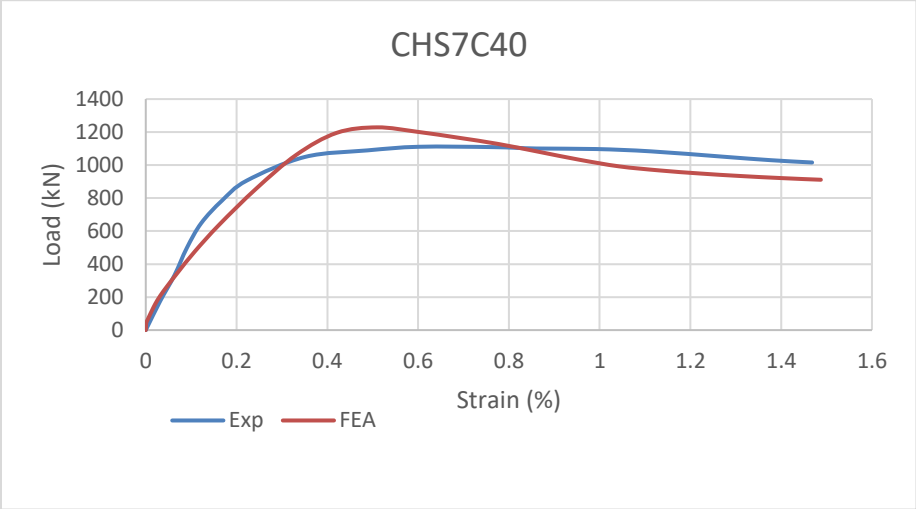

(A)

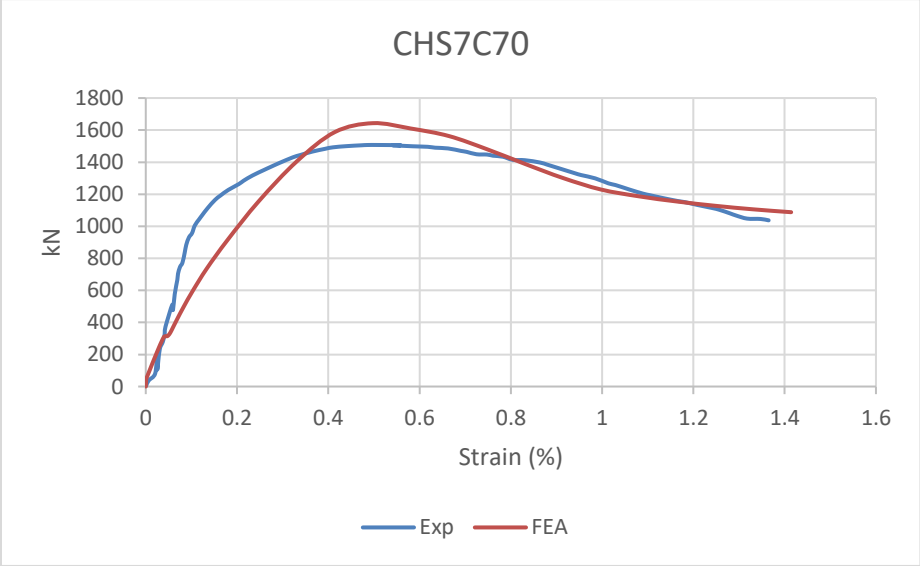

(B)

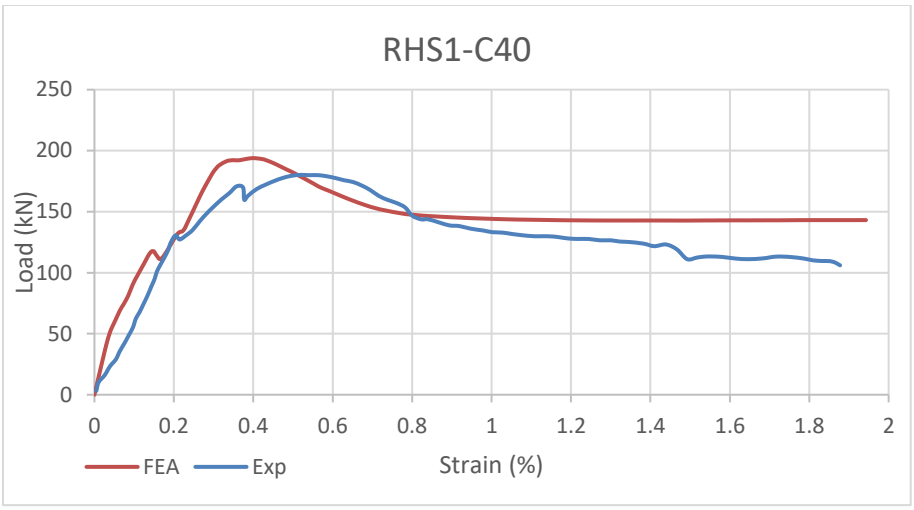

(C)

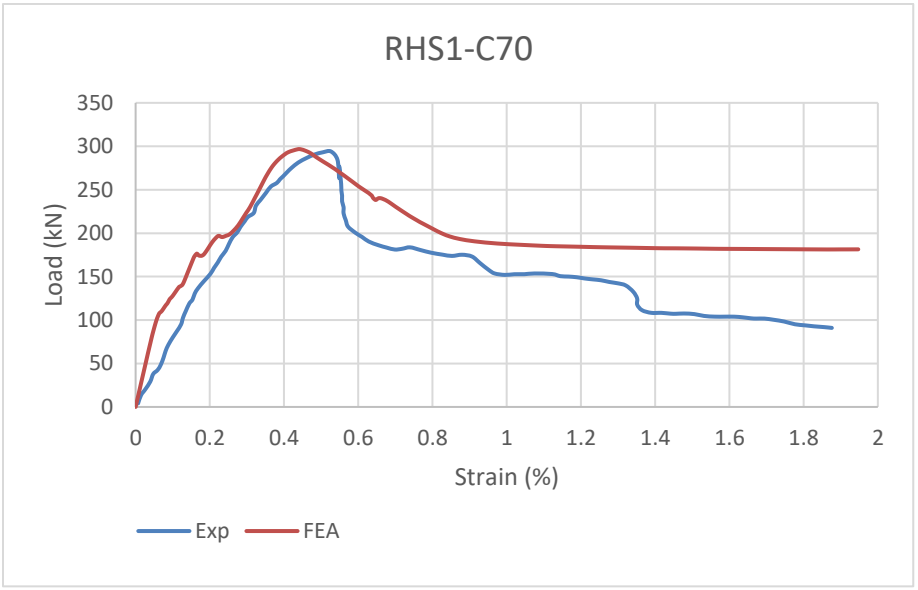

(D)

Figure 4.1 Experimental Versus Current FE Model for Columns.

4.4 Parametric Study

Experimental testing is constrained by high costs, specialised facilities, and the necessity for experienced staff members; however, Finite Element Modelling (FEM) offers a cost-effective alternative for conducting extensive parametric studies covering a significant number of variables. After the FE models were validated, an extensive parametric analysis was conducted to assess the impact of various factors, including geometric shape, aluminium strength, concrete strength, and

aluminium thickness, on the short column's structural performance. In total, 34 (CAFT) columns were modelled in this study.

The investigations are divided into four groups that present the influence of different parameters on the behaviour of a concrete filled with short aluminium columns, which have different cross-section shapes, different aluminium proof stress, different concrete cylinder strength, and different wall thicknesses of aluminium tubes.

4.4.1 Specimens Labelling

The column for test specimens is marked to denote the aluminium proof stress, cross-section shape, aluminium tube wall thickness, and the strength of the nominal concrete cylinder. The name labelling is explained below:

- T6 indicates 6061-T6 (high-strength material) heat-treated aluminium alloy, and T5 indicates 6063-T5 (normal-strength material) heat-treated aluminium alloy.
- Second letters are identifying the aluminium tube cross-section shape, with (C) indicating the circular hollow section.
- The second number specifies the aluminium tube thickness, where 2 indicates 2mm wall thickness.
- The designations (C70) and (C40) refer to concrete cylinder strength, where (C70) represents (f'_c=70.2MPa), and (C40) represents (f'_c=44.8MPa).

4.4.2 Specimens Details

The parametric study presented by six different cross-section groups with equivalent section area, length and volume of the circular cross-section reference columns. 34 specimens were used in a parametric investigation to understand the effect of cross-section shape on the (CFAT) columns' performance. They consist of 6 different cross-sections as shown in Figure 4.2. Two of them are circular and rectangular, which are two of the most prevalent in practical construction applications. The remaining cross-sections are elliptical, round-ended, hexagonal and octagonal. All specimens' details are explained in the tables (Table 4.6 to Table 4.9); therefore, the dimensions are in (mm) units, the aluminium proof stress (f_y) in (MPa), and the compressive concrete strength (f'_c) in (MPa). Dimensions are explained in tables (Table 4.6 to Table 4.9), where D and B are outer dimensions of the aluminium tubes, L is column height, and t is the aluminium tube thickness.

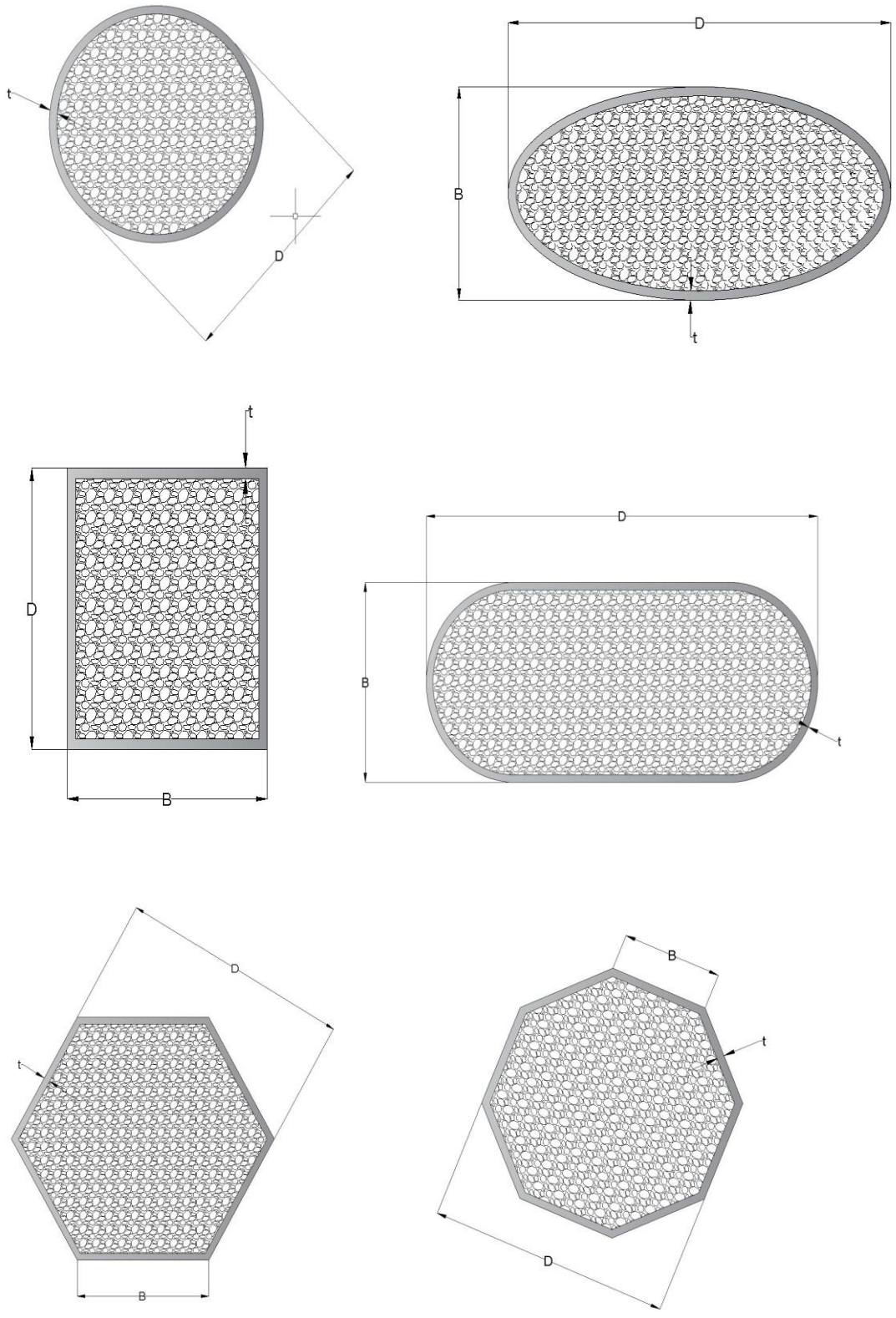

Figure 4.2 Specimens Shapes.

Table 4.6 Specimens' Details of Parametric Study for Group One.

Section	Specimen	L (mm)	t (mm)	B (mm)	D (mm)	A (mm2)	$\frac{D}{t}$	$\frac{Kl}{r}$	f_y	f'_c
Circular	T6C2C40	215	2	-	66	3421.2	33	13.03	267.9	44.8
	T6C3C40	440	3	-	135	14313.9	45	13.03	267.9	44.8
	T6C4C40	765	4	-	235	43373.7	58.7	13.02	267.9	44.8
Rectangular	T6R2C40	215	2	47.7	71.6	3421.5	35.8	15.58	267.9	44.8
	T6R3C40	440	3	97.7	146.5	14317.9	48.8	15.58	267.9	44.8
	T6R4C40	765	4	170	255	43373.4	63.7	15.58	267.9	44.8
Elliptical	T6E2C40	215	2	46.6	93.3	3420.5	46.6	18.42	267.9	44.8
	T6E3C40	440	3	95.4	190.9	14313.6	63.6	18.42	267.9	44.8
	T6E4C40	765	4	166.1	332.3	43373.6	83.1	18.41	267.9	44.8
Round Ended	T6RE2C40	215	2	43.7	87.5	3418.9	43.7	18.03	267.9	44.8
	T6RE3C40	440	3	89.5	179.1	14311.1	59.6	18.03	267.9	44.8
	T6RE4C40	765	4	155.8	311.7	43371.5	77.9	18.02	267.9	44.8
Hexagonal	T6H2C40	215	2	36.2	62.8	3421.5	31.4	12.97	267.9	44.8
	T6H3C40	440	3	74.2	128.5	14313.9	42.8	12.97	267.9	44.8
	T6H4C40	765	4	129.2	223.7	43375.4	55.9	12.97	267.9	44.8
Octagonal	T6O2C40	215	2	26.6	64.2	3421.5	32.1	17.68	267.9	44.8
	T6O3C40	440	3	54.4	131.4	14313.6	43.8	17.69	267.9	44.8
	T6O4C40	765	4	94.7	220.8	43374.7	55.2	17.68	267.9	44.8

Table 4.7 Specimens' Details of Parametric Study for Group Two.

Section	Specimen	L (mm)	t (mm)	B (mm)	D (mm)	A (mm2)	$\frac{D}{t}$	$\frac{Kl}{r}$	f_y	f'_c
Circular	T5C2C40	215	2	-	66	3421.2	33	13.03	185.9	44.8
	T5C3C40	440	3	-	135	14313.9	45	13.03	185.9	44.8
	T5C4C40	765	4	-	235	43373.7	58.7	13.02	185.9	44.8
	T6C2C40	**21**5	2	-	66	3421.2	33	13.03	267.9	44.8
	T6C3C40	440	3	-	135	14313.9	45	13.03	267.9	44.8
	T6C4C40	765	4	-	235	43373.7	58.7	13.02	267.9	44.8
Rectangular	T5R2C40	215	2	47.7	71.6	3421.5	35.8	15.58	185.9	44.8
	T5R3C40	440	3	97.7	146.5	14317.9	48.8	15.58	185.9	44.8
	T5R4C40	765	4	170	255	43373.4	63.7	15.58	185.9	44.8
	T6R2C40	215	2	47.7	71.6	3421.5	35.8	15.58	267.9	44.8
	T6R3C40	440	3	97.7	146.5	14317.9	48.8	15.58	267.9	44.8
	T6R4C40	765	4	170	255	43373.4	63.7	15.58	267.9	44.8

Table 4.8 Specimens' Details of Parametric Study for Group Three.

Section	Specimen	L (mm)	t (mm)	B (mm)	D (mm)	A (mm2)	$\frac{D}{t}$	$\frac{Kl}{r}$	f_y	f'_c
Circular	T6C2C40	215	2	-	66	3421.2	33	13.03	267.9	44.8
	T6C3C40	440	3	-	135	14313.9	45	13.03	267.9	44.8
	T6C4C40	765	4	-	235	43373.7	58.7	13.02	267.9	44.8
	T6C2C70	215	2	-	66	3421.2	33	13.03	267.9	70.2
	T6C3C70	440	3	-	135	14313.9	45	13.03	267.9	70.2

	T6C4C70	765	4	-	235	43373.7	58.7	13.02	267.9	70.2
Rectangular	T6R2C40	215	2	47.7	71.6	3421.5	35.8	15.58	267.9	44.8
	T6R3C40	440	3	97.7	146.5	14317.9	48.8	15.58	267.9	44.8
	T6R4C40	765	4	170	255	43373.4	63.7	15.58	267.9	44.8
	T6R2C70	215	2	47.7	71.6	3421.5	35.8	15.58	267.9	70.2
	T6R3C70	440	3	97.7	146.5	14317.9	48.8	15.58	267.9	70.2
	T6R4C70	765	4	170	255	43373.4	63.7	15.58	267.9	70.2

Table 4.9 Specimens' Details of Parametric Study for Group Four.

Section	Specimen	L (mm)	t (mm)	B (mm)	D (mm)	A (mm2)	$\frac{D}{t}$	$\frac{Kl}{r}$	f_y	f'_c
Circular	T6C5C40	440	5	-	135	14313.9	27	13.025	267.9	44.8
	T6C3C40	440	3	-	135	14313.9	45	13.026	267.9	44.8
	T6C1.9C40	440	1.9	-	135	14313.9	71	13.025	267.9	44.8
Rectangular	T6R5C40	440	5	97.7	146.55	14317.9	29.3	15.58	267.9	44.8
	T6R3C40	440	3	97.7	146.55	14317.9	48.8	15.58	267.9	44.8
	T6R1.9C40	440	1.9	97.7	146.55	14317.9	77	15.58	267.9	44.8

4.4.2.1 Cross-Sectional Slenderness

According to AISC 360, [60] can classify the slenderness of cross-sections of circular and rectangular section shapes, which are the only classifications of cross-section available in the AISC 360. Due to the lack of a slender rating of the aluminium concrete composite columns' cross-section in codes, it was necessary to use the classification specific to steel in AISC 360 and substitute the aluminium value instead of the steel value. Following the approach taken by researchers in previous studies [32], [61]. According to AISC 360, the slenderness of a cross-section is classified as slender, noncompact, or compact. The cross-section is classified as a slender section if the diameter to-wall-thickness ratio is bigger than λr. The cross-section is classified as a noncompact section if the external diameter to wall thickness ratio is bigger than λp and lower than λr. The cross-section is classified as compact when the ratio of diameter to tube thickness is less than λp. According to Table I1.1a in the structural steel buildings specification, AISC 360, 2016. As a result, the study was conducted on a range of external diameter to wall thickness ratios of rectangular and circular section samples that include compact, noncompact, and slender sections, as shown in Table 4.10.

To discuss the effect of the tube thickness parameter, the four groups use different tube thicknesses with a constant value of the external dimension of the tube for circular and rectangular sections. This helps us to understand the effect of using a different range of tube thickness. The four groups also contain a range of diameter to wall thickness ratios of circular and rectangular section tubes that include compact, noncompact, and slender sections. The following equations (from Equation 4.1 to Equation 4.3) are used to classify the cross sectional slenderness of a circular shape. For classification of cross-sectional slenderness, for rectangular shapes, Equations (from Equation 4.4 to Equation4.6) are used.

For circular sections: -

$$\lambda_p = \frac{0.15\,E}{f_y} \quad (4.1)$$

$$\lambda_r = \frac{0.19\,E}{f_y} \quad (4.2)$$

$$\text{Maximum permitted} = \frac{0.31\,E}{f_y} \quad (4.3)$$

For rectangular sections: -

$$\lambda_p = 2.26 \times \sqrt{\frac{E}{f_y}} \quad (4.4)$$

$$\lambda_r = 3 \times \sqrt{\frac{E}{f_y}} \quad (4.5)$$

$$\text{Maximum permitted} = 5 \times \sqrt{\frac{E}{f_y}} \quad (4.6)$$

Table 4.10 Details of Cross-Sectional Slenderness Classification.

Section	Specimen	λ	λ_p	λ_r	Maximum permitted	AISC360 section type
Circular	T6C2C40	33	36.338	46.02836	75.098	Compact
	T6C3C40	45	36.338	46.02836	75.098	Noncompact
	T6C4C40	58.75	36.338	46.02836	75.098	Slender
	T6C5C40	25	36.338	46.02836	75.098	Compact
	T6C1.9C40	69.05	36.338	46.02836	75.098	Slender
	T5C2C40	33	54.14	68.57	111.89	Compact
	T5C3C40	45	54.14	68.57	111.89	Compact
	T5C4C40	58.7	54.14	68.57	111.89	Noncompact
Rectangular	T6R2C40	32.82	35.1758	46.6935	77.82264	Compact
	T6R3C40	45.85	35.1758	46.6935	77.82264	Noncompact
	T6R4C40	60.767	35.1758	46.6935	77.82264	Slender
	T6R5C40	26.31	35.1758	46.6935	77.82264	Compact
	T6R1.9C40	74.13	35.1758	46.6935	77.82264	Slender
	T5R2C40	32.82	42.9	56.99	94.9	Compact
	T5R3C40	45.85	42.9	56.99	94.9	Noncompact
	T5R4C40	60.767	42.9	56.99	94.9	Slender

4.4.2.2 Column Height

Column specimens used in this investigation are classified as short columns to exclude the global buckling of columns and focus on the cross-section shape effect. All specimens are classified according to ACI 318-19 [62] as short columns, which are often used to indicate a column with a strength equal to that computed for its cross-section. The slenderness ratios of all columns (Kl/r)

are under 22 (for columns not braced against side sway) to confirm all columns are classified as short as shown in Table 4.11, where the radius of gyration is obtained by equation 4.7

$$r = \sqrt{\frac{I_g}{A_g}} \quad 4.7$$

Table 4.11 Details of Columns Height Classification

Section	Specimen	D (mm)	t (mm)	A (mm)	I (mm^4)	Radius of gyration (mm)	$\frac{Kl}{r}$	Column height
Circular	T6C2C40	66	2	3421	931422	16	13.02	Short
	T6C3C40	135	3	14313	16304443	33.75	13.02	Short
	T6C4C40	235	4	43373	149707088	58.75	13.02	Short
	T6C5C40	135	5	14313	16304443	33.75	13.02	Short
	T6C1.9C40	135	1.9	14313	16304443	33.75	13.02	Short
Rectangular	T6R2C40	71	2	3421	650380	13.787	15.58	Short
	T6R3C40	146	3	14317	11389070	28.2035	15.58	Short
	T6R4C40	255	4	43373	104514294	49.088	15.58	Short
	T6R5C40	146	5	14317	11389070	28.2035	15.58	Short
	T6R1.9C40	146	1.9	14317	11389070	28.2035	15.58	Short

4.4.2.3 Ductility Index

In structural engineering, ductility is an important measure of how effectively columns work. It describes how efficiently a member can handle a lot of plastic deformation without losing its ability to bear weight or structural rigidity all of a sudden [63].

The ductility index can be calculated using the load-displacement curve by dividing the (Δ0.85) by (Δu). as shown in Figure 4.3. Thus, the ductility is obtained by equation 4.8 [64]

$$DI = \frac{\Delta_{0.85}}{\Delta_u} \quad 4.8$$

Were

Δ 0.85 is the displacement at (0.85 from ultimate load) in plastic region.

Δ u is the displacement at ultimate load

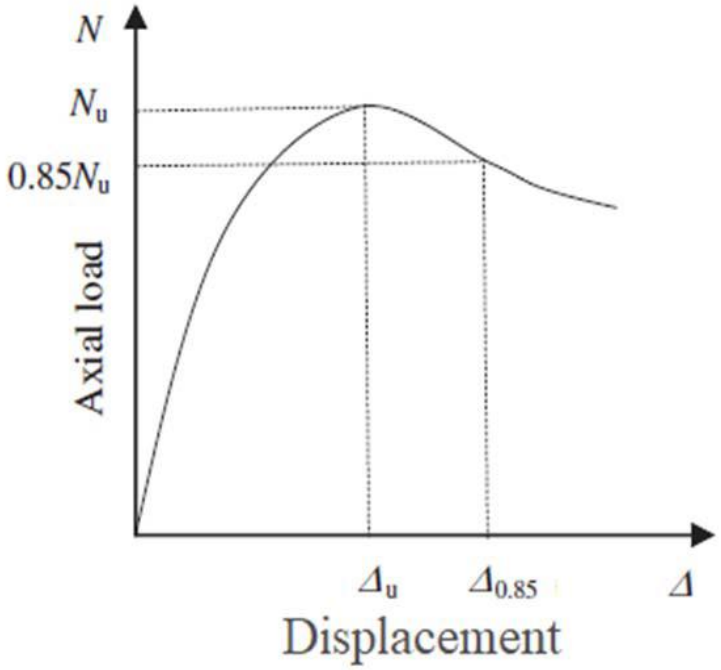

Figure 4.3 Illustrate of Ductility Index.[64]

4.4.2.4 Material Properties

The experimentally determined material characteristics of the concrete core and aluminium tubes by [6], and [25] were employed in this parametric investigation. Table 4.12 explained properties for 6061-T6 and 6063-T5 aluminium alloys.

Aluminium material is a sort of nonlinearity classification, which doesn't have a sharp yielding stress point, so the stress in 0.2% plastic strain (0.2% aluminium proof stress) was dependent in this study, which is a widely adopted concept. Specimens of group one, group three, and group four are made of 6061-T6 (high-strength material) heat-treated aluminium alloy. Zhou and Young's (2009) [6] experimental data showed that the (T6) tubes of aluminium in (group CHS7) with high-strength had a nonlinear stress-strain response, with a proof stress of 267.9MPa. Specimens of Group Two using 6063-T5 (normal strength material) heat-treated aluminium alloy. The specimen (N-C2-NW), which is made of a normal-strength aluminium tube, displays a non-linear stress-strain behaviour, measured by [25], with a proof stress of 185.9 MPa.

Table 4.12 Aluminium Property of Parametric Study [6][25].

Aluminium alloy	E_o (GPa)	$\sigma_{0.2}$ (MPa)	σ_u (MPa)	ε_f (%)
6063-T5	67.1	185.9	207.7	10.4
6061-T6	64.9	267.9	282.9	10.1

For specimens of group one, group two, and group four, the compressive concrete cylinder strength equal to 44.8MPa, as presented by [6], was adopted for the concrete infill. On the other hand, for specimens of group three, the compressive concrete cylinder strength of 70.2 MPa, as presented by [6], was adopted for the concrete infill.

4.4.3 Effect of Cross-Section Shape (Group One)

Commonly, stub columns are utilised in both experimental and numerical studies to decrease the effects of global buckling and thus isolate the performance of composite members against axial compression. The cross-sectional geometry of aluminium -filled concrete stub columns, however, is an important factor that controls the interaction between the cover of the aluminium and the concrete core, thus affecting ultimate load, stiffness degradation, ductility and failure modes.

The present group of experiments is aimed at investigating the structural behaviour of different cross-sections of aluminium -filled concrete stub columns under axial compression. The comparison of these different geometries allows one to analyse the cross-sectional shape influence on the load-carrying capacity, confinement efficiency, and failure mechanisms. The results will not only clarify the mechanical behaviour of the combined (aluminium -concrete) columns with varying cross-sections but also help provide the correct data to contribute later, more efficient design approaches for the majority of aluminium -filled concrete short members with proper cross-sections for the target requirement.

This group presents six different cross-section groups with equivalent section area, length, wall thickness, and volume of the circular cross-sections as reference columns to make the specimens comparable and uses the same material properties for all the specimens of this group. 18 specimens were used in this group to understand how the cross-section shape affects (CFAT) columns' behaviour. This group branches into two branches, which are curved or rounded cross-sections and polygon cross-sections with sharp corners. The curved or rounded cross-sections include circular, elliptical, and round-ended cross-sections. These curved cross-sections have the feature that the outer edges are smooth and rounded. The main objective of this branch is to investigate how the degree of curvature impacts the performance of the column in terms of axial behaviour, ultimate load, stiffness, and ductility for short, unreinforced concrete columns confined with aluminium. A lot of investigations have been done on circular concrete columns filled with aluminium tubes, but little attention has been put on columns with polygon cross-sections, which, although they are good at handling architectural and structural applications. Sharp-cornered sections, like rectangular, hexagonal, and octagonal sections, totally change the confinement and stress distribution patterns when compared to smooth or rounded sections.

4.4.3.1 Results and Discussion

(A) Ultimate load

Table 4.13 indicates that circular cross-sections always outperformed the remaining geometric shapes regarding the ultimate load capacity for all of the different diameter-to-thickness ratios that were studied. In circular sections, the compressive stresses are distributed continuously around the perimeter, which reduces local stress concentrations and delays the initiation of buckling or crushing. This geometric advantage becomes especially important when the diameter-to-thickness ratio changes, because the circular shape can maintain a more stable confinement mechanism over a wider range of slenderness conditions. Loading stresses in circular cross-section columns have equal distribution across the entire perimeter, thus avoiding stress concentrations observed in the corners of polygonal shapes. Another important reason is the confinement effect. In columns such as concrete-filled aluminium tubes, the circular aluminium shell provides nearly uniform lateral confinement to the concrete core. This improves the compressive strength and ductility of the core concrete, allowing the column to sustain higher loads before failure. Because the confinement is uniform in a circular section, the aluminium tube and concrete core interact more effectively than in other sections, where the confinement is nonuniform and weaker at corners.

The columns having elliptical cross-sections (T6E2C40, T6E3C40, T6E4C40) exhibited ultimate load decreases of 6%, 5%, and 3%, respectively, compared with their circular reference equivalents. The small decreases come due to the elliptical shape's lower consistency in curvature, which slightly lowers the smallest moment of inertia in the major axis direction and induces uneven stress distribution. The circular section has a constant radius in every direction, which means its geometric stiffness is the same for any in-plane axis. This gives it a more uniform resistance to compression and stress concentration. By contrast, an elliptical section has different major and minor axes, so the curvature is not constant and the distance of the boundary from the centroid varies with direction. As a result, the moment of inertia changes with axis orientation, and the section becomes weaker along the axis with the smaller radius.

The columns having round-ended cross-sections (T6RE2C40, T6RE3C40, T6RE4C40) exhibited decreases of 5%, 4%, and 4%, respectively, compared with their circular reference equivalents. The rounded ends improve performance by lowering the concentration of stress at corners; however, elliptical and round ended cross-section columns remain less efficient compared to complete circular shaped columns. round-ended sections, although smoother than rectangular or square sections, still include transition regions where curvature is not perfectly uniform, and these regions slightly disturb the stress flow. This makes the structural response less efficient than a complete circle.

The columns having a hexagonal cross-section (T6H2C40, T6H3C40, T6H4C40) indicated reductions of 10%, 11%, and 9%, respectively, compared with their circular reference equivalents. The octagonal changes (T6O2C40, T6O3C40, T6O4C40) displayed decreases of 9%, 10%, and

9%, respectively, compared with their circular reference equivalents. When the section becomes hexagonal or octagonal, the presence of flat faces and corners changes the stress path, so the load is no longer carried as smoothly as in the circular case. This can reduce the effective structural efficiency even if the total area is similar. Corners are important because they act as zones of stress concentration and can trigger earlier localized yielding under compressive load, especially in thin-walled tubular members.

The columns having rectangular cross-sections (T6R2C40, T6R3C40, T6R4C40) exhibited the lowest efficiency, displaying reductions of 12%, 14%, and 12%, respectively, compared with their circular reference equivalents. The cause of this effect corresponds to the considerable asymmetry in the moment of inertia (at least across the weakest axis), increased slenderness within one direction, and sharp corners, which act like buckle initiators, leading to an early development of damaging failure.

The columns having polygonal cross-sections, which have sharp edges, indicate that those having a larger number of corners, like octagonal shapes, provide a greater ultimate load capacity compared to hexagonal shapes, which exceed rectangular shapes. This order basically comes from the theories of stress distribution from structural mechanics. The polygons having a greater number of edges closely correspond to a circular shape, therefore improving the moment of inertia and decreasing stress concentrations at sharp corners, where stress risers may result in early failure beneath axial compression. Sharp corners in polygons having fewer sides (such as rectangles having four edges) create concentrated high-stress areas, decreasing buckling resistance and ultimate load. The hexagons, having six corners, improve this by enabling smooth curve transformations, while octagonal shapes, having eight edges, achieve a more uniform distribution of load, reaching the uniform strength found in circular sections.

The higher ultimate load observed in columns with curved cross-sections such as circular, elliptical, and round-ended sections can be attributed primarily to their more uniform stress flow under compression. Unlike sharp-edged polygonal sections, curved geometries do not contain corners that intensify local stresses, so the axial load is distributed more evenly around the perimeter. This reduces premature localized yielding and delays the formation of critical weak zones, allowing the column to sustain a larger compressive load before failure.

Table 4.13 Specimen's Details and Results (Group One).

Section	Specimen	$\frac{D}{t}$	$P_{FEA\ (kN)}$	DI	Change %
Circular	T6C2C40	33	297	3.03	1.93
	T6C3C40	45	1109	1.99	1.29
	T6C4C40	58.7	3027	1.8	1.23

Rectangular (control DI)	T6R2C40	35.8	262	1.57	0
	T6R3C40	48.8	959	1.54	0
	T6R4C40	63.7	2677	1.46	0
Elliptical	T6E2C40	46.6	279.7	1.77	1.13
	T6E3C40	63.6	1051.8	1.58	1.03
	T6E4C40	83.1	2933.8	1.51	1.03
Round Ended	T6RE2C40	43.7	280.7	1.65	1.05
	T6RE3C40	59.6	1064.8	1.55	1.006
	T6RE4C40	77.9	2911	1.49	1.02
Hexagonal	T6H2C40	31.4	268	1.71	1.09
	T6H3C40	42.8	982.1	1.59	1.03
	T6H4C40	55.9	2741	1.54	1.05
Octagonal	T6O2C40	32.1	270.6	2.47	1.57
	T6O3C40	43.8	998.6	1.69	1.1
	T6O4C40	55.2	2755.7	1.57	1.08

(B) load-axial deformation curves

The resulting load-axial deformation graph was determined and drawn for all concrete-filled aluminium tube column specimens with different cross-sections. Figure 4.4 displays the estimation achieved by ABAQUSE (2019) using the current finite element model.

During the elastic area, the initial stiffness, defined as the slope along the curve, shows little variation with respect to sectional shape at low diameter-to-wall thickness (D/t) ratios, clearly seen in Figure 4.4(A). It is because of the dominance of global axial stiffness based on the characteristics of the combined material and the little effect of local geometrical parameters at small slenderness.

On the other hand, at greater D/t ratios, the elastic slope was considerably higher in curve cross-sections as compared with sharp-cornered sections [Figure 4.4(B, C)]. The enhancement is due to improved yielding resistance in curved sections, which delays the development of geometric nonlinearity by enabling an even radial distribution of stresses and lowering concentrations of stress in corners.

The ultimate load of columns displayed some variation according to section shape, corresponding to the previous paragraph.

Table 4.13 proved ductility significantly enhances with circular-section columns (T6C2C40, T6C3C40, T6C4C40) with an increase in the ductility index of (3.03, 1.99, 1.8), specifically by (1.93%, 1.29%, 1.23%) respectively, higher than rectangular section control columns (T6R2C40,

T6R3C40, T6R4C40). because of the better radial confinement of the concrete core, increasing post-yield absorbing energy from higher shear transferring and crack bonding.

The elliptical cross-section columns (T6E2C40, T6E3C40, T6E4C40) with increasing in ductility index of (1.77, 1.58, and 1.51) specifically (1.13%, 1.03%, and 1.03%) respectively higher than rectangular section control columns. The round-ended cross-section columns (T6RE2C40, T6RE3C40, T6RE4C40) with increasing ductility index of (1.65, 1.55, and 1.49) specifically (1.05%, 1.006%, and 1.02%) higher than the rectangular section control columns respectively. The improved ductility of the elliptical and round-ended columns is scientifically explained by reduced stress concentration, better confinement, delayed concrete crushing, and a more stable post-peak response. The elliptical section performed best because its geometry provided the smoothest stress flow and the most effective deformation capacity.

The hexagonal cross-section columns (T6H2C40, T6H3C40, T6H4C40) with increasing in ductility index of (1.71, 1.59, and 1.54) specifically (1.09%, 1.03%, and 1.05%) higher than the rectangular section control columns respectively. The ductility in polygonal-section columns increased linearly with the number of edges, showing an improved estimate of circular symmetry, which decreases stress concentrations at angles and improves total deformability through distribution yielding. This can be observed in octagonal cross-sectional columns (T6O2C40, T6O3C40, T6O4C40) with an increase in ductility index of (2.47, 1.69, and 1.57) specifically by (1.57%, 1.1%, and 1.08%) higher than the rectangular section control columns respectively.

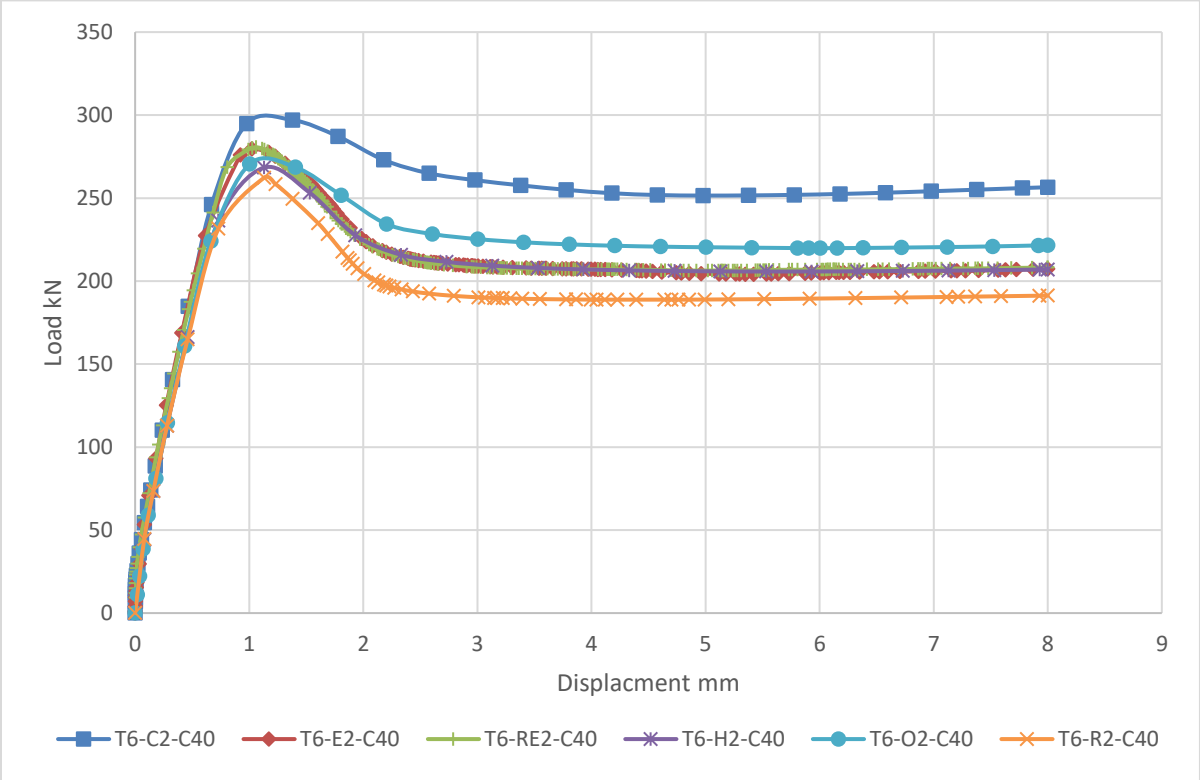

(A)

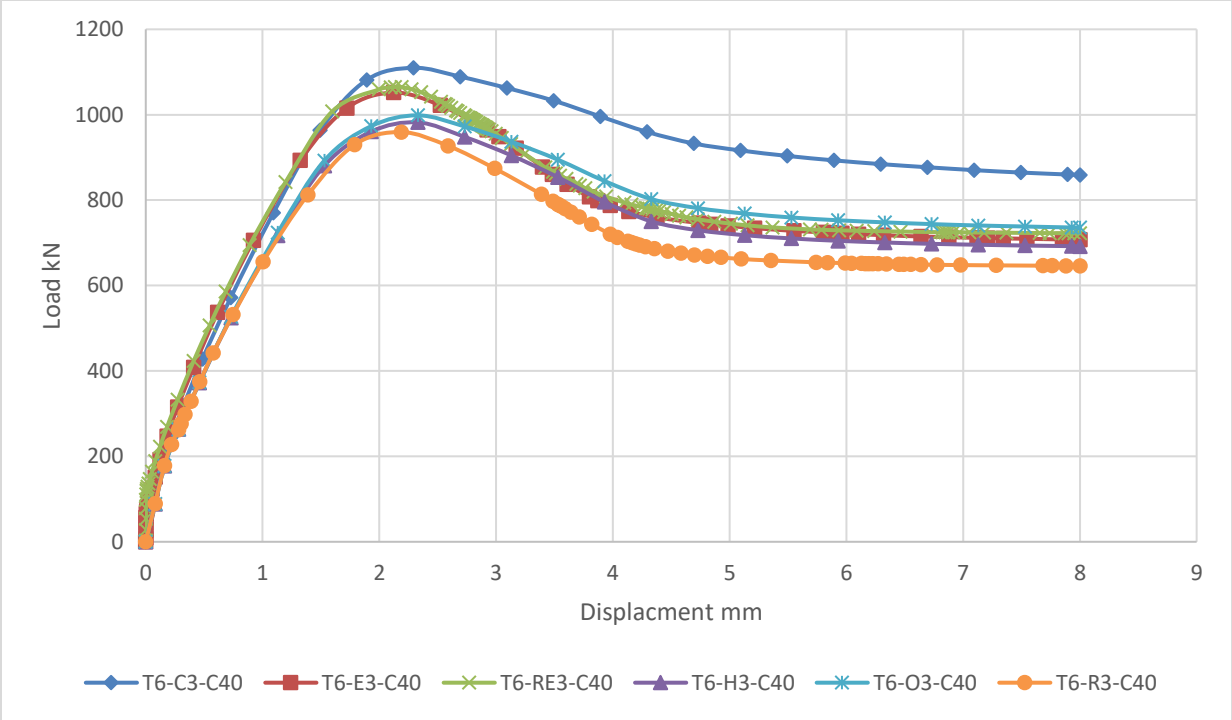

(B)

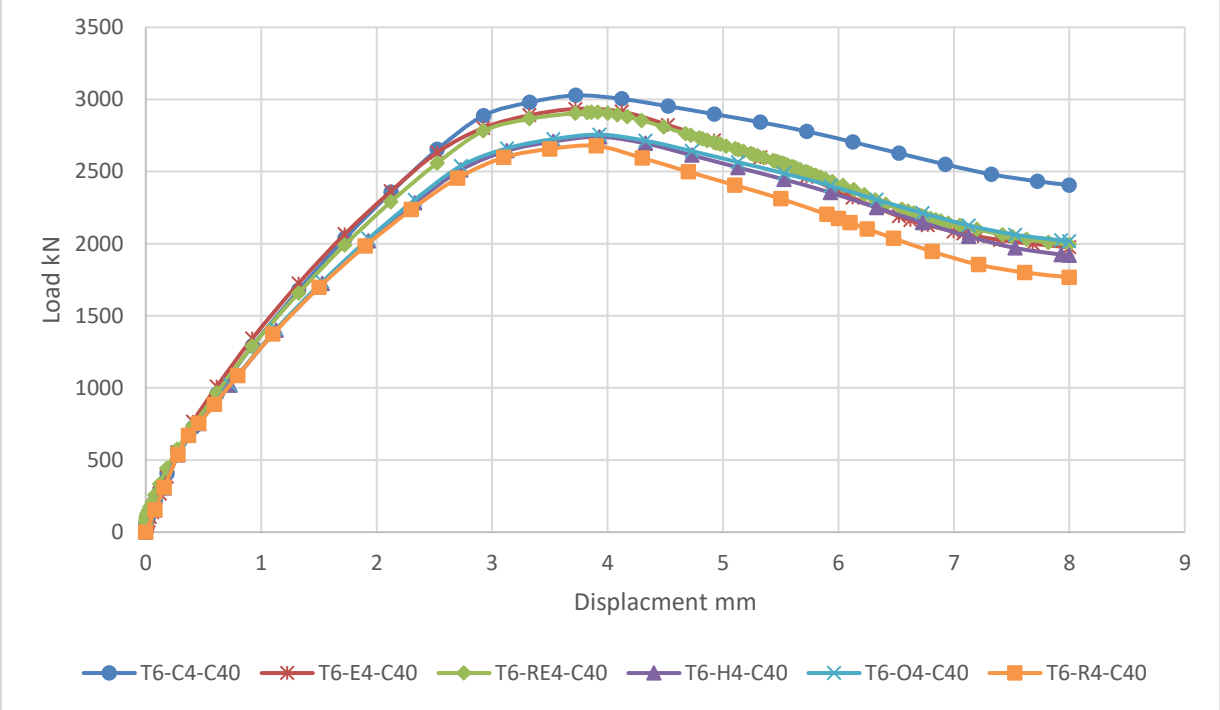

(C)

Figure 4.4 Load-Axial Displacement Relationship for Group One

(C) Mode of failure

One of the important things in column investigations is the mode of failure. In concrete-filled aluminium tubular (CFAT) stub column specimens, the mode of failure depends on the properties of the materials that comprise it (in filled concrete and aluminium tube) and the geometry of the column that led to the failure mechanism. Short (CFAT) column specimen's failure with the (local buckling), and it may be subdivided into shear failure and crushing of concrete. Aluminium tube local buckling occurs due to compression failure of the concrete core. From Figure 4.5 to Figure 4.10 a comparative study of the typical failure modes found in the specimens having different cross-sections tested with axial compression is provided.

All the specimens with circular cross-sections exhibited concrete crushing within the middle of the column height as shown in Figure 4.12 of stress cloud diagram, with one exception for the noncompact cross-section column T6C3C40, which failed in shear mode within the middle of the column height as shown in Figure 4.11. This condition indicates that, for this noncompact cross-section, the shear capacity of an aluminium tube had been exceeded before the entire formation of a typical concrete crushing pattern.

In columns having elliptical cross-sections, concrete crushing usually occurred within the middle of the column height. This occurrence can be attributed to unequal stiffness around the perimeter and the ability of the elliptical section to show greater bends at the middle height beneath axial compression, thus increasing the local instabilities of the outer wall.

Round-ended section columns exhibited concrete crushing at different places across the column's height, dependent on the D/t ratio. In the specimen (T6RE2C40) with a D/t = 43.76 ratio, concrete crushing developed at middle of the column height, showing a quite stocky cross-section in which instability occurs in the region of highest compressive stress. In the specimen (T6RE3C40), D/t = 59.68 ratio, concrete crushing occurred near to the loading plate, indicating higher wall slenderness and an increased impact of load application and end constraint settings on the instability behaviour. The slenderest specimen (T6RE4C40), having D/t = 77.93, displayed concrete crushing near to the support plate, in which concentrations of stress and constraint factors enhance early local instability.

On the other hand, samples having polygonal cross-sections showed a typically uniform concrete crushing focused on the middle height, regardless of the studied D/t range. This effect may be explained by the even stiffness distribution and unique flat-plate parts of polygonal walls, which promote asymmetric stress distribution, leading to a more secure and expected uniform concrete crushing action that is not as affected by differences in cross-section slenderness over the analysed range.

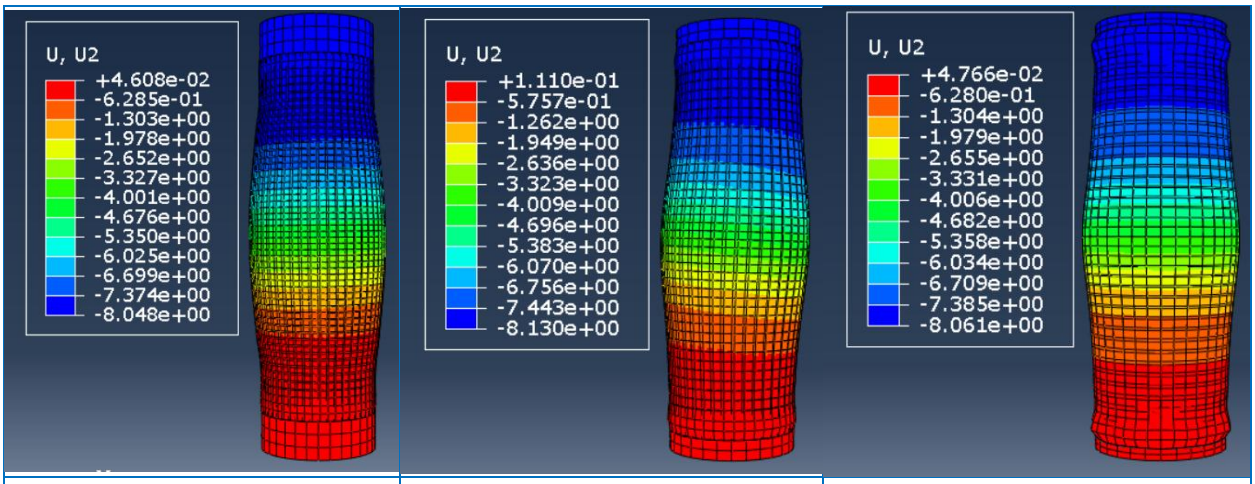

T6C2C40	T6C3C40	T6C4C40

Figure 4.5 Mode of Failure (Circular Section Columns – Group One)

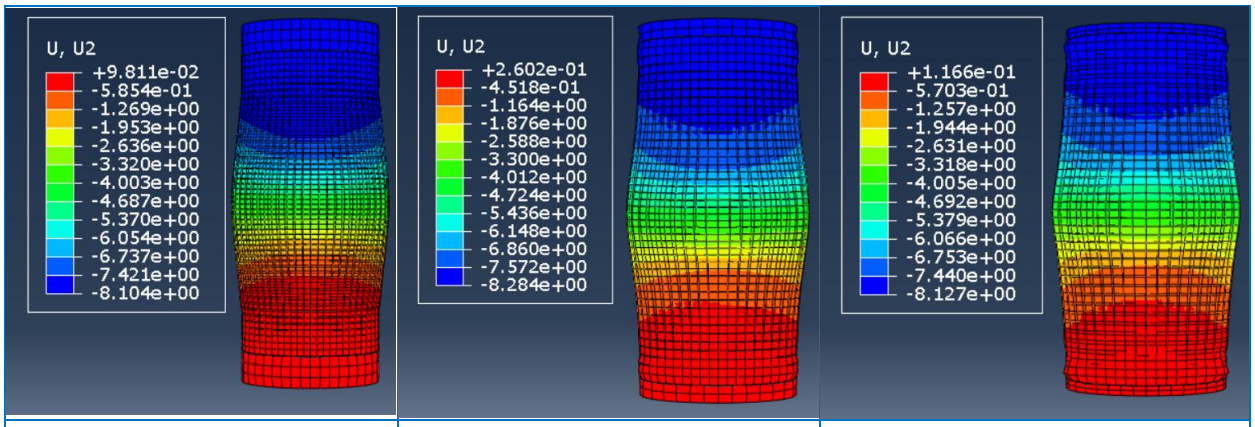

T6E2C40	T6E3C40	T6E4C40

Figure 4.6 Mode of Failure (Elliptical Section Columns – Group One)

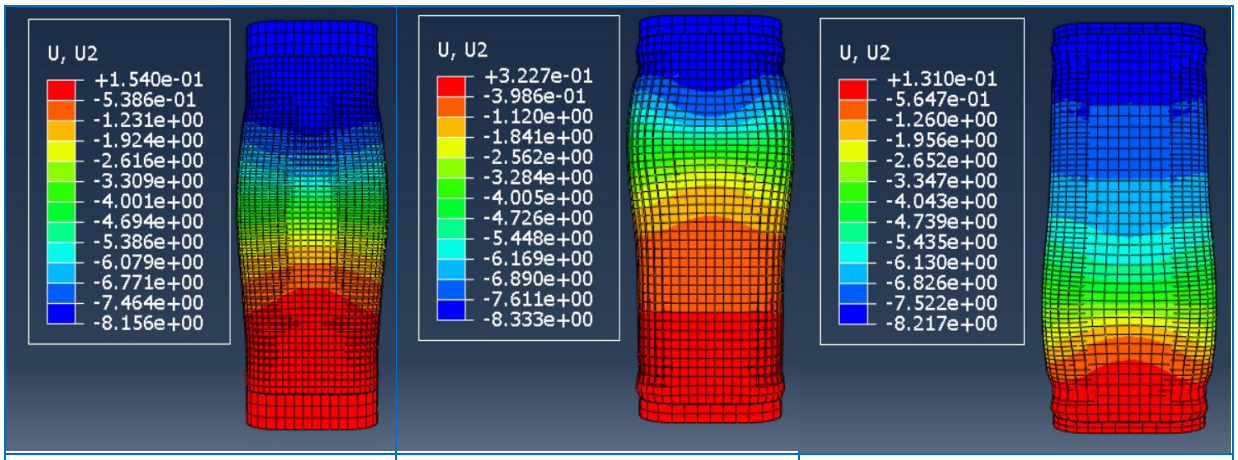

T6RE2C40	T6RE3C40	T6RE4C40

Figure 4.7 Mode of Failure (Round Ended Section Columns – Group One)

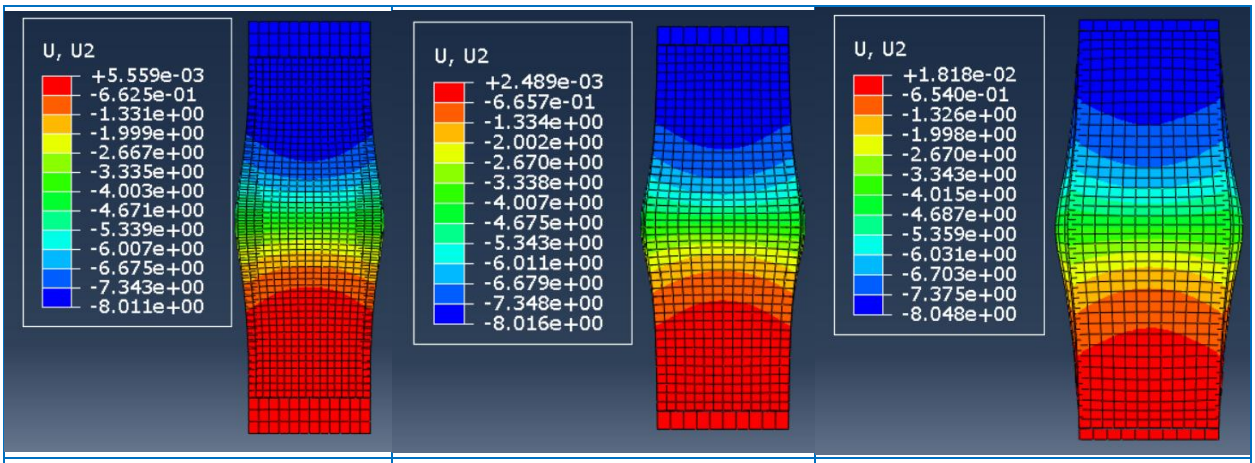

T6R2C40	T6R3C40	T6R4C40

Figure 4.8 Mode of Failure (Rectangular Section Columns – Group One)

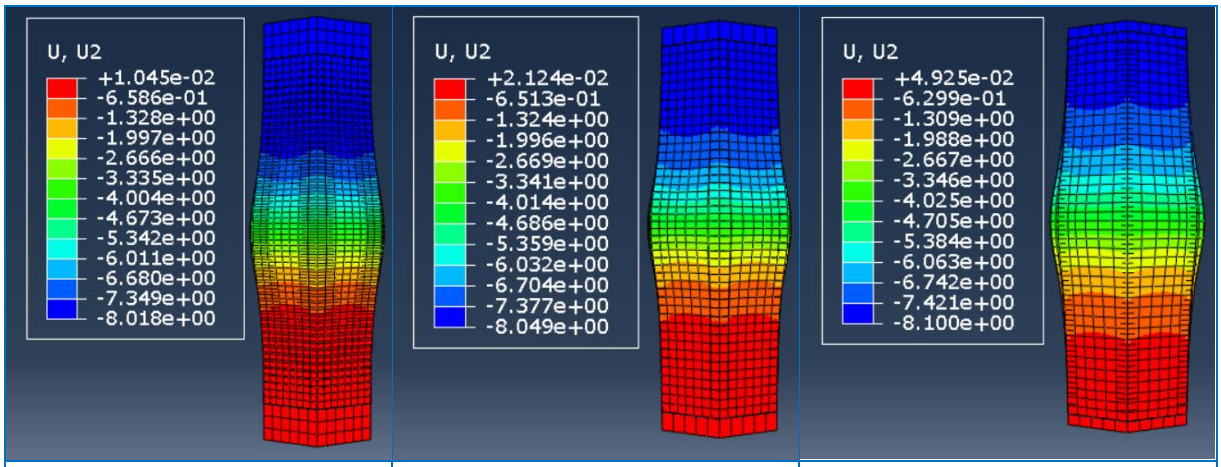

T6H2C40	T6H3C40	T6H4C40

Figure 4.9 Mode of Failure (Hexagonal Section Columns – Group One)

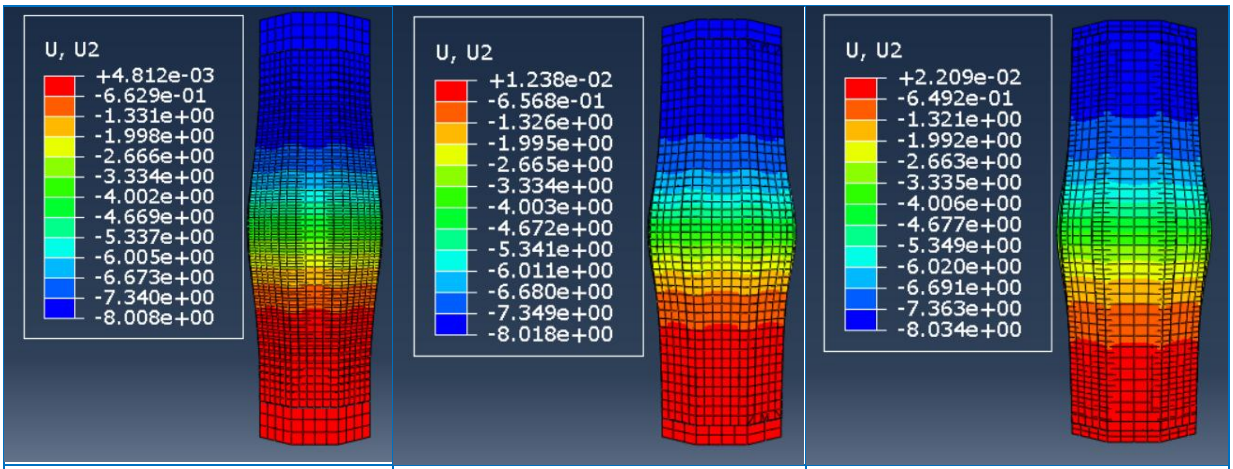

T6O2C40	T6O3C40	T6O4C40

Figure 4.10 Mode of Failure (Octagonal Section Columns – Group One)

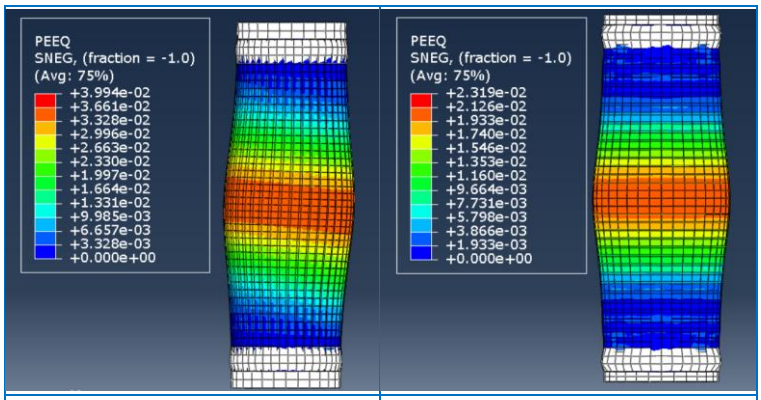

T6C3C40	T6C4C40

Figure 4.11Mode of Failure (PEEQ)

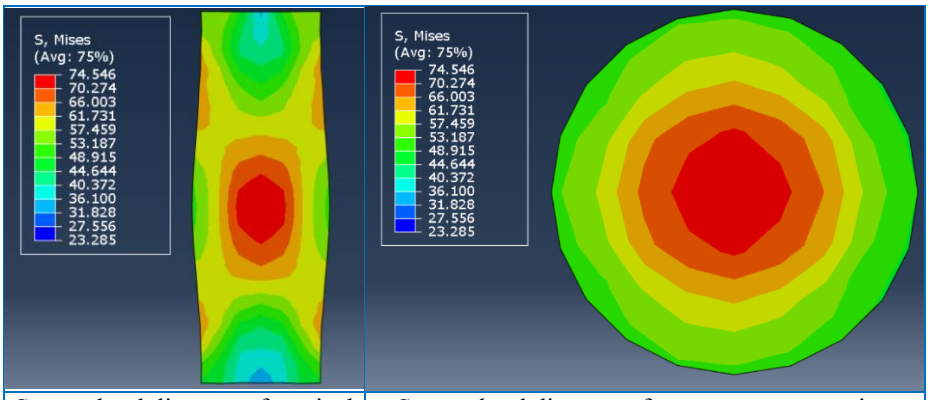

Stress cloud diagram of vertical section (failure load).	Stress cloud diagram of concrete cross-section (peak load).

Figure 4.12 Stress cloud diagram.

4.4.4 Effect of Proof Stress of Aluminium (Group Two)

The influence of changing proof stress of aluminium tubes on the structural behaviour of concrete-filled aluminium columns was studied utilising the proposed finite element model. Employing in this group different aluminium alloys, which are 6063-T5 (normal strength material), heat-treated aluminium alloy with proof stress equal to 185.9 MPa, and 6061-T6 (high strength material), heat-treated aluminium alloy with proof stress equal to 267.9 MPa. The impact of different proof stresses of aluminium tubes on the ultimate Load, mode of failure, and load-axial shortening of (CFAT) with circular and rectangular sections was analysed. All the details of materials properties and dimensions of specimens are explained in Table 4.7 for circular sections and for rectangular sections. For this group, the proposed finite element model of 12 specimens were used with a constant compressive strength of concrete equal to 40 MPa to focus on the impact of aluminium proof stress.

4.4.4.1 Results and Discussion

(A) Ultimate load

Table 4.14 illustrates a clear increase in the ultimate load-carrying capacity of tested specimens as the rise of aluminium proof stress rises from 185.9 to 267.9 MPa, regardless of whether the cross-sections are rectangular or circular. This improvement comes from the enhanced proof stress, resulting in better resistance to initial yielding and deformation against compressive loads, in turn delaying the start of modes of failure such as local buckling or crushing.

The columns with the smaller value of (D/t), which are the (T6C2C40, T6R2C40) specimens having aluminium proof stress equal to 267.9 MPa, displayed an increase in ultimate load of 20% and 18% for circular and rectangular sections, respectively, when compared to columns that had aluminium proof stress equal to 185.9 MPa. Columns with intermediate values of (D/t), which are the (T6C3C40, T6R3C40) specimens having aluminium proof stress equal to 267.9 MPa, displayed an improvement in ultimate load of 17% and 14% for circular and rectangular sections, respectively, when compared to columns with aluminium proof stress equal to 185.9 MPa. Lastly, columns with the larger value of (D/t), which are (T6C4C40, T6R4C40) specimens having aluminium proof stress equal to 267.9 MPa, indicated an enhancement in ultimate load of 14% and 12% for circular and rectangular sections, respectively, when compared with columns with aluminium proof stress equal to 185.9 MPa.

The result indicates that the rise in ultimate load, resulting from aluminium proof stress from 185.9 MPa to 267.9 MPa, is nonlinear relation as the (D/t) ratio rises, with the most significant rise noticed in specimens with the lowest value of (D/t) ratio, both rectangular and circular. The observed increase in ultimate load after raising the aluminium proof stress from 185.9 MPa to 267.9 MPa is nonlinear because the structural response is governed by an interaction between material strength, concrete crushing resistance, and cross-sectional slenderness rather than by proof stress alone. This effect is more pronounced at low (D/t) ratios because thicker or less slender sections can exploit the increase in material strength more effectively before instability governs the failure mode.

Table 4.14 Specimen's Details and Results (Group Two)

Section	DI control column	Specimen	f_y	$\frac{D}{t}$	P_{FEA} (kN)	DI	Change %
Circular	control	T5C2C40	185.9	33	246.5	2.72	0
		T5C3C40	185.9	45	944.6	1.72	0
		T5C4C40	185.9	58.7	2649.4	1.65	0

	-	T6C2C40	267.9	33	297	3.03	1.11
		T6C3C40	267.9	45	1109	1.99	1.16
		T6C4C40	267.9	58.7	3027	1.8	1.09
Rectangular	control	T5R2C40	185.9	35.8	222.4	1.59	0
		T5R3C40	185.9	48.8	841	1.55	0
		T5R4C40	185.9	63.7	2398	1.54	0
	-	T6R2C40	267.9	35.8	262	1.57	0.98
		T6R3C40	267.9	48.8	959	1.54	0.99
		T6R4C40	267.9	63.7	2677	1.46	0.95

(B) load-axial deformation curves

The resulting load-axial deformation graph was determined and drawn for all the concrete-filled aluminium tube column samples with different aluminium proof stress. Figure 4.13 displays the estimation achieved by ABAQUSE (2019) using the current finite element model. The slope of the curve in the region of elasticity displays no enhancement with increasing the aluminium proof stress from 185.9 to 267.9MPa, regardless of whether the cross-sections are rectangular or circular. On the other hand, it was observed that the ultimate load was improved as the aluminium proof stress increased. The increased aluminium proof stress delays the beginning of aluminium yielding, enabling improved load redistribution to the concrete core and delaying concrete crushing failure modes, as shown by extended post-peak deformation plateaus in finite element analyses.

Table 4.14 proved that with increasing the aluminium proof stress from 185.9 to 267.9MPa the ductility slightly enhances with circular-section columns (T6C2C40, T6C3C40, T6C4C40) with an increase in the ductility index of (3.03, 1.99, and 1.8), specifically by (1.11%, 1.16%, and 1.09%) respectively, higher than circular section control columns having aluminium proof stress equal to 185.9MPa, namely (T5C2C40, T5C3C40, T5C4C40). No noticeable change in ductility with increasing the aluminium proof stress from 185.9 to 267.9MPa with rectangular cross-section composite columns (T6R2C40, T6R3C40, T6R4C40) with a decrease in ductility index of (1.57, 1.54, and 1.46), specifically by (0.98%, 0.99%, and 0.95%) respectively, lower than rectangular section control columns having aluminium proof stress equal to 185.9MPa, namely (T5R2C40, T5R3C40, T5R4C40). The most defensible explanation is that the circular sections benefited more from the higher aluminium proof stress because their geometry provides more uniform confinement, better suppression of local buckling, and a more stable post-peak load path. In contrast, the rectangular sections already experience non-uniform stress transfer and stress concentrations at corners and flat plates, so increasing proof stress produced little or no additional ductility and, in some cases, slightly reduced it.

Figure 4.13 indicates that a carefully planned cross-sectional design enables the replacement of rectangular sections that have proof stress of aluminium (267.9 MPa) with lower aluminium proof stress circular sections (185.9 MPa), which gives similar structural performance with slight enhancements in stiffness and ductility. This equivalent behaviour exists regardless of the ratio of diameter to aluminium thickness, due to the improved buckling resistance of circular shapes from identical radial confinement and reduced eccentricity effects.

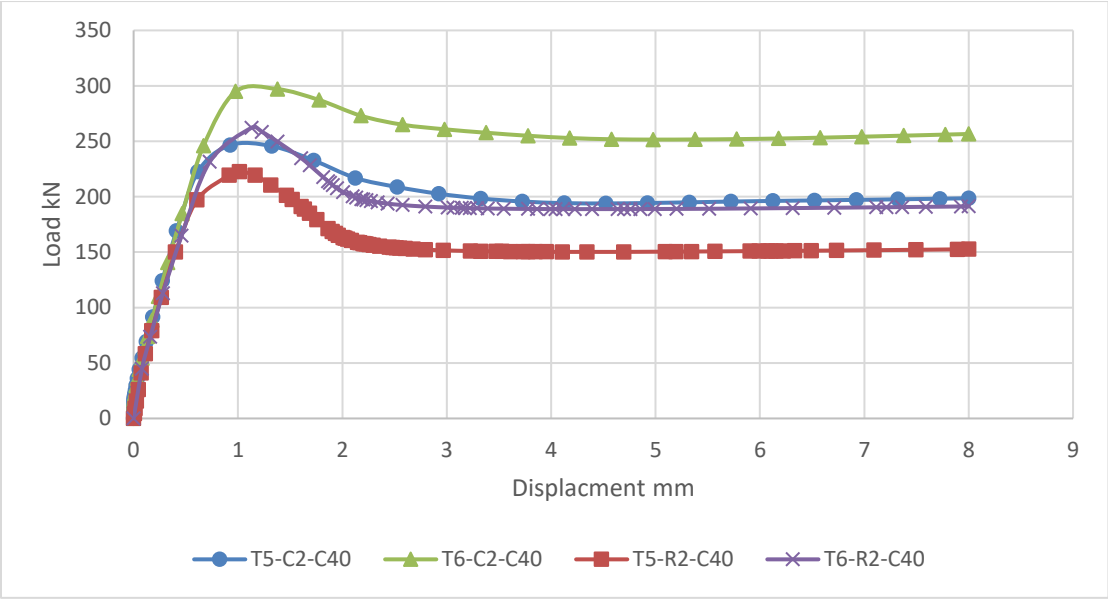

(A)

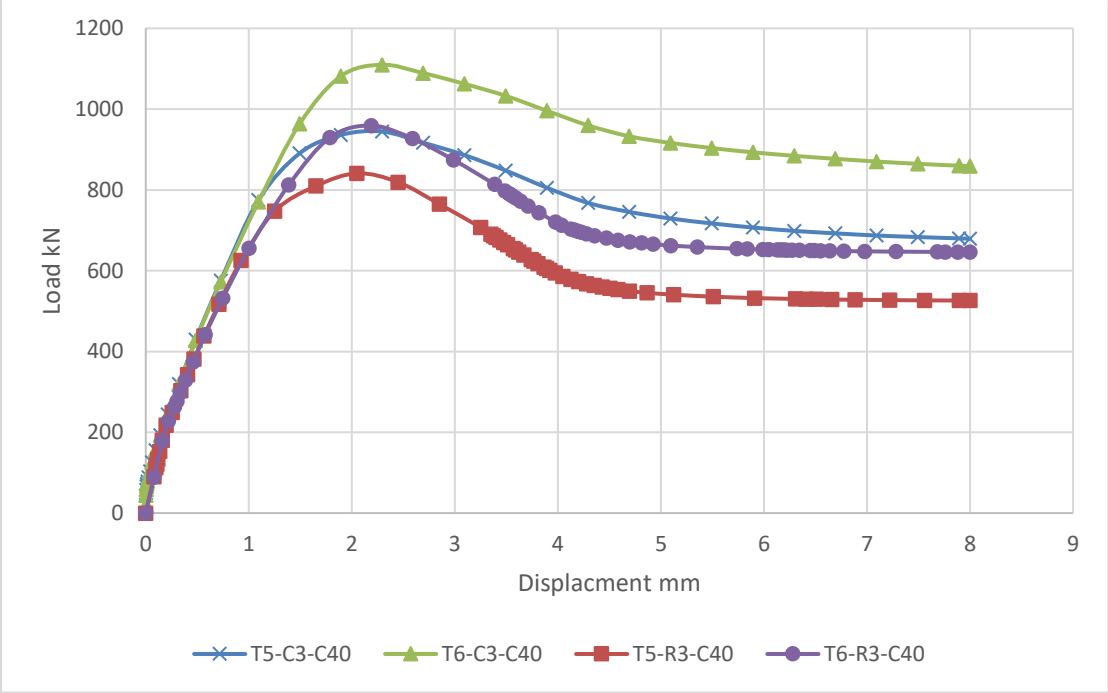

(B)

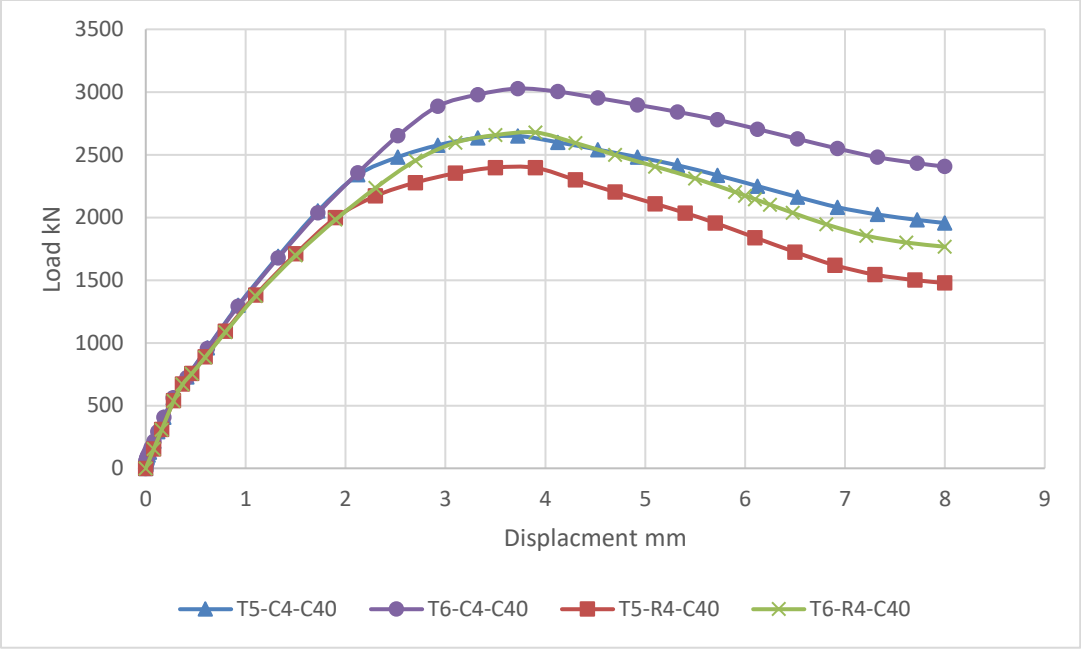

(C)

Figure 4.13 Load-Axial Displacement Relationship for Group Two.

(C) Mode of failure

From Figure 4.14 to Figure 4.17 a comparative analysis of the typical failure modes observed in samples subjected to axial compression, confined with different proof stresses of aluminium tube is displayed. In circular cross-sections, concrete crushing often occurred in the middle height of the column across all specimens because of the concentration of inelastic strains and geometric weaknesses under compressive pressures.

Notable exceptions have been observed in circular cross-sections T5C3C40 (f_y = 185.9 MPa) and T6C3C40 (f_y = 267.9 MPa), in addition to in the specimen T5C2C40 (f_y = 185.9 MPa), where shear failure dominated at middle of the column height as shown in Figure 4.18. The differences are caused by not enough lateral confinement provided by the aluminium tube, leading to early shear band formation before concrete crushing, particularly in sections with an intermediate value of (D/t = 45) ratio, which show reduced post-yield ductility and greater sensitivity to shear stresses.

On the other hand, rectangular cross-sections displayed uniform concrete crushing at the middle column height, independent of proof stresses of aluminium tube. This unity results from the parallel form of rectangular tubes, which enhances a symmetric deformation pattern and strain transferring under compression, thus decreasing local weakness.

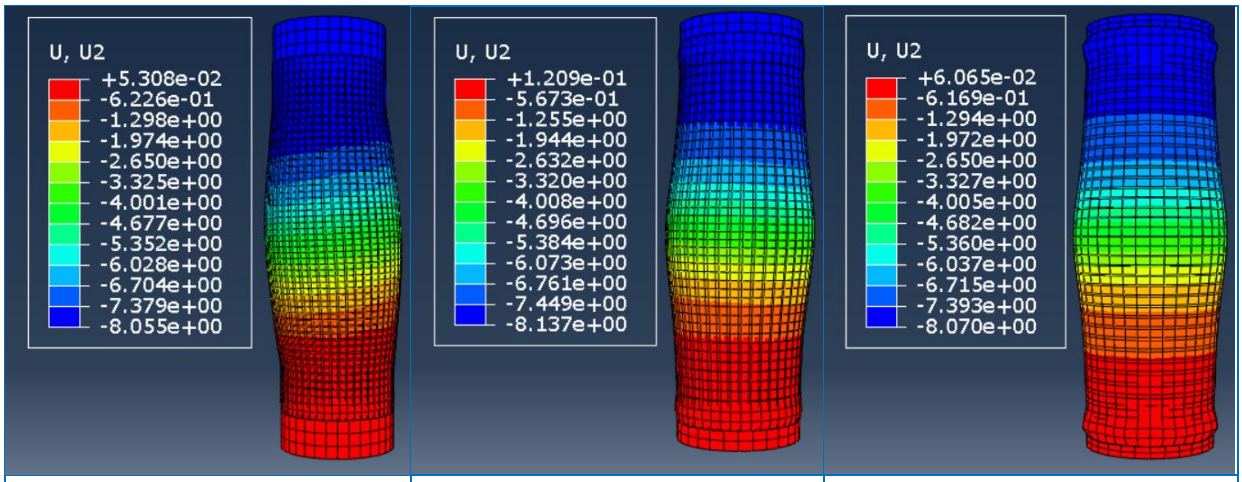

T5C2C40	T5C3C40	T5C4C40

Figure 4.14 Mode of Failure (Circular Section Columns – Group Two)

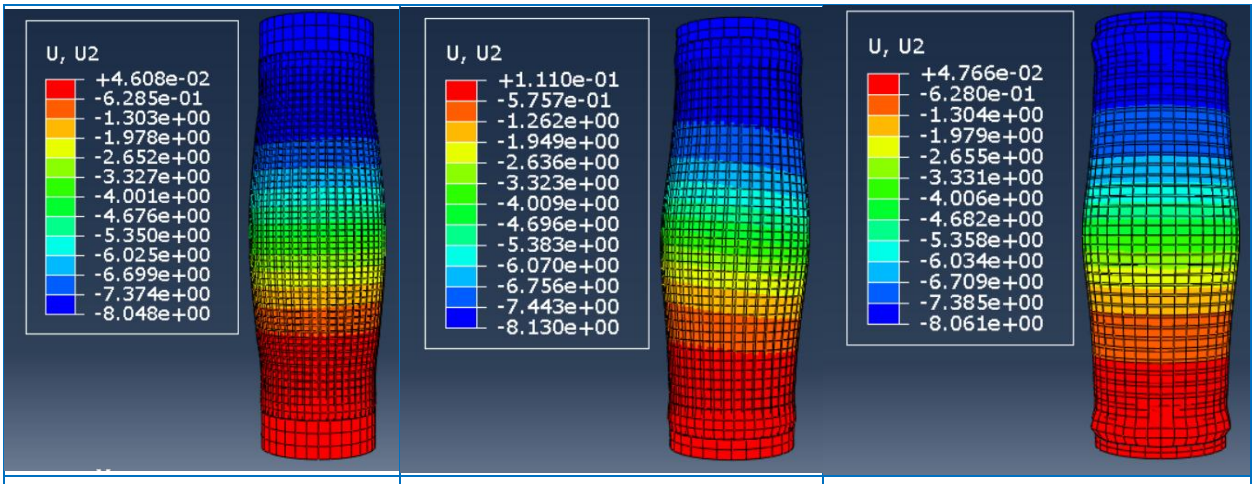

T6C2C40	T6C3C40	T6C4C40

Figure 4.15 Mode of Failure (Circular Section Columns – Group Two)

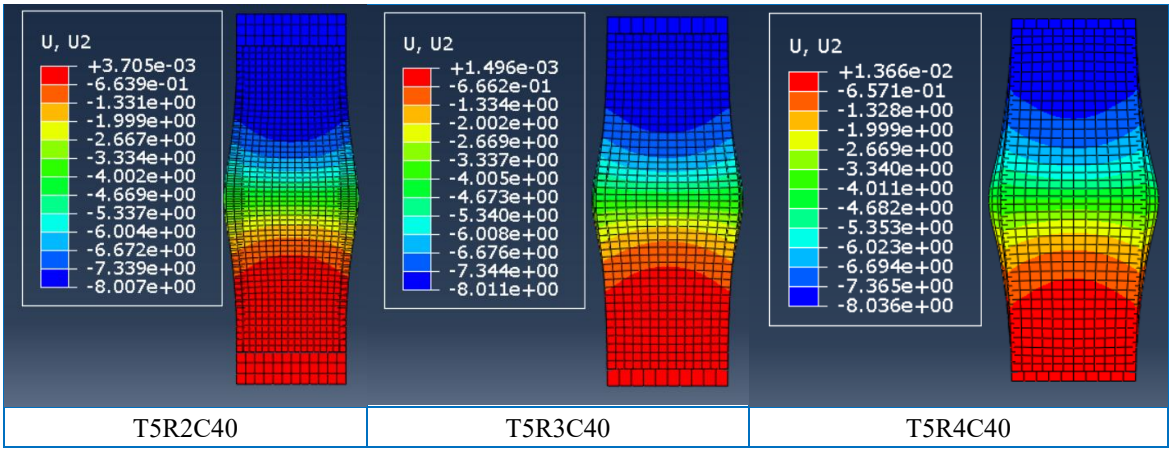

T5R2C40	T5R3C40	T5R4C40

Figure 4.16 Mode of Failure (Rectangular Section Columns – Group Two)

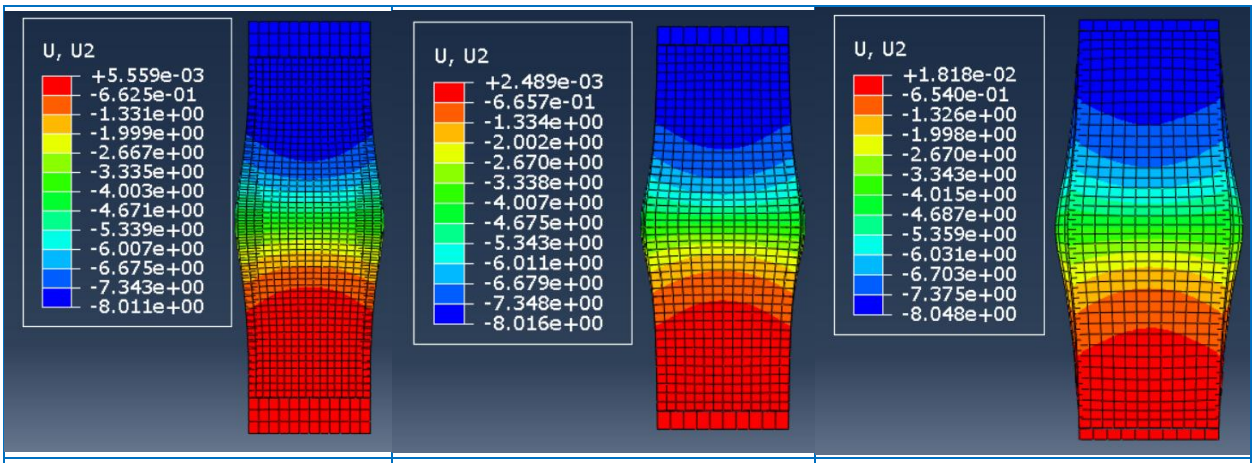

T6R2C40	T6R3C40	T6R4C40

Figure 4.17 Mode of Failure (Rectangular Section Columns – Group Two)

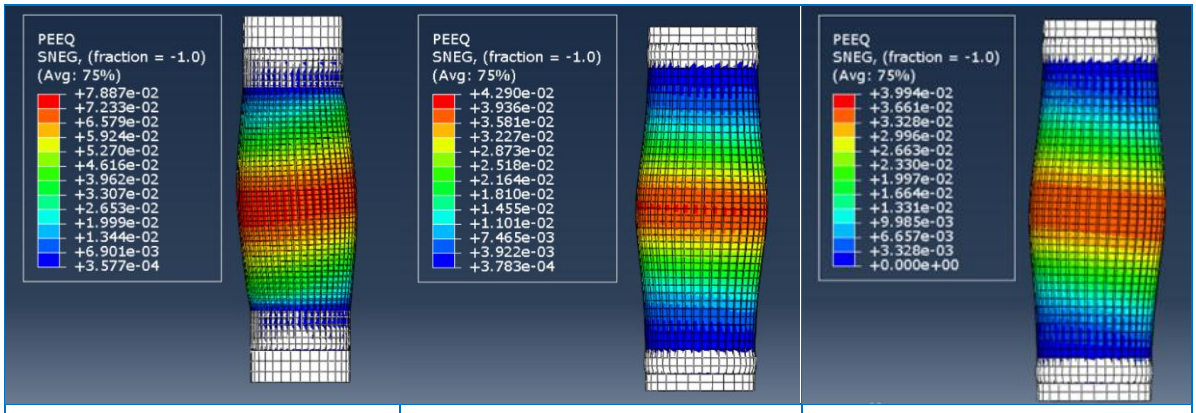

T5C2C40	T5C3C40	T6C3C40

Figure 4.18 Mode of Failure (PEEQ)

4.4.5 Effect of Compressive Concrete Strength (Group Three)

Nowadays, high-quality building components, like high-strength concrete, have become widely employed in engineering designs because of continuing developments in materials technology. Employing concrete with different compressive strengths, such as 40 MPa (normal-strength) and 70 MPa (high-strength), enables designers to enhance performance for varying load requirements and design limitations. In this group, the impact of different compressive strengths of concrete (f'_c) on the ultimate load, mode of failure, and load-axial shortening of (CFAT) with circular and rectangular sections was analysed by changing the strengths of concrete from 40 to 70MPa. All the details of material properties and dimensions for specimens are explained in Table 4.8 for circular sections and for rectangular sections. In this group, using the proposed finite element model of 12 specimens, the concrete compressive strength impact on the structural response of the concrete-filled aluminium tube samples was studied.

4.4.5.1 Results and Discussion

(A) Ultimate load

Table 4.15 illustrates a clear increase in the capacity of the ultimate load of tested specimens as the strength of concrete rises from 40 to 70 MPa, regardless of whether the cross-sections are rectangular or circular. Enhancement comes from the key function of concrete compressive strength to determine concrete's axial and confining capacities, as higher-strength concrete provides stronger resistance to compressive stress.

The columns with compact sections, having a concrete compressive strength equal to 70MPa, displayed an increase in ultimate load of 25% and 26% for circular and rectangular sections, respectively, when compared to columns that had concrete compressive strength equal to 40MPa. Noncompact column sections having a concrete compressive strength equal to 70MPa displayed an improvement in ultimate load of 28% and 32% for circular and rectangular sections, respectively, when compared to columns with a concrete compressive strength of 40 MPa. Lastly, columns with slender sections having a concrete compressive strength of 70MPa indicated an enhancement in ultimate load of 33% and 36% for circular and rectangular sections, respectively, when compared with columns with concrete compressive strength equal to 40MPa.

The result indicates that the rise in ultimate load, resulting from increasing the strength of concrete from 40 MPa to 70MPa, is linear as the ratio of depth-to-thickness (D/t) rises, having the most significant rise noticed in slender cross-sections, both rectangular and circular. The most significant improvement in slender sections comes from increasing concrete crushing resistance resulting from higher concrete compressive strength, enhancing the concrete confining effect and delaying yielding in the aluminium tube, thus enhancing total column efficiency.

Table 4.15 Specimen's Details and Results (Group Three)

Section	DI control	Specimen	f'_c	$\frac{D}{t}$	P_{FEA} (kN)	DI	Change %
Circular	control	T6C2C40	44.8	33	297	3.03	0
		T6C3C40	44.8	45	1109	1.99	0
		T6C4C40	44.8	58.7	3027	1.8	0
	-	T6C2C70	70.2	33	374	1.94	0.64
		T6C3C70	70.2	45	1425	1.76	0.88
		T6C4C70	70.2	58.7	4031	1.62	0.9

Rectangular	control	T6R2C40	44.8	35.8	262	1.57	0
		T6R3C40	44.8	48.8	959	1.54	0
		T6R4C40	44.8	63.7	2677	1.46	0
	-	T6R2C70	70.2	35.8	331	1.4	0.89
		T6R3C70	70.2	48.8	1265	1.61	1.04
		T6R4C70	70.2	63.7	3638	1.51	1.03

(B) load-axial deformation curves

The resulting load-axial deformation graph was determined and drawn for all specimens of the aluminium concrete composite column with various concrete compressive strengths. Figure 4.19 displays the estimation achieved by ABAQUSE (2019) using the current finite element model. The slope of the curve in the region of elasticity became steeper for higher concrete infill strengths, namely grade 70 MPa.

On the other hand, ductility was reduced in the samples that had increasing concrete infill strengths, namely from grade 40 to 70MPa. Can be noticeable with circular and rectangular section columns (T6C2C70, T6C3C70, T6C4C70, T6R2C70) with a decrease in the ductility index of (1.94, 1.76, 1.62, 1.4), specifically by (0.64%, 0.88%, 0.9%, 0.89%), respectively lower than circular and rectangular section control columns having concrete compressive strengths equal to 40MPa namely (T6C2C40, T6C3C40, T6C4C40, T6R2C40). It was observed that there was a major difference in curves throughout columns with high-strength infill compared to those with normal-strength infill. When the high-strength concrete core reaches its ultimate load, the aluminium tube around it approaches its yield point. On the other hand, within specimens with normal strength filling, the aluminium tube achieves yield stresses early from the concrete-filled reaching ultimate load.

There is one exception: in noncompact and slender rectangular cross-section columns, with increasing the concrete infill strengths from 40 to 70MPa, the ductility slightly enhances with (T6R3C70, T6R4C70) with an increase in the ductility index of (1.61, 1.51) specifically by (1.04%, 1.03%) respectively, higher than rectangular section control columns having concrete infill strengths equal to 40MPa namely (T6R3C40, T6R4C40). This unexpected improvement is due to the higher-strength concrete infill's better confinement effect, which keeps the noncompact and slender sections from concrete crushing too quickly.

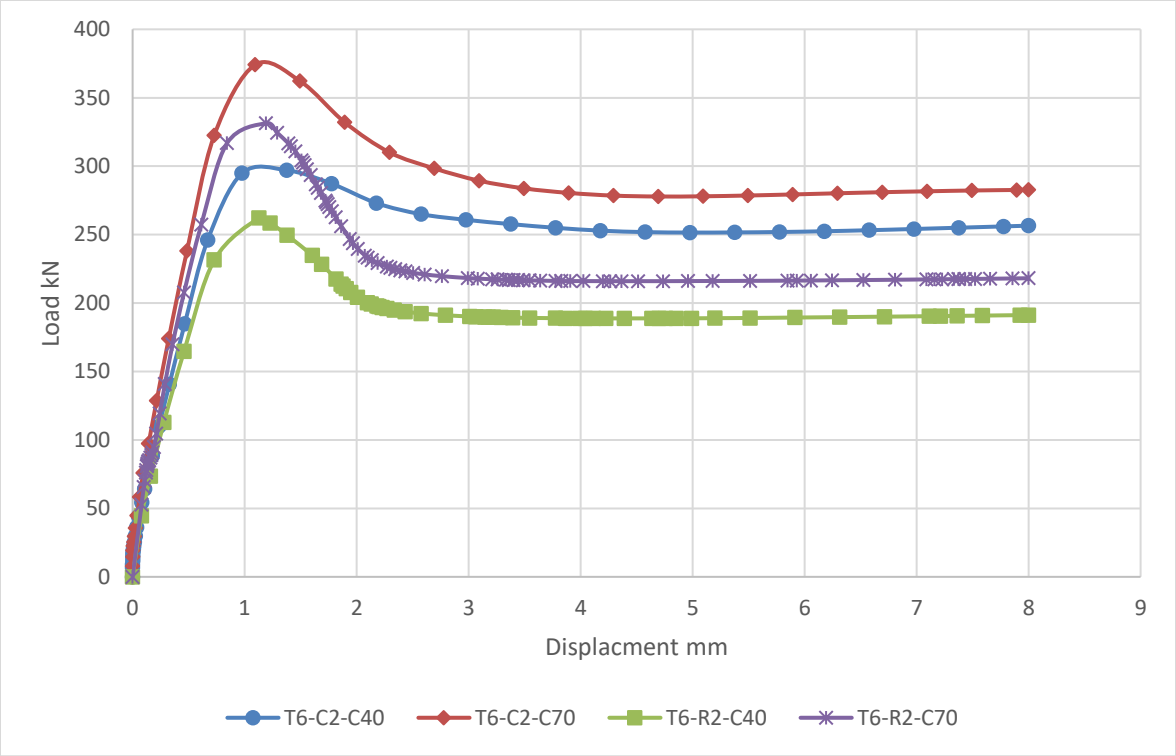
400
350
300
250
200
150
100
50
0
Load kN
0
1
2
3
4
5
6
7
8
9
Displacment mm
T6-C2-C40
T6-C2-C70
T6-R2-C40
T6-R2-C70

(A)

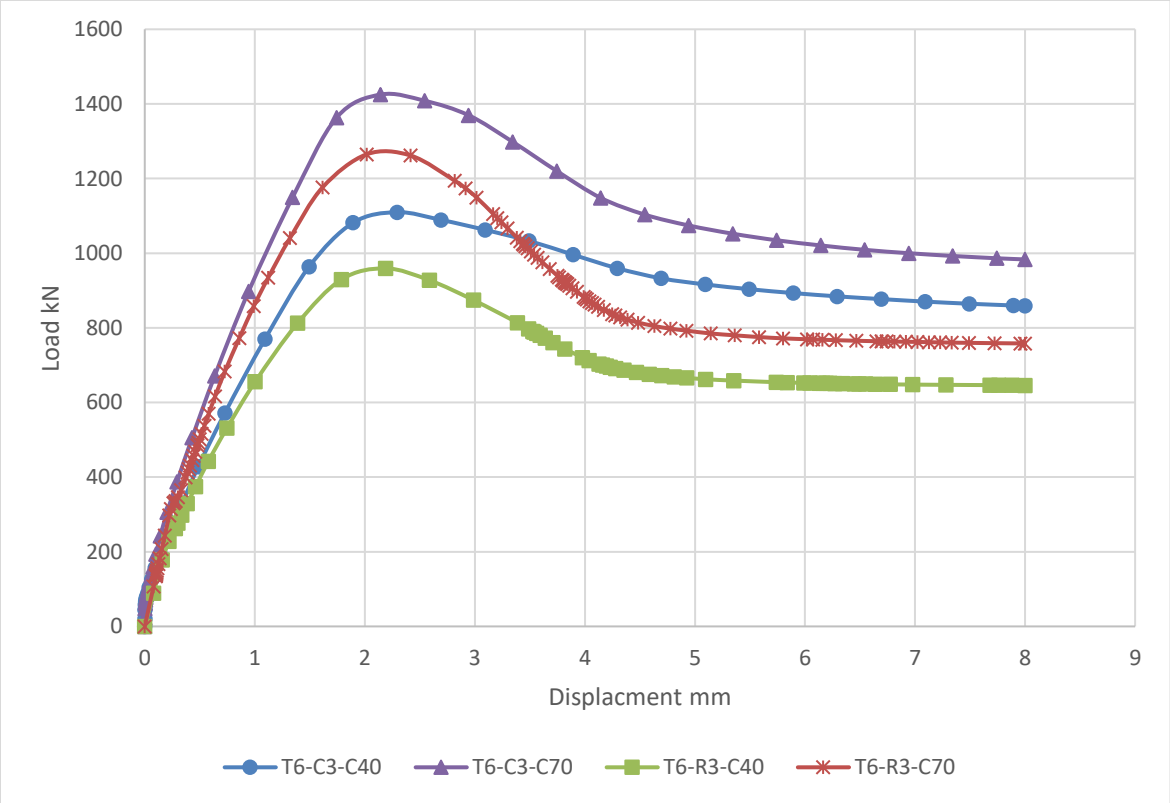
1600
1400
1200
1000
800
600
400
200
0
Load kN
0
1
2
3
4
5
6
7
8
9
Displacment mm
T6-C3-C40
T6-C3-C70
T6-R3-C40
T6-R3-C70

(B)

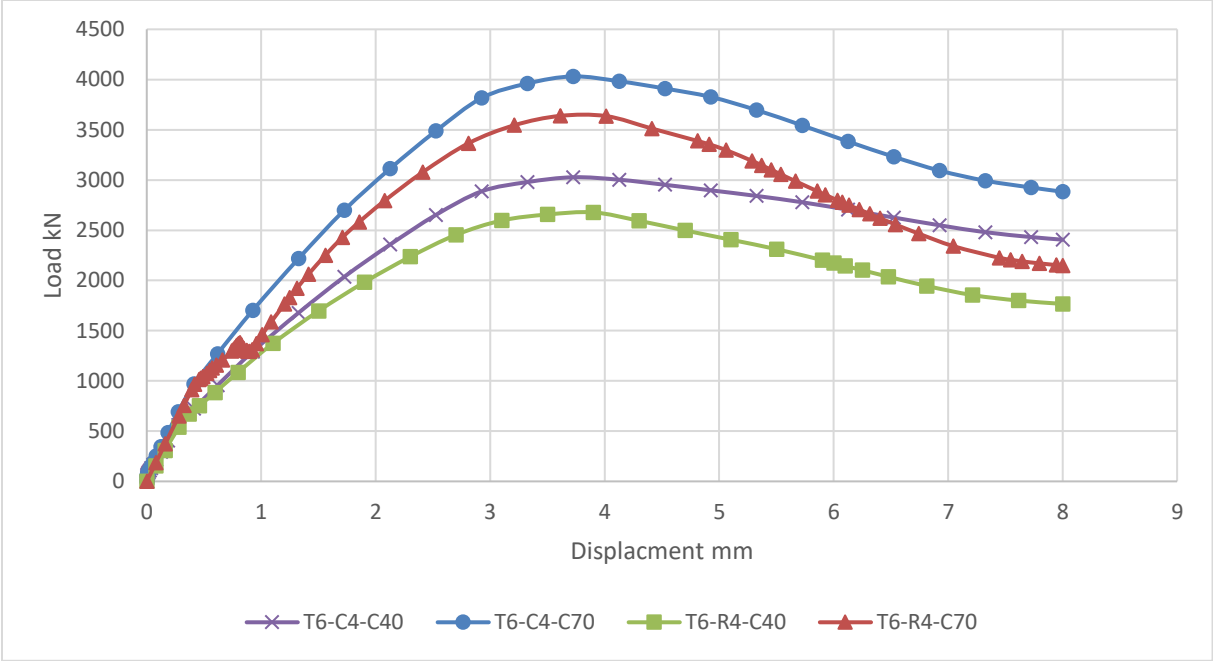

(C)

Figure 4.19 Load-Axial Displacement Relationship for Group Three.

(C) Mode of Failure

From Figure 4.20 to Figure 4.23 a comparative analysis of the typical failure modes observed in samples subjected to axial compression, filled with different concrete compressive strengths is displayed. In circular cross-sections, concrete crushing often occurred in the middle height of the column across all specimens because of the concentration of inelastic strains and geometric weaknesses under compressive pressures.

Exceptions occurred in the noncompact cross-sections T6C3C40 and T6C3C70, which have strengths of concrete of 40MPa and 70MPa, respectively, and with a compact cross-section T6C2C70, which has a strength of concrete of 70 MPa, that shear failure occurred in the middle of the column height as shown in Figure 4.24. The difference is caused by increased concrete confinement with higher-strength concrete, which delays concrete crushing by enhancing the tube's lateral confinement (through the concrete-core expansion effect), thus enabling shear-dominated failure, which includes diagonal cracking and decreasing post-yield ductility.

On the other hand, rectangular cross-sections displayed uniform concrete crushing at the middle column height, independent of concrete compressive strength, due to the parallel stiffness and the stress concentrations at sharp corners, which encourage local yield and collapse beneath uniform compression.

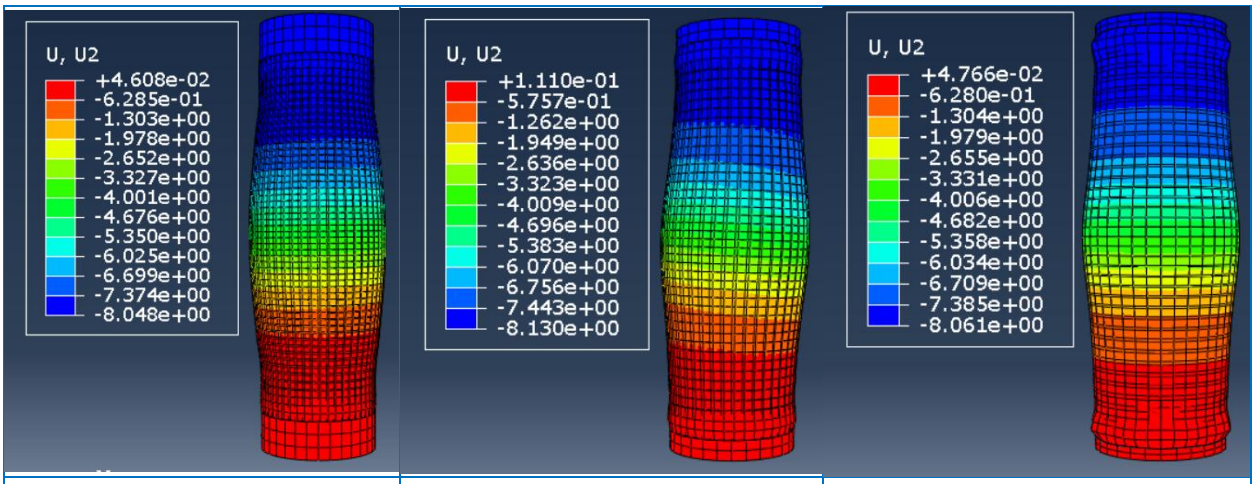

T6C2C40	T6C3C40	T6C4C40

Figure 4.20 Mode of Failure (Circular Section Columns – Group Three)

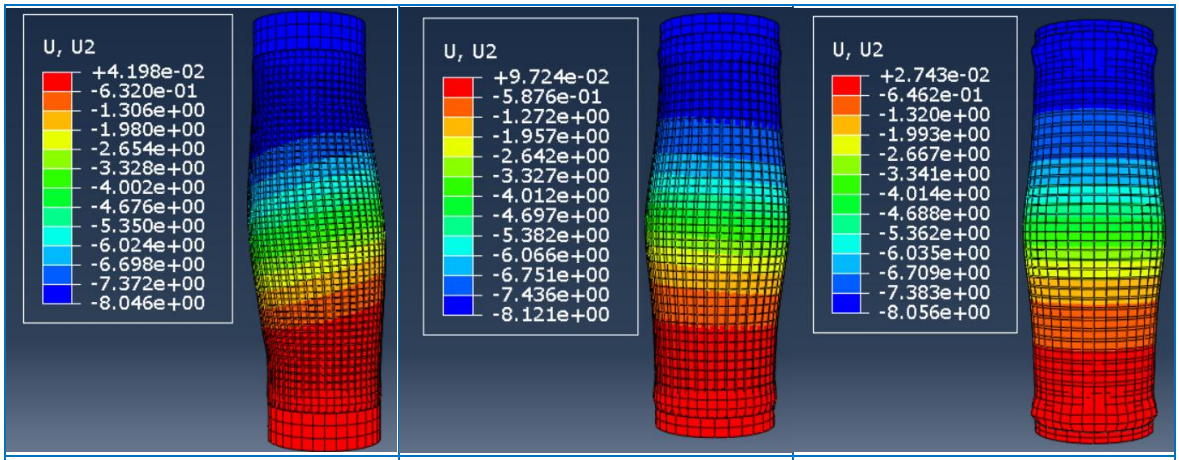

T6C2C70	T6C3C70	T6C4C70

Figure 4.21 Mode of Failure (Circular Section Columns – Group Three)

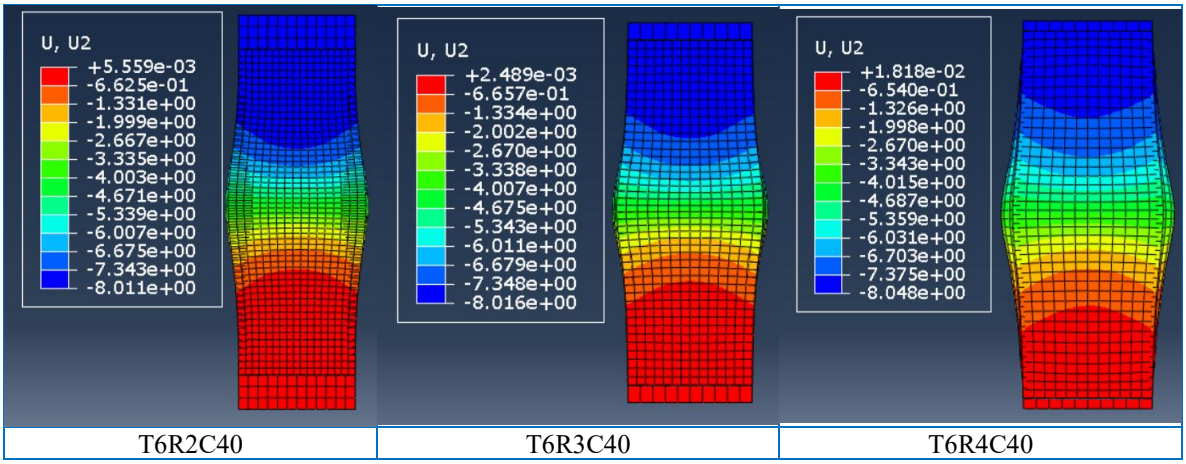

T6R2C40	T6R3C40	T6R4C40

Figure 4.22 Mode of Failure (Rectangular Section Columns – Group Three)

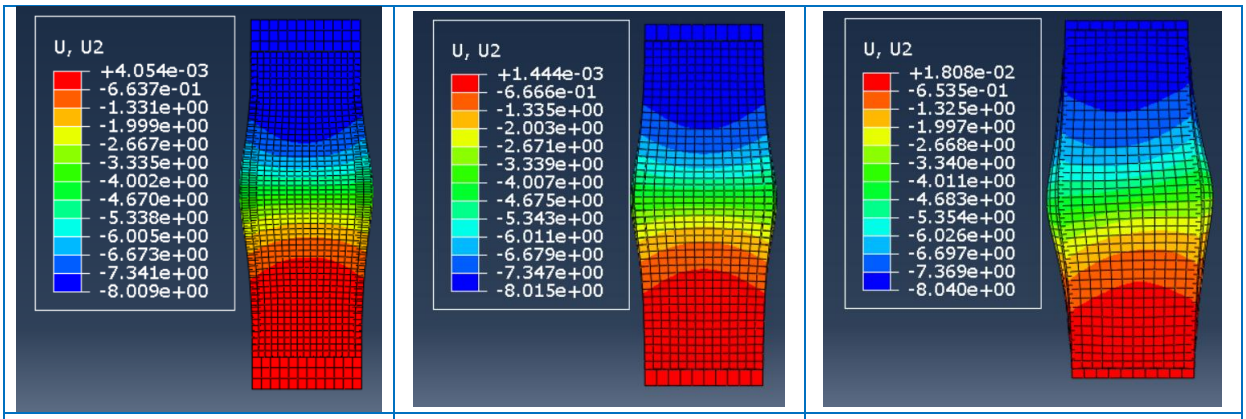

T6R2C70	T6R3C70	T6R4C70

Figure 4.23 Mode of Failure (Rectangular Section Columns – Group Three)

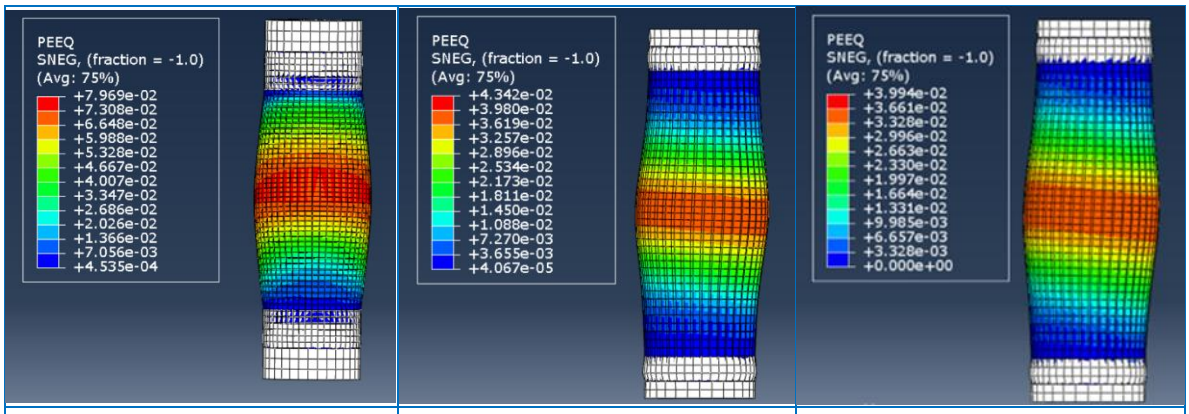

T6C2C70	T6C3C70	T6C3C40

Figure 4.24 Mode of Failure (PEEQ)

4.4.6 Effect of Aluminium Tube Thickness (Group Four)

This group investigates how the ratio of (D/t) affects the structure of (CAFT) column performance. The depth-to-thickness (D/t) ratio is systematically changed via increasing the thickness of aluminium tubes and keeping the tube's diameter fixed, therefore defining the effect on key performance indicators.

The columns that have slender, noncompact, and compact sections— classified according to slenderness criteria in applicable standards for design (AISC) are assessed based on each of the three aluminium wall thicknesses: 1.9 mm, 3 mm, and 5 mm. The collection includes different D/t ratios that represent varying failure forms, therefore providing complete insight into the ratio's impact on the enhancing confines of the concrete component as well as the whole composite behaviour.

4.4.6.1 Results and Discussion

(A) Ultimate load

Table 4.16 clearly displays an increasing improvement in the ultimate load-bearing capacity of the studied samples with a rise in aluminium wall thickness, no matter whether their cross-sections are rectangular or circular.

For noncompact section columns that had an aluminium wall thickness of 3 mm, the ultimate load increased about 22% for circular sections and 19% for rectangular sections, compared with slender cross-section columns having a wall thickness of 1.9 mm. Also, compact cross-section columns having a 5 mm wall thickness exhibited improvements of 58% and 56% for circular and rectangular sections, respectively, compared to the same slender section.

The theoritical results indicate that increasing the aluminium wall thickness leads to a marked improvement in the ultimate axial load capacity of both circular and rectangular composite columns. This enhancement is attributed to the greater stiffness and improved concrete crushing resistance of the thicker aluminium walls, which allow more effective confinement of the concrete core. The improved confinement delays concrete crushing, promotes a more favorable triaxial stress state, and strengthens the composite interaction between the aluminium shell and the infill. The circular specimens exhibited slightly higher strength gains than the rectangular specimens because of their more uniform confinement efficiency and more stable stress distribution under axial compression.

Table 4.16 Specimen Details and Results (Group Four)

Section	DI control	Specimen	t (mm)	$\frac{D}{t}$	P_{FEA} (kN)	DI	Change %
Circular	-	T6C5C40	5	27	1435.3	3.1	1.67
	-	T6C3C40	3	45	1109	1.99	1.07
	Control	T6C1.9C40	1.9	71	907.5	1.86	0
Rectangular	-	T6R5C40	5	29.3	1256.8	1.6	1.2
	-	T6R3C40	3	48.8	959	1.54	1.15
	Control	T6R1.9C40	1.9	77	806.9	1.33	0

(B) Load-axial deformation curves

The resulting load-axial deformation graph was determined and drawn for all specimens of the (CFAT) columns with different thicknesses of aluminium tube. Figure 4.25 displays the estimation achieved by ABAQUSE (2019) using the current (FEM).

During the area of elasticity, the beginning slope of the curves rises together with a rise in the tube thickness of the concrete filled aluminium tube columns (from 1.9mm to 3mm and 5mm), no matter if the cross-sectional shape is rectangular or circular. In concrete-filled aluminium tubes, the tube restrains the lateral dilation of the concrete core. When wall thickness increases, the tube can provide stronger confinement, so the concrete and tube act more compatibly under compression and the composite section behaves more rigidly. This stronger interaction delays early micro-cracking and reduces slip or local instability at the interface.

The ultimate load capacity was different depending on the section shape, corresponding to the previous paragraph.

Table 4.16 proved ductility is highly enhanced with compact circular-section columns with a 5 mm wall thickness (T6C5C40) with an increase in the ductility index of (3.1), specifically by (1.67%), higher than the circular-section control column with a 1.9mm wall thickness (T6C1.9C40). The ductility also enhances with noncompact circular-section columns with a 3 mm wall thickness (T6C3C40) with an increase in the ductility index of (1.99) specifically by (1.07%), higher than the slender circular-section control column with a 1.9mm wall thickness (T6C1.9C40). The compact circular shape is especially efficient because circular sections distribute stresses more uniformly around the perimeter. This uniformity reduces stress concentration and promotes a more stable post-yield response, so the column can absorb more deformation energy before reaching ultimate failure. In practical terms, the thicker circular tube behaves like a more restrained and stable shell, so the load is maintained over a larger displacement range.

The ductility also enhances with rectangular-section columns with a 3mm, 5mm wall thickness (T6R3C40, T6R5C40) with an increase in the ductility index of (1.54, 1.6) specifically by (1.15%, 1.2%) higher than the slender rectangular section control column with a 1.9mm wall thickness (T6R1.9C40). For the rectangular columns (T6R3C40 and T6R5C40), the ductility improvement is also expected, but the increase is usually less pronounced than in circular columns. Rectangular sections have flat plate elements that are more susceptible to local buckling because compressive stresses concentrate in the plates rather than being distributed smoothly around the perimeter. Even when the wall thickness increases, the corners and flat sides do not confine deformation as uniformly as a circular section, so the ductility enhancement remains moderate.

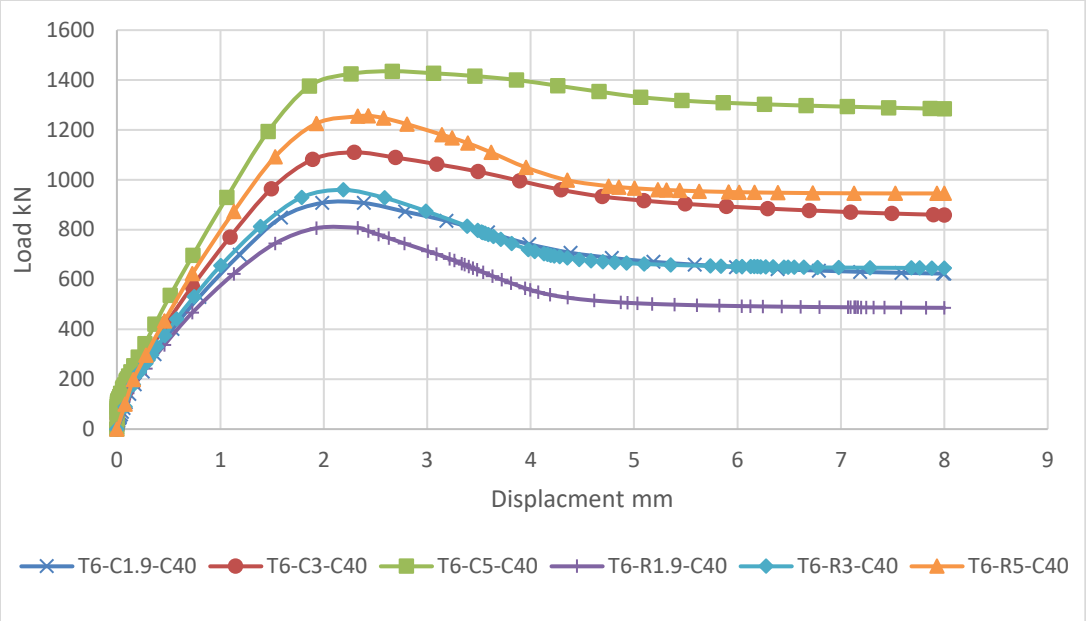

Figure 4.25 Load-Axial Displacement Relationship for Group Four.

(C) Mode of Failure

Figure 4.26 and Figure 4.27 display a comparative analysis of the typical failure modes observed in samples subjected to axial compression, confined with different aluminium tube thicknesses.

Circular slender cross-section columns and noncompact cross-section columns limited by 1.9 mm and 3 mm thick walls exhibited shear mode failure at the middle column height as shown in Figure 4.28. This behaviour develops because of insufficient lateral confinement and therefore does not prevent shear banding, a localised shear deformation mode observed in unconfined thin components under axial forces.

On the other hand, compact cross-sections (low λ, high local stability) having a 5 mm thickness of tube displayed ductile "drum-like" deformation indicated by bending at middle height where the outer diameter exceeds that at the ends, absent of local buckling indication. The improvement in confinement stiffness resulting from a thicker wall provides greater radial constraint, increasing the critical buckling stress, leading to stable, post-elastic expansion instead of instability.

Rectangular in slender and noncompact cross-sections (1.9 mm and 3 mm thickness) typically displayed uniform concrete crushing at the middle column height. This unity results from the parallel form of rectangular tubes, which enhances a symmetric deformation pattern and strain transferring under compression, thus decreasing local weakness.

One exceptional situation occurred in the compact cross-section rectangular column T6R5C40 (5 mm thickness), showing uniform concrete crushing localised by the upper half of the column hight. The difference probably results from varied stress distribution, cancelling the intended entire stable enhancement from improved confinement.

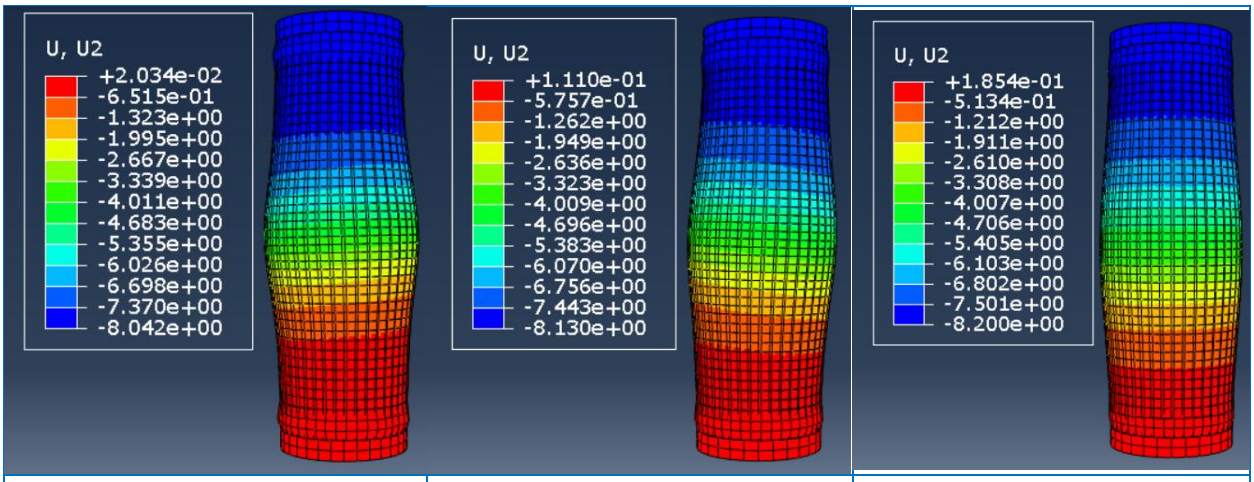

T6C1.9C40	T6C3C40	T6C5C40

Figure 4.26 Mode of Failure (Circular Section Columns – Group Four)

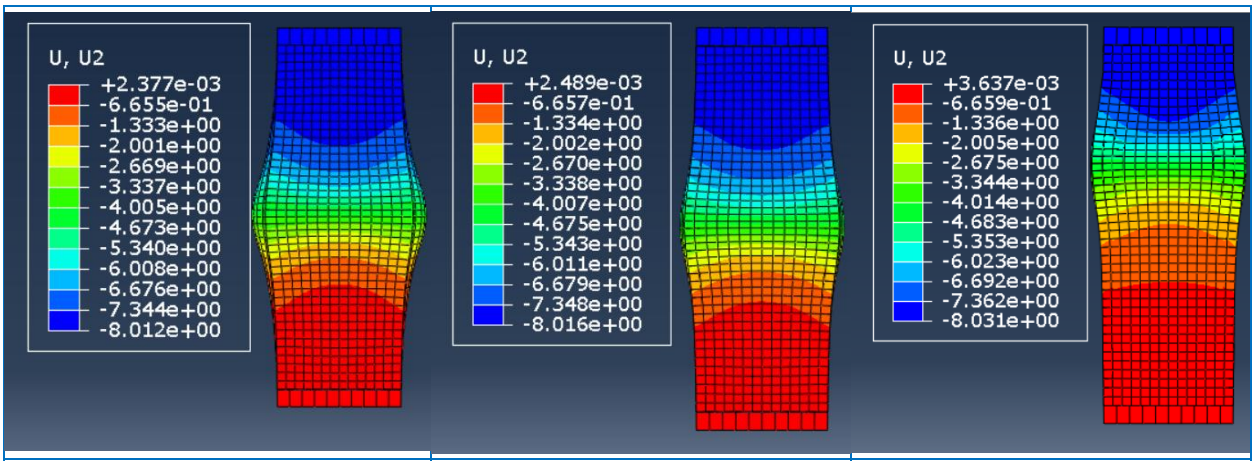

T6R1.9C40	T6R3C40	T6R5C40

Figure 4.27 Mode of Failure (Circular Section Columns – Group Four)

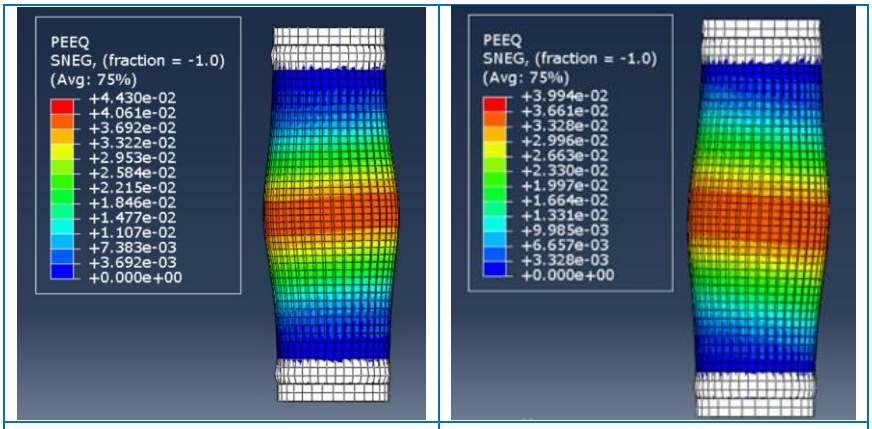

T6C1.9C40	T6C3C40

Figure 4.28 Mode of Failure (PEEQ)

Chapter Five: Conclusion and Recommendations

5.1 Conclusion

The presented numerical investigation focuses on the behaviour of an aluminium concrete composite column with various cross-sections using the Abaqus program for finite element analysis (FEM).

1- The theoretical results, which were comparable to previous experimental results, indicated that the structural behaviour of the aluminium concrete composite short column model can be accurately predicted, showing a high comparability range between 0.90 and 0.99.

2- The circular section specimens exhibited a significant outperformance in the ultimate load compared to other sections of columns within all ranges of (D/t) ratios performed in the current investigation, regardless of the compressive strength or aluminium proof stress. The columns, which have a circular section provide improved structural effectiveness and even load distribution in comparison to various cross-section designs. The shapes ranged in strength from the weakest to the strongest in the following sequence (rectangular, hexagonal, octagonal, elliptical, round ended, circular).

3- The elliptical shaped columns with aluminium wall thicknesses of (2, 3, and 4 mm) display a reduction in ultimate load of 6%, 5%, and 3%, respectively, when compared with circular shaped specimens. The round-ended shape columns with aluminium wall thicknesses of (2, 3, and 4 mm) showed a reduction of 5%, 4%, and 4%, respectively, in ultimate load compared to the circular equivalent columns. The slight losses come in the elliptical and rounded shapes due to the lower uniformity in shape, resulting in unequal stress distribution.

4- Columns with hexagonal sections aluminium wall thickness of (2, 3, and 4 mm), illustrate reductions of ultimate load of 10%, 11%, and 9%, respectively, compared to the circular section's columns. The octagonal section specimens, with aluminium wall thicknesses of (2, 3, and 4 mm), when compared to circular shaped specimens, display a reduction in ultimate load of 9%, 10%, and 9%. The rectangular shaped columns, with aluminium wall thicknesses of (2, 3, and 4 mm), indicate the minimum structural efficiency, with a reduction in ultimate load of 12%, 14%, and 12%, respectively, compared to their equivalent circular cross-section specimens. Columns with polygonal cross-sections and sharp edges show increasing ultimate load capacity with more corners. This follows structural mechanics principles, as polygons with more edges approximate a circle, enhancing moment of inertia and reducing stress concentrations at corners that cause early axial failure.

5- Throughout the test of six sections shaped columns, the slope of the elastic area shows no clear changes with specimens that have a low D/t ratio. On the other hand, at greater D/t ratios, the elastic slope was considerably higher in curve cross-sections as compared with sharp-cornered sections. The enhancement is due to improved yielding resistance

in curved sections, which delays the development of geometric nonlinearity by enabling an even radial distribution of stresses and lowering concentrations of stress in corners.

6- samples having polygonal cross-sections showed a typically uniform concrete crushing focused on the middle height, regardless of the studied D/t range. This effect may be explained by the even stiffness distribution and unique flat-plate parts of polygonal walls, which promote asymmetric stress distribution, leading to a more secure and expected uniform concrete crushing action that is not as affected by differences in cross-section slenderness over the analysed range.

7- For rectangular and circular shapes, columns that display aluminium proof stress increased from 185.9 MPa to 267.9 MPa, and an increase in the ultimate load was observed, varying from 12% to 20%. This variation depends on the nonlinear relationship between the ultimate load and the (D/t) ratio, where the highest increase in ultimate load was noticed in the lowest (D/t) ratio columns because less slender sections can exploit the increase in material strength more effectively before instability governs the failure mode.

8- The result indicates that the rise in ultimate load, resulting from increasing the strength of concrete from 40 MPa to 70MPa, is linear as the ratio of depth-to-thickness (D/t) rises, having the most significant rise noticed in slender cross-sections, both rectangular and circular. The most significant improvement in slender sections comes from increasing concrete crushing resistance resulting from higher concrete compressive strength, enhancing the concrete confining effect and delaying yielding in the aluminium tube, thus enhancing total column efficiency.

9- The intermediate (D/t = 45) ratio circular section columns display shear mode failure, regardless of the aluminium tube proof stress or concrete compressive strength. This situation means that, for this kind of form, the shear strength of an aluminium wall was exceeded early, before the complete formation of a typical concrete crushing form.

10- Theoretical analyses reveal that increasing aluminium wall thickness enhances the ultimate axial load capacity of circular and rectangular composite columns by 19%–58% relative to slender counterparts. This improvement stems from heightened stiffness and superior concrete-crushing resistance, fostering effective core confinement that postpones crushing, induces a beneficial triaxial stress state, and bolsters aluminium-concrete composite synergy.

11- In the elastic range, the initial slope of the stress-strain curves for concrete-filled aluminium tube columns steepens with increasing tube wall thickness (1.9 mm to 3 mm and 5 mm), irrespective of rectangular or circular cross-sections. Thicker tubes enhance confinement of the concrete core, promoting composite action under axial compression. This intensified interaction mitigates early micro-cracking, interfacial slip, and local instability, thereby enhancing overall sectional rigidity.

5.2 Recommendation for Future Works

More comprehensive studies are needed for an inquiry into the basic behavioural properties of CFAT columns.

Some recommended suggestions in the following:

1- Filling the aluminium tubes with different types of concrete and comparing them with each other (self- compacting, recycled aggregate concrete and lightweight concrete).
2- Aluminium reinforcement with CFRP layers with different patterns.
3- Using steel reinforcement to delay the concrete failure.
4- Develop the aluminium alloys to become close to the properties of steel while preserving the properties of aluminium.

References

[1] Wameedh Issa Braidi, "Nonlinear Analysis of Solid and Hollow Slender Rc Columns Strengthened By Sfr Subjected To Concentric And Eccentric Loads," Collage of Engineering, University of Misan, 2022.

[2] Athar Luaibi Mhawi and Abbas Oda Dawood, "Experimental Investigation of Concrete Filled Steel Tubular Columns with Partially Sand Replacement," College of Engineering, University of Misan, 2020.

[3] F. K. Idan, "Finite element analysis of concrete-filled aluminum tube columns," *International Journal of Applied Engineering Research*, vol. 12, no. 12, pp. 3054–3062, 2017.

[4] S. Bin Ali, *Structural behaviour and design of aluminium alloy-concrete composite structural members*. Liverpool John Moores University (United Kingdom), 2023.

[5] F. Zhou and B. Young, "Tests of concrete-filled aluminum stub columns," *Thin-Walled Structures*, vol. 46, no. 6, pp. 573–583, 2008.

[6] F. Zhou and B. Young, "Concrete-filled aluminum circular hollow section column tests," *Thin-Walled Structures*, vol. 47, no. 11, pp. 1272–1280, 2009.

[7] J. Dwight, *Aluminium design and construction*. CRC Press, 1998.

[8] F. M. Mazzolani, "3D aluminium structures," *Thin-Walled Structures*, vol. 61, pp. 258–266, 2012.

[9] Y. Sun, "The use of aluminum alloys in structures: Review and outlook," in *Structures*, Elsevier, 2023, p. 105290.

[10] F. Soetens and J. Mennink, *Aluminium building and civil engineering structures*. Elsevier, 1999.

[11] M. Chybiński, Ł. Polus, and M. Szumigała, "Aluminium members in composite structures–a review," *Archives of Civil Engineering*, pp. 253–274, 2022.

[12] Luck M. Snell, "Aluminium in concrete: A simple solution to a complex problem," *Arizona Contractor and Community*, Apr. 2021.

[13] S. F. Resan, "Structural Behavior of Simply Supported Ferrocement Aluminium Composite Beams," College of Engineering of The University of Basrah, 2012.

[14] X. You *et al.*, "A review of research on aluminum alloy materials in structural engineering," *Developments in the built environment*, vol. 17, p. 100319, 2024.

[15] A. C. I. Committee, "Building code requirements for structural concrete (ACI 318-08) and commentary," American Concrete Institute, 2025.

[16] T. Wang, X. Liu, and H. Zhao, "Experimental Study of the Seismic Performance of L-Shaped Columns with 500 MPa Steel Bars," *The Scientific World Journal*, vol. 2014, no. 1, p. 105826, 2014.

[17] J. An, "Study on Optimization Design of Reinforced Concrete Special-shaped Column Frame Structure," *Chem. Eng. Trans.*, vol. 62, pp. 1075–1080, 2017.

[18] J. Liu, H. Song, and Y. Yang, “Research on mechanical behavior of L-shaped multi-cell concrete-filled steel tubular stub columns under axial compression,” *Advances in Structural Engineering*, vol. 22, no. 2, pp. 427–443, 2019.

[19] Hayder Lateef Naji, “Behavior of Reinforced Concrete Column Strengthening with HPFRC under Eccentric Loads,” College of Engineering, University of Misan, 2025.

[20] Murtaza Allawi Raheemah, “EXPERIMENTAL INVESTIGATION OF SLENDER PLASTIC CONCRETE COMPOSITE COLUMNS,” College of Engineering, University of Misan, 2019.

[21] A. Ilanthalir, J. J. Regin, and J. Maheswaran, “Concrete-filled steel tube columns of different cross-sectional shapes under axial compression: A review,” in *IOP Conference Series: Materials Science and Engineering*, IOP Publishing, 2020, p. 012007.

[22] J. Becque, “Analytical modeling of concrete columns confined by FRP,” 2000.

[23] Y. Hu, B. Davison, I. Burgess, and R. Plank, “Multi-scale modelling of flexible end plate connections under fire conditions,” 2010.

[24] F. E. Richart, A. Brandtzaeg, and R. L. Brown, “A study of the failure of concrete under combined compressive stresses,” *University of Illinois. Engineering Experiment Station. Bulletin; no. 185*, 1928.

[25] J.-H. Zhu and B. Young, “Experimental investigation of aluminum alloy circular hollow section columns,” *Eng. Struct.*, vol. 28, no. 2, pp. 207–215, 2006.

[26] F. Zhou and B. Young, “Numerical analysis and design of concrete-filled aluminum circular hollow section columns,” *Thin-walled structures*, vol. 50, no. 1, pp. 45–55, 2012.

[27] K. Z. Nasser, “Structural behavior of concrete filled aluminum tubular columns,” *Basrah Journal for Engineering Science*, vol. 12, no. 1, pp. 46–49, 2012.

[28] K. Z. Nasser, “Experimental and Computational Study of Concret Fill Aluminum Tubular Column Under Axial Loads,” *Kufa Journal of Engineering*, vol. 5, no. 2, pp. 29–46, 2014.

[29] S. F. Resan, “Experimental investigation of aluminum-lightweight concrete composite columns,” *Basrah Journal for Engineering Science*, vol. 14, no. 1, pp. 13–25, 2014.

[30] S. F. Resan, “Behavior of aluminum columns enhanced with CFRP and filled by light weight concrete,” *Engineering and Technology Journal*, vol. 32, no. 11, pp. 2658–2672.

[31] G. Nayak, K. K. Shetty, and S. Abdalla, “Effect of depth to thickness ratio and length to depth ratio on hollow section aluminium tubes filled with self-compacting concrete,” *Int. J. Res. Eng. Technol.*, vol. 3, no. 3, pp. 675–678, 2014.

[32] A. J. H. Alshimmeri, “Structural behavior of confined concrete filled aluminum tubular (CFT) columns under concentric load,” *Journal of Engineering*, vol. 22, no. 8, pp. 125–139, 2016.

[33] M. A. Al-Mazini and A. H. Chkhewier, “Behavior of concrete filled aluminum square and rectangular hollow section columns under axial loads: Experimental and analytical study,” *Journal of Babylon University/Engineering Sciences*, vol. 25, no. 2, pp. 712–726, 2017.

[34] F.-C. Wang, H.-Y. Zhao, and L.-H. Han, “Analytical behavior of concrete-filled aluminum tubular stub columns under axial compression,” *Thin-Walled Structures*, vol. 140, pp. 21–30, 2019.

[35] P. Jinlong, L. Guanhua, and J. Cai, “Numerical analysis of circular and square section concrete filled aluminum tubes under axial compression,” *Fracture and Structural Integrity*, vol. 14, no. 54, pp. 169–181, 2020.

[36] V. I. Patel, Q. Q. Liang, and M. N. S. Hadi, “Numerical simulations of circular high strength concrete-filled aluminum tubular short columns incorporating new concrete confinement model,” *Thin-Walled Structures*, vol. 147, p. 106492, 2020.

[37] E. Georgantzia, S. Bin Ali, M. Gkantou, G. S. Kamaris, K. Kansara, and W. Atherton, “Structural response of aluminium alloy concrete filled tubular columns,” *ce/papers*, vol. 4, no. 2–4, pp. 614–620, 2021.

[38] Z.-J. Zhang, F.-X. Han, and Q. Liu, “Experimental and Finite Element Study on 7A04 Aluminum Alloy Tube Confined High Strength Concrete Long Column,” *Geofluids*, vol. 2022, no. 1, p. 4692054, 2022.

[39] J. Bu, Q. Liu, Y. Yu, and Q. Qiu, “Axial compression performance and bearing capacity calculation of round-ended concrete-filled aluminum tube column,” *Applied Sciences*, vol. 13, no. 13, p. 7918, 2023.

[40] B. R. Jean, “Troubleshooting Finite-Element Modeling with Abaqus: With Application in Structural Engineering Analysis,” 2020.

[41] J. E. Akin, *Finite element analysis concepts: via SolidWorks*. World Scientific Publishing Company, 2010.

[42] A. Khennane, *Introduction to finite element analysis using MATLAB® and abaqus*. CRC Press, 2013.

[43] S. Johnson, “Comparison of nonlinear finite element modeling tools for structural concrete,” *university of Illinois at Urbana Champaign,(December 15, 2006)*, 2006.

[44] F. Hejazi and H. M. Esfahani, *Solving complex problems for structures and bridges using ABAQUS finite element package*. CRC Press, 2021.

[45] K. J. Bathe, “Finite element procedures,” 1996, *Prentice Hall New Jersey*.

[46] J. N. Reddy, *An introduction to the finite element method*, vol. 3. McGraw-Hill New York, 2005.

[47] R. D. Cook, *Concepts and applications of finite element analysis*. John wiley & sons, 2007.

[48] O. C. Zienkiewicz and R. L. Taylor, *The finite element method set*. Elsevier, 2005.

[49] E. Georgantzia, S. Bin Ali, M. Gkantou, G. S. Kamaris, K. D. Kansara, and W. Atherton, “Flexural buckling performance of concrete-filled aluminium alloy tubular columns,” *Eng. Struct.*, vol. 242, p. 112546, 2021.

[50] B. I. Karlsson and E. P. Sorensen, *ABAQUS Analysis User’s Guide Volume III: Materials*, vol. 3. 2006.

[51] S. Garner, J. Strong, and A. Zavaliangos, “The extrapolation of the Drucker–Prager/Cap material parameters to low and high relative densities,” *Powder Technol.*, vol. 283, pp. 210–226, 2015.

[52] B. I. Karlsson and E. P. Sorensen, *ABAQUS Analysis user’s guide volume IV: Elements*. 2006.

[53] *Dassault Systèmes: Analysis User’s Guide Volume III*. 2010.

[54] P. Kmiecik and M. Kamiński, “Modelling of reinforced concrete structures and composite structures with concrete strength degradation taken into consideration,” *Archives of civil and mechanical engineering*, vol. 11, no. 3, pp. 623–636, 2011.

[55] D.-D. Pham and P.-C. Nguyen, “Behavior Analysis and Design of Concrete-Filled Steel Circular-Tube Short Columns Subjected to Axial Compression,” *arXiv preprint arXiv:2107.06488*, 2021.

[56] X. Yun, Z. Wang, and L. Gardner, “Full-range stress–strain curves for aluminum alloys,” *Journal of Structural Engineering*, vol. 147, no. 6, p. 04021060, 2021.

[57] U. Brian, “Local and postlocal buckling of fabricated steel and composite cross sections,” *Journal of Structural Engineering*, vol. 127, no. 6, pp. 666–677, 2001.

[58] J. G. Stoner, “Finite element modelling of GFRP reinforced concrete beams,” Doctoral dissertation, University of Waterloo, 2015.

[59] B. I. Karlsson and E. P. Sorensen, *ABAQUS Analysis user’s manual volume V: Prescribed conditions, constraints and interactions* . 2006.

[60] A. Specification, “Specification for structural steel buildings,” *ANSI/AISC*, vol. 36010, 2005.

[61] X.-F. Yan, M. Ahmed, and M.-N. He, “Behavior and design of axially loaded high-strength concrete-filled circular aluminum tubular short columns,” in *Structures*, Elsevier, 2022, pp. 357–371.

[62] *Design Guide on the ACI 318 Building Code Requirements for Structural Concrete*, First. 2020.

[63] T. Sheehan, “Cyclic behaviour of hollow and concrete-filled circular hollow section braces,” Doctoral dissertation, University of Warwick, 2013.

[64] N. Jamaluddin, “Behaviour of elliptical concrete-filled steel tube (CFT) columns under axial compression load,” Doctoral dissertation, University of Leeds, 2011.

الخلاصة

تقدم هذه الدراسة تحقيقًا عدديًا لسلوك الأعمدة المصنوعة من الألمنيوم والمملوءة بالخرسانة ذات مقاطع عرضية مختلفة. شملت الدراسة البارامترية 34 نموذجًا مقسمة إلى أربع مجموعات، حيث تُبيّن تأثير معاملات مختلفة على سلوك أعمدة الألمنيوم القصيرة المملوءة بالخرسانة، والتي تختلف في أشكال المقاطع العرضية، وإجهاد الخضوع للألمنيوم، ومقاومة الخرسانة الأسطوانية، وسمك جدران أنبوب الألمنيوم.

تتناول المجموعة الأولى تحليل سلوك المقاطع العرضية، حيث تم دراسة ستة أشكال مختلفة للمقاطع لها نفس مساحة المقطع والطول والحجم مقارنةً بالأعمدة المرجعية ذات المقطع الدائري. وقد أظهرت هذه المجموعة أن المقاطع الدائرية تتفوق دائمًا على باقي الأشكال الهندسية. كما أظهرت الأعمدة ذات المقاطع المستطيلة أقل كفاءة بين جميع الأشكال، حيث انخفض الحمل الأقصى بنسبة تراوحت بين 12% و14% مقارنةً بنظيراتها الدائرية. وقد تراوحت قوة الأشكال من الأضعف إلى الأقوى وفق الترتيب التالي: (المستطيل، السداسي، المثمن، الإهليجي، ذو النهايات الدائرية، الدائري).

درست المجموعة الثانية تأثير اختلاف إجهاد الخضوع للألمنيوم، حيث تم اعتماد قيمتي 267 و185 ميغا باسكال. واستخدمت هذه المجموعة مقاطع دائرية ومستطيلة بهدف فهم تأثير إجهاد الخضوع على سلوك هذه المقاطع. أظهرت الأعمدة ذات المقاطع الدائرية وبإجهاد خضوع مقداره 267 ميغا باسكال زيادة في الحمل الأقصى تراوحت بين 14% و20% مقارنةً بالأعمدة ذات إجهاد الخضوع 185 ميغا باسكال. كما أظهرت الأعمدة ذات المقاطع المستطيلة وبإجهاد خضوع 267 ميغا باسكال زيادة في الحمل الأقصى تراوحت بين 12% و18% مقارنةً بالأعمدة ذات إجهاد الخضوع 185 ميغا باسكال.

أما المجموعة الثالثة فقد تناولت تأثير مقاومة الخرسانة الأسطوانية المختلفة، حيث تم اعتماد قيمتي 44 و70 ميغا باسكال، واستخدمت مقاطع دائرية ومستطيلة لفهم تأثير مقاومة الخرسانة على سلوك هذه المقاطع. أظهرت الأعمدة ذات المقاطع الدائرية وبمقاومة ضغط خرسانية مقدارها 70 ميغا باسكال زيادة في الحمل الأقصى تراوحت بين 25% و33% مقارنةً بالأعمدة ذات مقاومة 40 ميغا باسكال. كما أظهرت الأعمدة ذات المقاطع المستطيلة وبمقاومة ضغط خرسانية مقدارها 70 ميغا باسكال زيادة في الحمل الأقصى تراوحت بين 26% و36% مقارنةً بالأعمدة ذات مقاومة 40 ميغا باسكال.

تناولت المجموعة الرابعة تحليل تأثير سمك جدران الألمنيوم المختلفة، والتي بلغت (1.9، 3، و5 ملم). واستخدمت هذه المجموعة مقاطع دائرية ومستطيلة لفهم تأثير السماكة على سلوك هذه المقاطع. بالنسبة للأعمدة ذات المقاطع غير المدمجة وبسماكة جدار 3 ملم، لوحظت زيادة في الحمل الأقصى بنحو 22% للمقاطع الدائرية و19% للمقاطع المستطيلة مقارنةً بالأعمدة ذات المقاطع النحيفة وبسماكة 1.9 ملم. كما أظهرت الأعمدة ذات المقاطع المدمجة وبسماكة 5 ملم تحسنًا بلغ 58% و56% للمقاطع الدائرية والمستطيلة على التوالي، مقارنةً بنفس المقاطع النحيفة.

جمهورية العراق
وزارة التعليم العالي والبحث العلمي
كلية الهندسة/ جامعة ميسان
قسم الهندسة المدنية

التحقيق العددي في سلوك أعمدة الألمنيوم المملوءة بالخرسانة ذات المقاطع العرضية المختلفة

اعداد الطالبة

روى ليث الجاروش

بكالوريوس هندسة مدني 2020

رسالة

مقدمة الى كلية الهندسة في جامعة ميسان

كجزء من متطلبات الحصول على درجة الماجستير في علوم الهندسة المدنية/ الانشاءات

بأشراف

الأستاذ الدكتور: محمد صالح عبد علي